

University of Alberta

CFD Simulation of Underground Coal Gasification

by

Ahad Sarraf Shirazi

A thesis submitted to the Faculty of Graduate Studies and Research
in partial fulfillment of the requirements for the degree of

Master of Science

in

Chemical Engineering

Department of Chemical and Materials Engineering

©Ahad Sarraf Shirazi

Fall 2012

Edmonton, Alberta

Permission is hereby granted to the University of Alberta Libraries to reproduce single copies of this thesis and to lend or sell such copies for private, scholarly or scientific research purposes only. Where the thesis is converted to, or otherwise made available in digital form, the University of Alberta will advise potential users of the thesis of these terms.

The author reserves all other publication and other rights in association with the copyright in the thesis and, except as herein before provided, neither the thesis nor any substantial portion thereof may be printed or otherwise reproduced in any material form whatsoever without the author's prior written permission.

Abstract

Underground Coal Gasification (UCG) is a process in which coal is converted to syngas in-situ. UCG has gained popularity recently as it could be used to extract energy of deep-lying coal seams, and it reduces the footprints attributed to the gasification process. In this study, two models have been developed to describe UCG process under in-situ conditions. Initially, a two-dimensional model was developed in COMSOL Multiphysics. Results and limitations of this model are discussed. The second model was developed in ANSYS FLUENT which includes all relevant reactions in a three-dimensional geometry. A detailed sensitivity analysis has been performed to investigate the effect of various parameters on the performance of the process. The results indicated particular importance of coal properties and variation of these properties with temperature. This study provides a strong basis for further extension of the model to the larger scales.

Acknowledgements

First, I would like to thank my supervisor, Dr. Gupta for providing the opportunity to work on this project. He has supported me throughout the project with his comments, patience and support.

I would also like to express my gratitude to Dr. Joe Mmbaga for his advice and valuable comments during this project.

I gratefully acknowledge Shayan Karimipour for his advice and contribution in this research. I am grateful in every possible way and hope to keep up our collaboration in the future.

I also want to thank Alberta Energy Research Institute (AERI) and the Canadian Centre for Clean Coal/Carbon and Mineral Processing Technologies (C5MPT) for the funding of this project.

Finally, I would like to thank Saba Roozbahani, my best friend, for support, enthusiasm, and patience throughout this project.

Table of contents

CHAPTER ONE: INTRODUCTION	1
1.1 COAL IN 21 ST CENTURY	1
1.2 WHAT IS UCG?	5
1.3 PROCESS OVERVIEW	6
<i>1.3.1 Drilling the wells</i>	6
<i>1.3.2 Linking</i>	8
<i>1.3.3 Ignition of coal</i>	10
<i>1.3.4 Gasification</i>	10
1.4 SUITABLE COAL SEAMS FOR UCG	11
1.5 RESEARCH OBJECTIVES	12
CHAPTER TWO: LITERATURE REVIEW	14
2.1 FIELD TRIALS, HISTORY AND CURRENT DEVELOPMENT	14
<i>2.1.1 Russia</i>	15
<i>2.1.2 European Union</i>	16
<i>2.1.3 USA</i>	18
<i>2.1.4 Australia</i>	24
<i>2.1.5 Other Countries</i>	26
2.1.5.1 South Africa	26
2.1.5.2 Canada	26
2.1.5.3 China	27
2.1.5.4 India	28
2.2 REVIEW OF EXPERIMENTS RELATED TO UCG	28
<i>2.2.1 Pilot-scale experiments</i>	28
<i>2.2.2 Coal block experiments</i>	31
2.3 SUMMARY OF TRIALS AND EXPERIMENTS	36
2.4 REVIEW OF UCG MODELING EFFORTS	37
<i>2.4.1 Packed bed models</i>	38

2.4.2	<i>Coal Slab models</i>	40
2.4.3	<i>Channel models</i>	44
2.4.4	<i>Other approaches for UCG modeling</i>	51
2.4.4.1	Reactor models	51
2.4.4.2	Probabilistic simulation	53
2.4.4.3	Process models	54
2.5	SUMMARY OF MODELING REVIEW	55
CHAPTER THREE: MODELING		57
3.1	GOVERNING EQUATIONS	57
3.1.1	<i>Conservation equations</i>	57
3.1.2	<i>Chemical reactions</i>	60
3.1.2.1	Drying	61
3.1.2.2	Pyrolysis	62
3.1.2.3	Heterogeneous reactions (Combustion and Gasification)	63
3.1.2.4	Homogenous reactions	66
3.2	IMPLEMENTATION IN COMSOL MULTIPHYSICS	67
3.2.1	<i>Numerical methods</i>	68
3.3	IMPLEMENTATION IN ANSYS FLUENT	70
3.3.1	<i>Numerical methods</i>	72
3.3.2	<i>Spatial discretization</i>	72
3.3.3	<i>Pressure-velocity coupling</i>	73
3.3.4	<i>Under-relaxation factor</i>	74
3.3.5	<i>Convergence criteria</i>	74
3.3.6	<i>Meshing</i>	75
CHAPTER FOUR: RESULTS AND DISCUSSION		76
4.1	RESULTS OF DEVELOPED MODEL IN COMSOL	76
4.1.1	<i>Shortcomings of developed model in COMSOL.</i>	82
4.2	RESULTS OF DEVELOPED MODEL IN ANSYS FLUENT	83
4.2.1	<i>Grid sensitivity analysis</i>	84
4.2.2	<i>Base case simulation</i>	85

4.2.3 <i>Effect of discretization scheme</i>	92
4.2.4 <i>Effect of operating pressure</i>	93
4.2.5 <i>Effect of inlet temperature</i>	93
4.2.6 <i>Effect of inlet flux</i>	94
4.2.7 <i>Effect of permeability</i>	96
4.2.8 <i>Effect of varying thermal properties of coal</i>	98
4.2.9 <i>Effect of moisture content</i>	101
CHAPTER FIVE: CONCLUSIONS AND RECOMMENDATIONS	103
5.1 CONCLUSIONS	103
5.2 RECOMMENDATIONS FOR FUTURE WORK	104
REFERENCES	106
APPENDIX A: USER-DEFINED FUNCTIONS	113

List of Tables

Table 1-1: Comparison of major coal gasification technologies	4
Table 2-1: Major government-funded UCG trials in the USA.	19
Table 2-2: Results of LVW and CRIP methods in Rocky Mountain trial (Modified from Beath and Davis, 2006)	23
Table 2-3: Major UCG experiments on coal blocks	31
Table 3-1: Main reactions in a gasification process	61
Table 3-2: Approximate relative rates of heterogeneous reactions of coal (800 C, 0.1 atm)	64
Table 3-3: Kinetic constants for reactions in coal	66
Table 3-4: Rate expressions and kinetic data for homogenous reactions	66
Table 4-1: Model parameters used for simulation of experiments of Forrester (1979)	77
Table 4-2: Proximate analysis of coal used in experiments of Forrester (1979)	77
Table 4-3: Dimensions of modeled geometry in COMSOL	78
Table 4-4: Proximate analysis of Alberta coal reservoir	78
Table 4-5: Parameters used for simulation of UCG in Alberta coal reservoir	79
Table 4-6: Bulk gas composition assumed for simulation of UCG (Perkins and Sahajwalla 2005)	79
Table 4-7: Dimensions of developed model in FLUENT	83
Table 4-8: Primary coal used in developed model in FLUENT	83
Table 4-9: Model parameters as used in FLUENT	84
Table 4-10: Boundary conditions for developed model in FLUENT	84
Table 4-11: Selected variables after 8500 seconds of process for various mesh cases	85
Table 4-13: Comparison of scaled dimensions of cavity with experiments	91
Table 4-14: Effect of discretization scheme after 8500 seconds of process	92
Table 4-15: Effect of operating pressure on UCG process after 6500 seconds of process	93
Table 4-16: Dimensions of the cavity for different injection rates	96

List of Figures

Figure 1-1: Global Distribution of fossil fuels in terms of gigatonnes of oil equivalent (Concluded from BP statistical review of World Energy, 2011) ..	2
Figure 1-2: World energy consumption by source (BP statistical review of World Energy, 2011).....	2
Figure 1-3: Life-cycle analysis of different power generation technologies	3
Figure 1-4: Various well configurations for UCG process: (a) Linked Vertical Wells (LVW) ; (b) Linear CRIP (c) Parallel CRIP (d) Steeply dipping seams	7
Figure 2-1: Thickness vs. depth of the field trials conducted worldwide (Modified from Pana, 2009).....	15
Figure 2-2: Projected shapes of cavity at Hanna II (Modified from Yeary (1989))	20
Figure 2-3: Plan view of Hoe Creek 3 cavity after 283 days of process (Modified from Thoesness and Creighton, 1983)	22
Figure 2-4: Long tunnel configuration in China (Couch (2009))	28
Figure 2-5: Typical cross-section of cavity in LBK experiments (Modified from Hill and Thorsness (1982))	30
Figure 2-6: Different reaction regimes in packed-bed model.....	39
Figure 2-7: Scheme of Coal Block models (Modified from Perkins and Sahajwalla (2005)).....	41
Figure 2-8: Reactions and Transport phenomena in channel model.....	45
Figure 2-9: UCG cavity defined in the work of Luo et al. (2009)	47
Figure 2-10: Channel formation in thin seams (Modified from Kuyper (1995)) .	48
Figure 2-11: Channel geometry in Kuyper's model (1996).....	50
Figure 2-12: Channel geometry in Perkins and Sahajwalla (2007)	51
Figure 2-13: Proposed reactor arrangement for cavity in works of Daggupati et al. (2011)	53

Figure 2-14: Probabilistic simulation of UCG process by possibility of movement of following interfaces: 1.Void-Rock; 2. Coal-Rock; 3. Void-Coal; 4.Void-Ash; 5. Ash-Void. (Biezen et al. (1995))	54
Figure 3-1: Surface area vs. conversion for different values of ψ	65
Figure 3-2: CRIP configuration for modeling UCG in COMOSL	67
Figure 3-3: Geometry for UCG modelling in FLUENT	70
Figure 4-1: Comparison of temperature distribution of simulation and experiments with gas temperature 1173 K. (Reproduced from Perkins (2005)).....	78
Figure 4-2: Cavity shape after 5 days of process	80
Figure 4-3: Rate of evolution of steam vs. temperature in a probe point in seam	80
Figure 4-4: Area of cavity vs. time	81
Figure 4-5: Outlet flow/Inlet flow for base case simulation	86
Figure 4-6: Composition of produced gas in base case simulation	87
Figure 4-7: Outlet temperature vs. time for base case simulation	88
Figure 4-8: Temperature distribution in coal seam after 9000 seconds of process	89
Figure 4-9: Reaction fronts in system after 4500 seconds of process: (a) combustion front, (b) pyrolysis front, (c) drying front	90
Figure 4-10: Cavity shape after 9000 seconds of process in base case simulation	90
Figure 4-11: Definition of characteristic dimension of cavity	91
Figure 4-12: Effect of inlet temperature on the cavity growth rate	94
Figure 4-13: Cavity volume vs. time for different inlet flow rates	95
Figure 4-14: Heating value of syngas for various injection rates	96
Figure 4-15: Cavity volume for seams with different initial permeability	97
Figure 4-16: Cavity shape for cases with different initial permeabilities (a) 1mD (b) 100 mD (c) 10 D.....	98
Figure 4-17: Thermal properties of coal as a function of temperature	100
Figure 4-18: Cavity volume for cases with temperature-dependant thermal properties.....	100
Figure 4-19: Cavity volume for cases with different initial moisture.....	102
Figure 4-20: Weight percent of steam in outlet	102

Nomenclature

C_2	Inertial resistance factor, 1/m
C_p	Specific heat capacity, J/(kg K)
d	Pipe diameter, m
D	Diffusion coefficient, m^2/s
E	Activation Energy, J/mol
k	Pre-exponential factor
k_c	Thermal conductivity, W/(m K)
L_e	Entrance length, m
M	Moisture content of coal
n	Power-law exponent
m^o	Mass flow rate, kg/s
p	Total Pressure, pa
Pe	Peclet number
R	Gas constant, J/(mol K)
R_p	Residual
$rate_i$	Reaction rate, $kg/(m^3 s)$
Re	Reynolds number
S	Specific surface area, 1/m
T	Temperature, K
U	Stream velocity, m/s
v	Velocity vector, m/s
VM	Volatile matter content of Coal
X	Char conversion
Y_i	Mass fraction of component i

Greek Letters

ΔH_i	Heat of reaction i , W/ m^3
φ	Porosity
Ψ	Structure parameter

μ	Kinematic viscosity of fluid, Pa.s
ρ	Density, kg/m ³
σ	Experimental parameter in permeability-porosity equation
Γ	Diffusion coefficient

Subscripts

g	gas
i	index
nb	neighbouring cells
s	solid

Abbreviations

1D	One-Dimensional
2D	Two-Dimensional
3D	Three-Dimensional
CFD	Computational Fluid Dynamics
CRIP	Controlled Retraction Injection Point
LLNL	Lawrence Livermore National Library
LVW	Linked Vertical Wells
RCL	Reverse Combustion Linking
SDS	Steeply Dipping Seams
UCG	Underground Coal Gasification

Chapter One: Introduction

1.1 Coal in 21st century

Coal is a carbon-rich rock formed by organic maturation of vegetal matter accumulations over thousands of years, which is called the coalification process. Coal is the most abundant and widespread type of fossil fuel and is estimated that 850 Gigatonnes of coal is economically recoverable using current technologies. Total amount of coal reserves that includes economically non-recoverable part is reported to be 18 Teratonnes (Couch, 2009). Figure 1-1 represents fossil fuel distribution around the world. US have the largest coal reserves in world with 223 billion tonnes of coal, followed by Russia and China. Canada has around 8 billion tonnes of coal reserves, most of which are located in western provinces (MIT Publication, 2007).

Currently, almost 90% of coal is used for power generation in developed countries, representing 30% of total electricity generation. Figure 1-2 shows world energy consumption based on its source.

With current trends of energy consumption, and rise of developing countries, these numbers is expected to be the same, while the total energy consumption increases around the world. In a recent study, it has been reported that coal consumption is expected to increase under any scenario due to its low price for

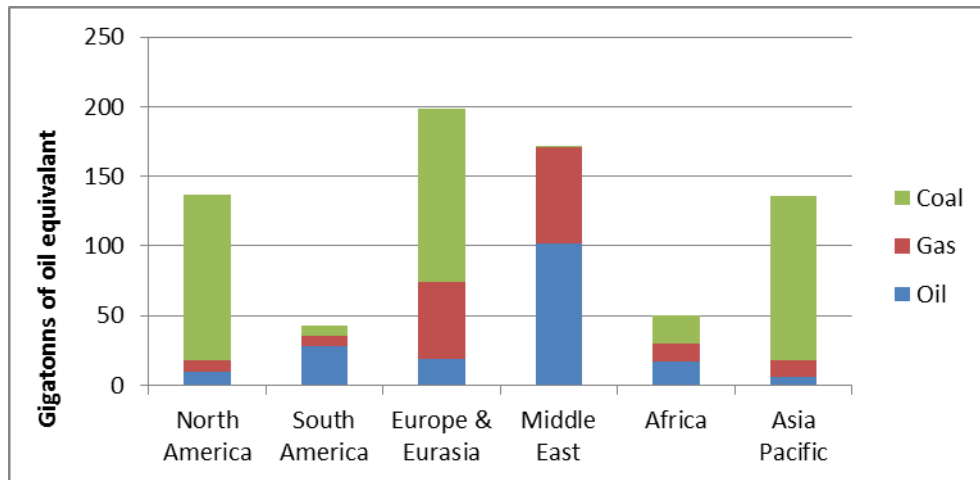


Figure 1-1: Global Distribution of fossil fuels in terms of gigatonnes of oil equivalent
(Concluded from BP statistical review of World Energy, 2011)

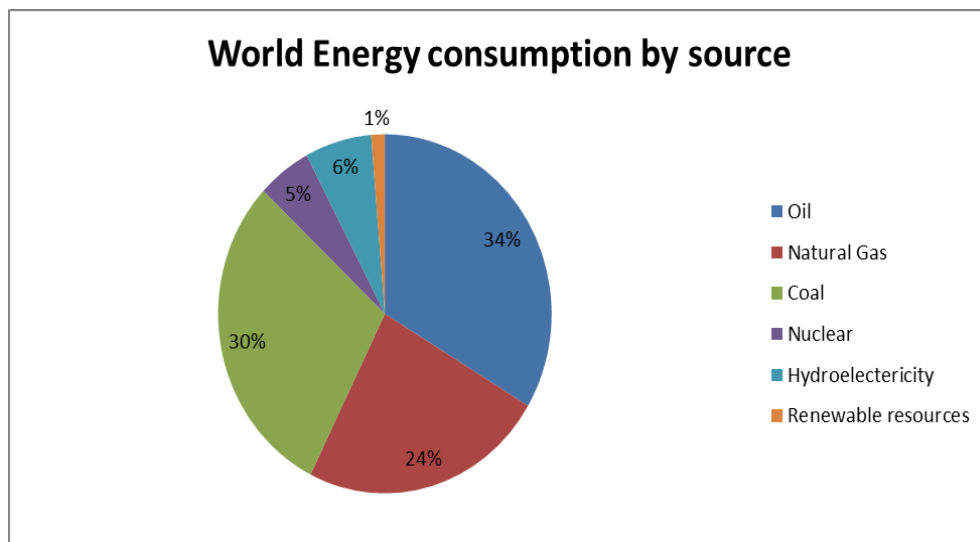


Figure 1-2: World energy consumption by source (BP statistical review of World Energy, 2011)

base-load power generation and availability around the world. However, as the governments are increasingly concerned with protecting environment, strict

regulations are passed to reduce Greenhouse Gas (GHG) emissions. Figure 1-3 shows emissions per generated electricity for different methods of power generation. As shown in Figure 1-3, compare to other power generation methods coal-fired power plants have higher GHG emission per generated energy due to lower efficiency of the process and higher carbon-to-hydrogen ratio of coal. Therefore, there is a significant push from governments for developing clean coal technologies that would enable them to use cheap coal and address environmental concerns at the same time.

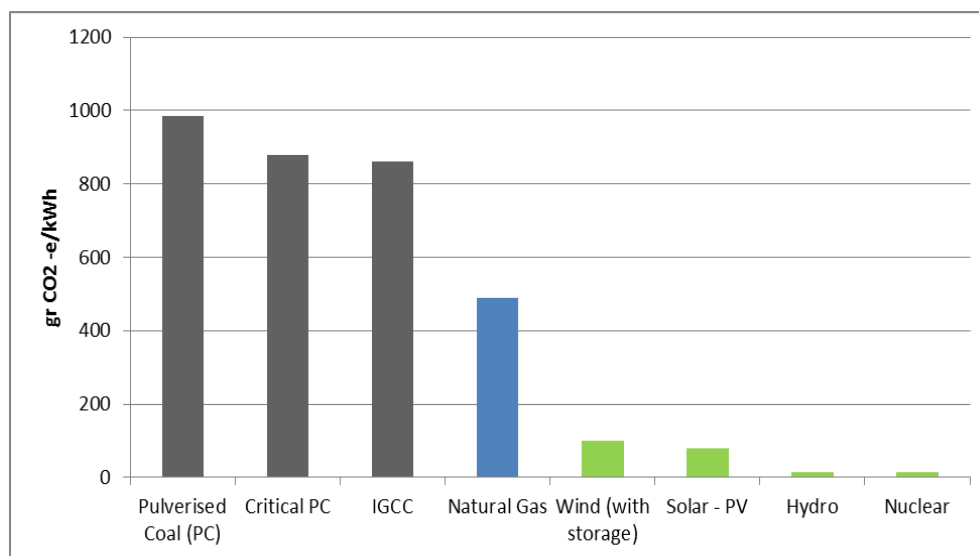


Figure 1-3: Life-cycle analysis of different power generation technologies
(Modified from Odeh and Cockerill, 2008)

Approaches for reducing emissions from coal-fired power plants could be divided in two categories: pre-combustion and post-combustion capture of CO₂.

In pre-combustion technologies, CO₂ is removed prior to combustion. In this method, coal is converted to a mixture of CO and H₂ which is called synthesis gas

or syngas, using gasification reactions. Syngas may further be transferred to shift reactors where CO is converted to H₂ and CO₂ using water/gas shift reaction.

Hydrogen is separated from CO₂ and used for power generation or fuel cells.

In post-combustion capture methods such as amine process, a chemical solvent is used to separate CO₂ from flue gas. Other approaches for reducing emissions from coal power plants include oxy-fuel combustion and using variations of pulverized coal combustion to increase efficiency of the process. Integration of gasification reactions with combined cycle (IGCC) has also resulted in reduction of emissions by 20 % and yielded a high pressure CO₂-rich stream in outlet ready for CO₂ capture and sequestration.

Different gasification reactors are developed over the years varying in gas flow configuration, coal particle size and operating conditions. Table 1-1 lists major gasification technologies currently being used in industry (Adams et al., 2009).

Table 1-1: Comparison of major coal gasification technologies

Reactor type	Moving bed (Lurgi)	Fluidised bed	Entrained flow (Shell)
Particle size	5-50 mm	0.5-5 mm	<250 µm
Fuel residence time	15-30 min	5-50 s	1-10 s
Pressure (atm)	28	25	28
Temperature (K)	1100-1350	1250-1400	1600-2200
O ₂ /Coal (kg/kg)	0.19	0.47	0.7
H ₂ O/O ₂	4.5	0.57	0.05

All of these gasification processes are occurring in surface, which requires mining, transportation, and grinding of the coal.

1.2 What is UCG?

Underground Coal Gasification is an alternative method for surface gasifiers. In this method coal is converted to syngas in-situ. This process involves burning coal underground with mixture of air/oxygen and steam. If the process is developed commercially, it would increase coal reserves by 60%. Even if 10% of this potential is met, it would provide a significant amount of additional energy source.

UCG has several advantages over conventional gasification process such as:

- Elimination of coal mining, which is considered a dangerous practice even with current equipment and safety regulations. For instance, China officially reported 6040 deaths in 2004 resulting from incidents in coal mines (USMRA Website).
- Lower capital investment due to the absence of surface gasification units.
- Elimination of ash handling operations, by keeping the ash underground.
- Lower water consumption.
- Generate possible sites for CO₂ sequestration

However, UCG introduces some challenges that should be addressed before the process can be adopted in large scale. Some of the main challenges are process stability, aquifer contamination and subsidence. The UCG performance is largely affected by properties of the coal seam, geological and hydro-geological conditions of the site which make prediction of UCG performance more difficult.

1.3 Process Overview

The UCG process involves four steps: drilling, linking, ignition, and gasification that are briefly described in following sections.

1.3.1 Drilling the wells

In the first step, injection and production wells should be drilled from surface to the coal seam. The basic layout of the process requires one borehole for injection of gases and one for production, however over the years three standard configurations of wells have been evolved which are:

- Linked Vertical Wells (LVW);
- Controlled Retraction Injection Point (CRIP);
- Steeply Dipping Seams (SDS).

Figure 1-4 shows a simple sketch of these well arrangements. The LVW configuration is based on the Soviet Union field trials and involves two wells that are connected by a linking method. The distance between wells depends on coal seam properties and its behaviour during linking and could be between 5-30 m. This method is generally suitable for shallow coal seams (<300 m). A modified version of LVW, named ϵ UCG, is currently licensed by Ergo Exergy® and was employed in Chinchilla field trial.

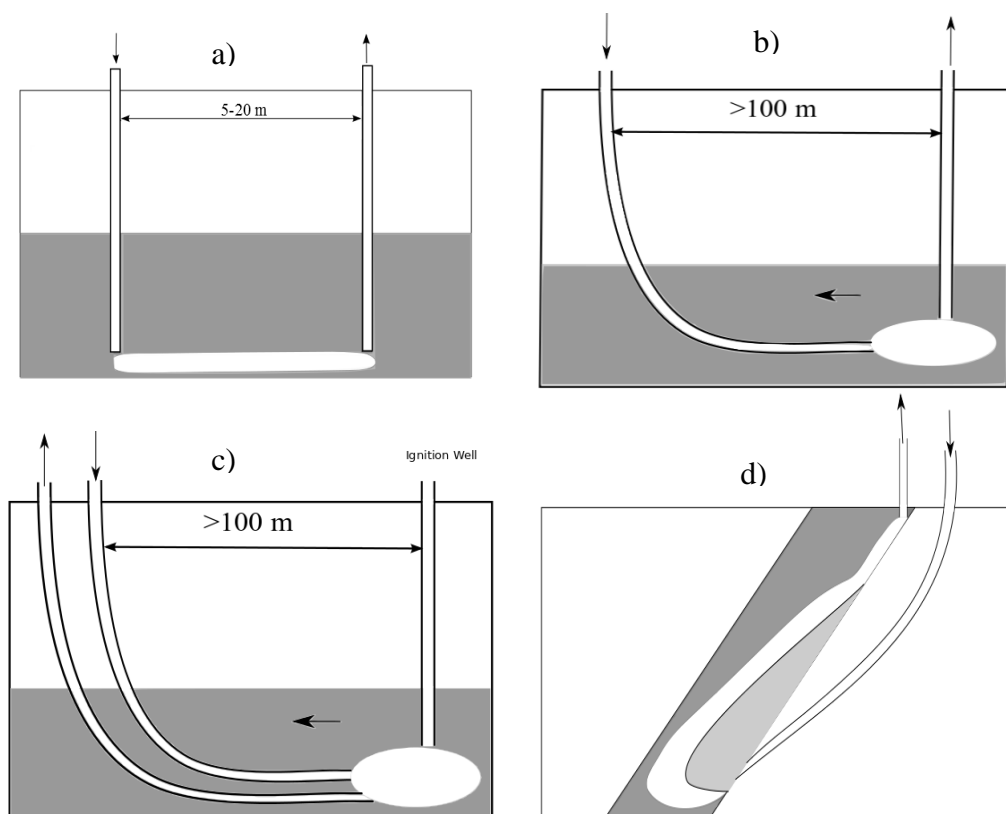


Figure 1-4: Various well configurations for UCG process: (a) Linked Vertical Wells (LVW) ; (b) Linear CRIP (c) Parallel CRIP (d) Steeply dipping seams

The CRIP method was pioneered in the works from Lawrence Livermore National Library (LLNL) during USA field trials (Thorsness and Creighton, 1983). It involves a movable injection point that is retracted when coal seam around the point is consumed. Gases will come in contact with coal when the liner is burnt away by ignition. This method provides greater control over gasification reactor, improves resource recovery, and requires comparatively fewer wells. Two variations of the CRIP technology have been practiced over the years. Linear CRIP in which a number of cavities are formed in series and parallel CRIP in which the cavity continuously grows along the coal until the whole coal seam is consumed.

To apply UCG in steep dipping seams (dip angle $> 50^\circ$), inclined injection should be used. In this method, injection well is drilled in lower part of the seam and production well is located in lower third of coal. In horizontal coal seams, inert roof material falls and remains unreacted as gases tend to move upward; while in steeply dipping seams, more char is accumulated around injection well that results in improved quality of produced gas (oxidation zone remains close to injection well, while reduction and pyrolysis zone would extend along the path of gas.). Few trials performed on SDB which resulted in higher gas qualities compared to horizontal seams. However, this method can only be conducted in certain seams and control of the process is a major challenge for this method. Furthermore, the difference in hydrostatic pressure along the seam makes it hard to control the ground water flow into the cavity (Davis and Ahner, 1982).

1.3.2 Linking

Since initial permeability of the coal seam does not allow sufficient gas flow for operation at large scale, a link which is a permeable path between injection and production wells should be established prior to start of gasification phase. Main methods for linking include reverse combustion, hydro-fracturing, directional drilling, and electro-linking. All of these methods increase the permeability of the coal in a narrow cylindrical channel.

Reverse combustion is conducted in following steps:

- Injection of high pressure air into the production well

- Combustion of air by electric heater
- Switching high pressure air from production to injection

These steps cause the flame front to move in opposite direction (from production to injection well). Reverse combustion has been used successfully in many trials; however direction and orientation of the generated link is hard to control. Application of this method in deeper seams introduces difficulties, as there is higher chance of spontaneous combustion in the base of the injection well (Gregg and Edgar, 1978).

In hydro-fracturing, high pressure fluid with a pressure higher than the rock strength is injected into the seam from injection well which usually form a circular permeable path at bottom of the seam. For this operation, mixture of water, thickening agent and sand would be pumped underground. Similar to the reverse combustion method, controlling location of permeable path is shown to be difficult (Gregg and Edgar, 1978).

Directional drilling is considered to be the most reliable method for linking. This method involves the drilling of a deviated borehole into the coal seam. Intersection of this borehole with injection and production boreholes provides the linking path. This method has been successfully used for linking of wells with up to 300-400 m distance. A detailed procedure for application of directional drilling in UCG is given elsewhere (Couch, 2009; DTI, 2006).

Electro-linking involves placing two electrodes at bottom of injection and production well and applying high intensity current. High electric current heats up the coal and removes moisture and volatile matter, which would increase the

permeability of coal. To use this method, electrical conductivity of original coal should be high and conductivity must increase as a result of heating. Applicability of this method is limited since it highly depends on electrical conductivity of coal and heterogeneous nature of seam. Therefore, this method is no longer used in field trials.

1.3.3 Ignition of coal

Igniting the coal is necessary for initiation of UCG process. There are little reliable data on ignition methods for UCG in open literature. Various methods of ignition that have been used in trials include use of pyrophoric compounds such as silane (SiH_4) and triethylborane (TEB), methane or propane gas, electrical ignition, dropping hot coke down the well, and spontaneous combustion of coal with pressurized oxygen. The only detailed description for ignition process is from large block experiments in which mixture of silane and propane was used (Hill and Thorsness, 1982).

1.3.4 Gasification

After the coal has been successfully ignited, a mixture of air/oxygen and steam would be injected into coal seam. This mixture would react with coal and synthesis gas would be recovered from production well. Consumption of coal would lead to development of an empty space, cavity, in underground seam. When the cavity reaches the production well, most of injection gas would bypass

before reacting with available coal resulting in lower quality of produced gases. For further continuation of operation, fresh coal should be made available to process. Produced gas includes hydrogen, carbon monoxide, carbon dioxide, methane and traces of other gases such as nitrogen and heavier hydrocarbons. It has been suggested to flush the cavities with water or steam after termination of process in order to remove pollutants and prevent them diffusing to surrounding environment.

1.4 Suitable coal seams for UCG

As mentioned earlier, UCG process is affected by properties of the seam. The primary geometric properties of seam include seam depth, thickness, and dip angle. Depth of coal seam is one of the most important parameters in the process. It determines operating pressure of process and also affects possibility of subsidence at surface. Operating pressure should be in equilibrium with hydrostatic pressure of surrounding that increases with a rate of 0.01 MPa/m depth. Therefore, operation at deeper seams will require more power for compression of injection gases, while offers greater stability and lower chances of subsidence. It has been suggested that coal seams deeper than 200-300 metres are suitable for UCG due to advantages mentioned earlier.

Seam dip angle has a significant effect on UCG performance. As discussed earlier, steeply dipping seams have resulted in higher quality of syngas; while introducing some challenges in process control and stability. Thickness of the coal

seam changes the behaviour of UCG reactor, as interaction with overburden in thin seams would considerably affect UCG performance. Based on the Soviet Union UCG trials, the thickness of the coal seam should be at least 2 m to be economically feasible. UCG practice is possible in all ranks of coal; however, previous trials have shown that low-rank coals that shrink upon heating are the most suitable for use in UCG. Higher-rank coals swell after pyrolysis resulting in blockage of the link path.

1.5 Research Objectives

The main goal of this research is to develop a model to describe cavity growth during UCG process in coal seams and to investigate the effect of various physical and operating parameters on performance of process.

This thesis has been divided into following sections:

- Literature Review: In this section a detailed review of major field trials, experiments and mathematical models along with their assumptions, approaches, and limitations are presented and their important results are presented.
- Modelling: Two different models are presented in this thesis. Models are solved using different commercial CFD codes. Each of these models and their assumptions, numerical methods, and equations are described in detail. A detailed comparison of two models is also presented.

- Results and Discussion: In this section, model results are presented and discussed in detail. Effects of various operating and physical parameters on process are investigated and most important parameters are identified.
- Conclusions and Future Work: In last part of thesis, important conclusions are made. Also, based on results of this research, important recommendations are made for further development of modelling on UCG.

Chapter Two: Literature Review

2.1 Field Trials, history and current development

Over 50 pilot UCG plants have been conducted worldwide since the 1930s. These developments have been concentrated in USSR, Europe, USA and China. USSR may be considered the first nation to heavily engage in UCG. However, detail information on the UCG trials in USSR is scarcely available. These trials were conducted in different coal seams with different depths and thicknesses. Compare to US and USSR trials, most of the European trials have been performed in deeper coal seams (Depth > 300 m) of lower rank coals and few efforts for using high-rank coals (anthracite and bituminous coals) were unsuccessful. In the following sub-sections, a brief review of important field trials and their findings are described based on their location.

Figure 2-1 summarizes all the UCG field trials performed worldwide in term of their depth and thickness of the coal seam. As can be seen, all of the trials except European efforts have been conducted in relatively shallow seams which are not currently targeted because shallow depth of seam limits the application of high operating pressures and increases the possibility of leakage.

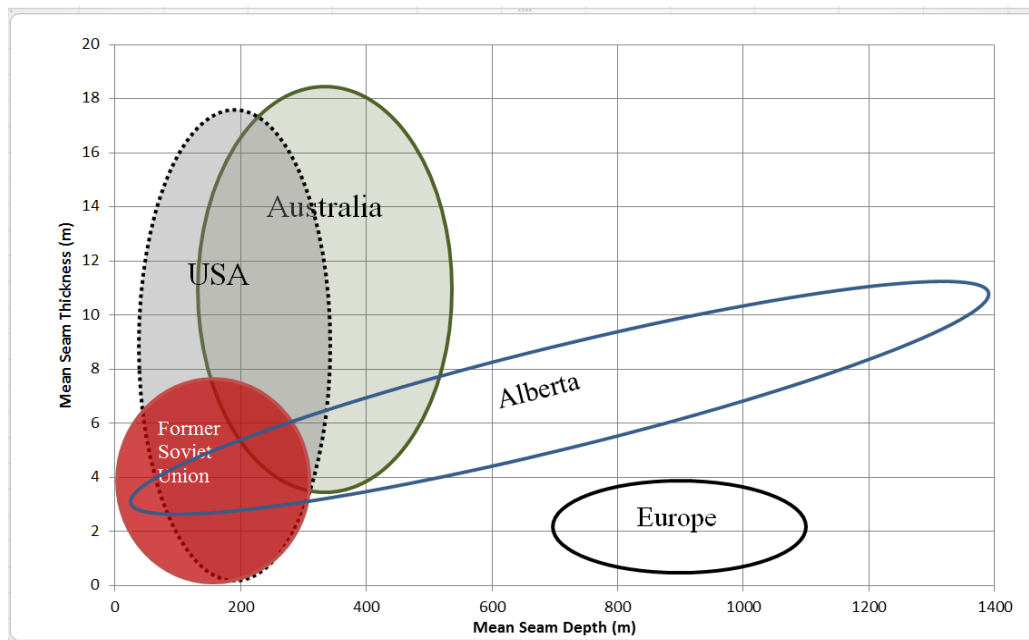


Figure 2-1: Thickness vs. depth of the field trials conducted worldwide (Modified from Pana, 2009)

2.1.1 Russia

The first pilot plants of UCG were built in former Soviet Union. Most of the operations were performed in shallow and thin coal seams depth < 100 m and thickness of 0.6-2.1 m and low operating pressure. Due to the shallow depth of the coal seam, extensive gas leakage of 5-30%, to surface was reported. Commercial-scale development of UCG was carried out in variety of geologic settings, which resulted in consumption of 17 Mt of coal in total. Air was usually used as oxidant which led to production of a syngas with a low heating value of $3-6 \text{ MJ/m}^3$. Use of oxygen and steam increased heating value of produced gas to $10-12 \text{ MJ/m}^3$. In these trials, reverse combustion and hydro-fracturing were investigated as economically favourable alternatives to directional drilling. Due to very low coal

permeabilities, establishment of a link was found to be necessary for continuous progression of the process. This found to decrease the sensitivity to initial coal permeability. These field trials also showed that lower thickness of the coal seam leads to a decreased heating value of the produced syngas. A detailed investigation of USSR trials is given elsewhere (Greg et al, 1976).

Development of UCG in Soviet Union was decreased and abandoned at around 1950s due to the discovery of large natural gas reservoirs. In harmony with the new wave of worldwide interest to UCG studies, Ukraine, Russia and Uzbekistan have started funding new research activities, noticeable from a significant increase in number of UCG-related patents that were published recently in those countries (Shafirovich and Varma, 2009).

2.1.2 European Union

Initial trials in Europe were conducted in UK from 1949 to 1959. Only low quality gas was produced in these tests due to unsuccessful linking. After termination of UK experiments in 1959, some other countries in Western Europe conducted trials at depths of more than 300 m. These trials were focused on establishing effective linking methods for deep coal seams. First series of these tests were performed in Bruay en Artois in France in an anthracite coal seam (thickness: 1.2 m, depth: 1170 m) to investigate the effect of coal reactivity and hydraulic linking between two wells. Poor hydraulic connection between wells forced them to use high pressure in the reverse combustion stage that led to self-

ignition of coal near injection well and failure of those trials. Another trial was conducted in France at Haute-Deule on a high-rank coal with a thickness of 1.8 m and depth of 880 m. A better linkage was established in this trial compared to the previous test which led to the continuation of the gasification reactions for almost two months. This test was finally ceased due to the blockage of the outlet by tars and coal particles (Couch, 2009). At the same time, a joint Belgium-Germany conducted trials at Thulin, Belgium in a coal seam of anthracite coals with 860 m depth and 6 m thickness. In the contrary to the previous trials, reverse combustion found to be unreliable as a primary linking method and directional drilling was found to be better suited for connecting the wells. This time, gasification continued for 200 days and was terminated because of excessive gas bypassing. These unsuccessful trials led to the conclusion that reverse combustion, hydrofracturing, and electro-linking are not suitable for establishing a link between injection and production wells in an anthracite coal seam due to its low volatile matter content. They also suggested conducting UCG trials in thinner seams of low rank coals. Initially, El Tremedal site in Spain was chosen due to its desirable depth (550 m) and extensive set of available borehole data. This seam contains high sulphur subbituminous coal with thickness of 2-4 m dipping at 30°. Linear CRIP was used in this trial along with directional drilling for linking as explained in section 1.3. The desirable temperature was achieved by igniting a methane burner using a Pyrophoric compound. The gasification reactions started afterwards. Coiled tubing was retracted seven times based on CRIP technology. Produced gas contained as much as 50% water due to excessive water influx into

cavity. Post-burn excavation of the site indicated that the cavity has undergone a huge side-wise growth and the cavity width is five times larger than seam thickness. The concentration methane was generally higher in the European tests due to higher operating pressure. El Tremedal test results demonstrated the feasibility of gasification at great depth, using directional drilling for well construction, and application of CRIP method for UCG in deep seams. Unfortunately, the trial was terminated due to an explosion of the accumulated methane after a short period. Methane concentration was generally higher in the European tests due to higher operating pressure (Couch, 2009).

Recently, European Union has started an initiative to investigate production of hydrogen-rich syngas from UCG in lignite coal seam (Stanczyk, 2009). This program also aims to study feasibility of the integration of UCG with Carbon Capture and Storage (CCS) technology

2.1.3 USA

A total of 31 tests were conducted in U.S. between 1973 and 1989, most of which were funded by the Department of Energy and performed in Wyoming sub-bituminous coal seams. Some trials were also funded by the private sector performed in Texas lignite seams. These tests are well-documented and results have been published in different reports and articles. Table 2-1 introduces the most important field trials in these series and their operational settings. As can be

seen, all of the trials except Pricetown, Wyoming, have been conducted in sub-bituminous coal seams.

Table 2-1: Major government-funded UCG trials in the USA.

Period	Location	Configuration	Coal rank	Seam thickness (m)	Seam depth (m)	Objective
1971-81	Hanna, WY	LVW-RCL	Sub-bituminous	7	45-152	Assessment of UCG methods used in USSR
1972-82	Hoe Creek, WY	LVW-RCL	Sub-bituminous	5	30-40	Investigation of various linking techniques
1977-80	Pricetown, WV	LVW-Drilled link	bituminous	3	270	Feasibility of UCG in bituminous seams
1976-82	Rawlins, WY	SDS	Sub-bituminous	7	120-200	Feasibility of UCG in steeply dipping seams
1981-85	Centralia, WA	CRIP	Sub-bituminous	6-8	20-50	Applicability of CRIP for UCG
1986-93	Rocky Mountain	LVW and CRIP	Sub-bituminous	7	75	Comparison of CRIP and LVW

LVW: Linked Vertical Wells; RCL: Reverse Combustion Linking; SDS: Steeply Dipping Seams; CRIP: Controlled Retraction Injection Point

A series of trials were conducted in Hanna, Wyoming spanned in a period of 10 years. The first phase of Hanna, Hanna I, was conducted to assess the feasibility of UCG in thick non-swelling coal seam. Excavation indicated that only the top part of the coal seam was consumed. This was related to the placement of the wells near the top of the coal seam. This problem was resolved in later phases of the project. In second phase of Hanna trials, Hanna II, reverse combustion and cavity growth patterns were studied in detail. The cavity was observed to grow upward and develop to a tear-drop region around the link between injection and production wells. The projected shape of the cavity is shown in Figure 2-2. The

lateral and vertical cavity growth in this experiment was determined to be 0.15-0.24 m/day, and 0.12-0.67 m/day, respectively.

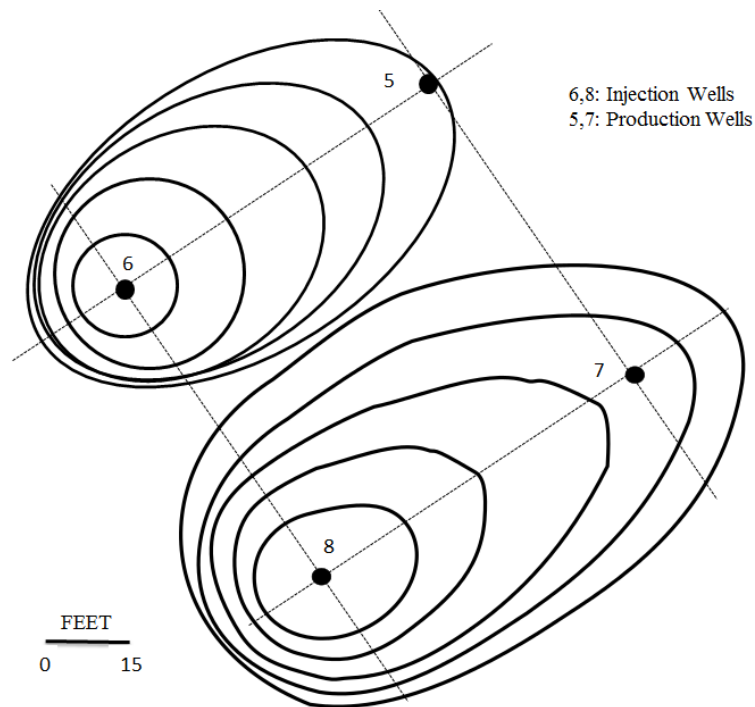


Figure 2-2: Projected shapes of cavity at Hanna II (Modified from Yearly (1989))

The third phase of the Hanna trials, Hanna III, was specifically designed to study the effect of UCG process on the quality of surrounding water resources. Results indicate that beyond gasification cavity, there is no sign of contaminant movement. Solubilized pyrolysis products were mostly found in cavities. Also, they have reported replacement of bicarbonate by sulphate compounds inside the cavity. (Cooke and Oliver, 1983)

Hanna IV was performed with an increased distance of 30 to 45 m between injection and production wells compared to the previous trials. Unsuccessful

operation of Hanna IV demonstrated that reverse combustion should not be used to establish linking over long distances.

Another series of UCG trials was attempted by Lawrence Livermore National Laboratory (LLNL) at Hoe Creek to investigate various linking techniques. Various methods including explosive fracture; reverse combustion; and directional drilling were tested. In Hoe Creek I, the forward gasification phase was able to continue only for 11 days using explosive fracturing for linking. Results of this phase indicated that explosive fracturing is not a viable method for developing a controlled region of high permeability as a link. The reverse combustion method was used in Hoe Creek II which led to the continuation of the trial for 43 days. Excessive water influx in this trial lowered the quality of the produced syngas. The operating pressure was increased by 20% to reduce the influx. This increased pressure resulted in significant gas loss to the surrounding environment. In Hoe Creek III, a combination of drilled link and reverse combustion was used for establishing the link near the bottom of the coal seam for a well spacing of 17-30 m. Due to the movement of the burned zone to the top sections of coal seam, significant gas losses of about 17% was reported. Post-burn coring exhibited a tear-drop cavity shape in the plan view and a bowl-like shape from side view. Cavity was filled with thermally affected rocks with a void at top. It is important to note the absence of unburned coal in cavity. Directional drilling was found to be an effective method for controlling the margins of the cavity. It was concluded that maintaining the injection point at lower part of seam would improve quality of syngas by 15% (Thorsness and Creighton, 1983).

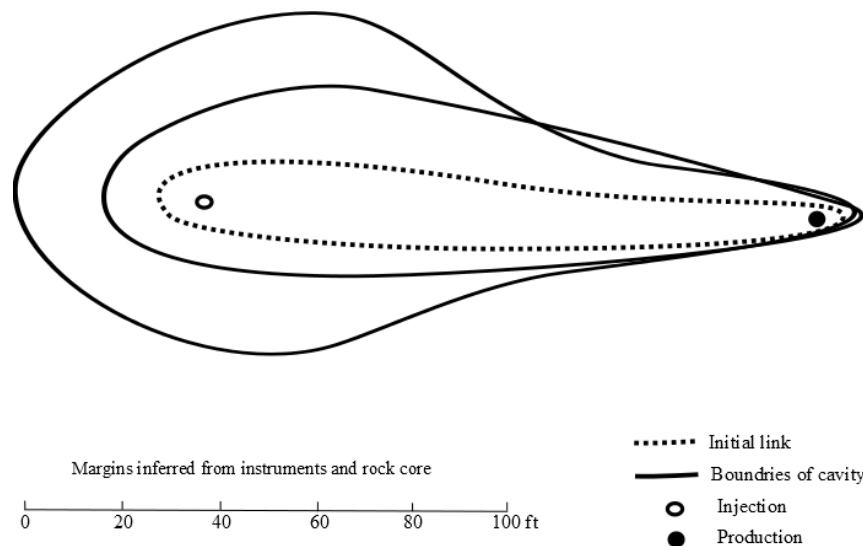


Figure 2-3: Plan view of Hoe Creek 3 cavity after 283 days of process (Modified from Thoesness and Creighton, 1983)

Due to shallow depth and weak roof of seam, these tests resulted in the propagation of subsidence to surface and contamination of the surrounding aquifers. This led to some serious concerns about environmentally hazardous effects of UCG. As a result of this test, CRIP technique was proposed for better control over location of reactions.

Pilot test at Pricetown was the only UCG trial in US that was conducted in a bituminous coal seam. Only 8-10 days of successful gasification was reported and the test was finally terminated because of low rates of gasification reactions. This was attributed to the agglomerating behaviour of the coal that sealed the walls and stopped the propagation of the cavity. This trial clearly showed the difficulties that may rise in the gasification of swelling coal seams.

Rawlins trials were conducted in inclined seams with dipping angle of 60°. These tests exhibited high thermal efficiency and low oxygen demand compared with horizontal seam (O₂/Coal: 0.2 compared to 0.4 for horizontal seams, Beath and Davis (2006)). Successful operation of this trial led to the proposal for building a UCG-to-Ammonia plant that was never built (Beath and Davis, 2006).

Objective of Centralia test was to investigate the effect of CRIP technique on the production gas and extent of coal recovery. This test showed that heating value of the gas may increase by 20% using CRIP technique. However, the roof collapsed into the cavity after intersecting with the overburden, which resulted a decline of 40% of the syngas heating value (Couch, 2009).

Trials at Rocky Mountains were performed to compare Linked Vertical Wells (LVW) and CRIP using the in-seam borehole. A mixture of steam and oxygen was used to produce a high-quality gas. Table 2-2 summarizes the data from these tests.

Table 2-2: Results of LVW and CRIP methods in Rocky Mountain trial (Modified from Beath and Davis, 2006)

Well Configuration	LVW	CRIP
Process Duration (Days)	65	90
Coal Consumption rate (Tons/Day)	70-100	70-200
Higher Heating Value of syngas (MJ/m ³)	8.5-10.34	9.24-11.85

CRIP operation was performed successfully and injection points were moved three times. New ignition points were started when there was a decline in heating value of the produce gas. CRIP technique resulted in 10-15% improvement in

syngas quality. A detailed operational procedure for CRIP operation was established as a result of this trial (Dennis, 2006).

Currently, two major UCG projects are ongoing in US, one in Wyoming and the other in Indiana. Site selection, characterization, and feasibility study for a UCG power plant have been completed for these projects. Possible CCS opportunities have also been identified in these projects (Gas Tech. Inc., 2007).

2.1.4 Australia

Australia has a considerable amount of low-rank coal in depth of 150 to 400 m that is suitable for UCG process. Three companies including Linc Energy Ltd., Cougar Energy Ltd. and Carbon Energy Ltd. are working toward commercialization of UCG in Australia and worldwide Pilot plants in these firms are close to the commercialization and appear to be most advanced compare to any other development around the world.

Linc Energy Ltd. conducted a series of trials from 1999 to 2002 at Chinchilla which is a Southern Australian coal seam. 9 pairs of injection/production vertical wells were drilled within a thick seam (10 m) at depth of 140 m in a sub-bituminous coal with 28% of ash. The operation continued below hydrostatic pressure of the surrounding to avoid unwanted mitigation of products and pollutants from cavity. There has been an extensive environmental assessment of the surrounding aquifers after shutdown and no pollution was reported. (Walker et al., 2001). 30 months of process operation at Chinchilla resulted in 95% resource

recovery of coal and steady gas production with a heating value of 4.5-5.7 MJ/m³.

The Linc Energy Ltd. has also built a demonstration plant for using UCG syngas in a Gas-to-Liquid (GTL) process. In 2007, they acquired an old UCG plant in Uzbekistan, and later at 2009, purchased Gas Tech Inc. in Wyoming, USA, that gives them control over 40,000 ha coal in Powder River Basin (Couch, 2009).

Carbon Energy Ltd. has cooperated with Commonwealth Scientific and Industrial Research Organization (CSIRO) to perform a pilot project at Bloodwood Creek, Australia. Initial stage of project consisted of 100 days of process at thick coal seam (10-12 m) with two parallel in-seam boreholes that intersect at the ignition point. Injection point can be retracted to provide fresh coal for the process. Successful operation of this project led to the development of a 5 MW power plant that uses UCG product gas for power generation. Next phases of the project will include a 25 and a 300 MW power plant (Carbon Energy website).

The Cougar Energy Ltd. started its UCG operations at Queensland at 2006. Vertical wells are with hydraulic fracturing and reverse combustion linking was used in thick coal seams. Also, Cougar Energy plans to conduct UCG at large brown coal deposits in Victoria, Australia. Recently, one of their pilot plants was shut down by Queensland government due to environmental concerns especially traces of benzene at surrounding potable water resources (Upstream news website).

2.1.5 Other Countries

2.1.5.1 South Africa

Along with Australia, South Africa is also working on commercial development of UCG process. Currently, there are two UCG developments in South Africa: one by Eskom and the other by Sasol. Eskom development is located close to a 4110 MW coal-fired power plant at Majuba. Eskom uses εUCG technology licensed from Ergo Exergy Inc.. Coal seam is 250-380 m deep and 1.8-4.5 m thick. A demonstration plant led to the production of 3-5000 m³/hr syngas which was used to generate 100 kWh electricity. The pilot project has been running steadily since 2007. They have announced their next development phase to be co-firing of UCG gas in the power plant boilers, design and operation of a 100-140 MW demonstration plant, and also design and commissioning of a commercial plant (Couch, 2009).

Sasol has recently started UCG tests in a sub-bituminous coal seam of 3 m thickness and 160 m depth. They have not released any information regarding their UCG operations (Sasol website).

2.1.5.2 Canada

Canada has approximately 10 billion tonnes of coal, which makes it the fifth largest coal reserves in the world. The Canadian UCG trials have been conducted in Alberta province that stores more than 40% of their coal. The first Canadian study was performed in 1977 at Forestburg (Pana, 2009). The main objective of

this test was to investigate the volume of the affected coal by UCG. Since 2009, Swan Hills Inc. has started a pilot UCG project using a single pair of wells in a 1400 m deep coal seam, makes it the deepest UCG test conducted till now. Great depth of the seam necessitated a high injection pressure of 14 MPa. The drilling costs would also be significantly higher compare to other cases. Fortunately, there is little risk of water contamination at this depth and higher pressure would contribute to the stability of the process. The initial pilot trials were claimed to be successful by the company and a combined-cycle power plant using UCG syngas has been proposed. The Laurus Energy Inc., another Canadian company that licensed a modified version of the LVW technology, is assessing Nova Scotia coal seams for possible UCG operation (Laurus Energy website).

2.1.5.3 China

Chinese studies have been mainly focused on the production of hydrogen-rich syngas from abandoned shallow coal mines (Depth <150 m). They followed a somehow different approach to achieve high concentrations of hydrogen. In this approach, they switched the injected gases between steam and oxygen in a cyclic manner. A long tunnel arrangement of wells was established as a result of these trials (Couch, 2009). It is shown that this method is capable of producing high quality syngas with a heating value of 12-14 MJ/m³.

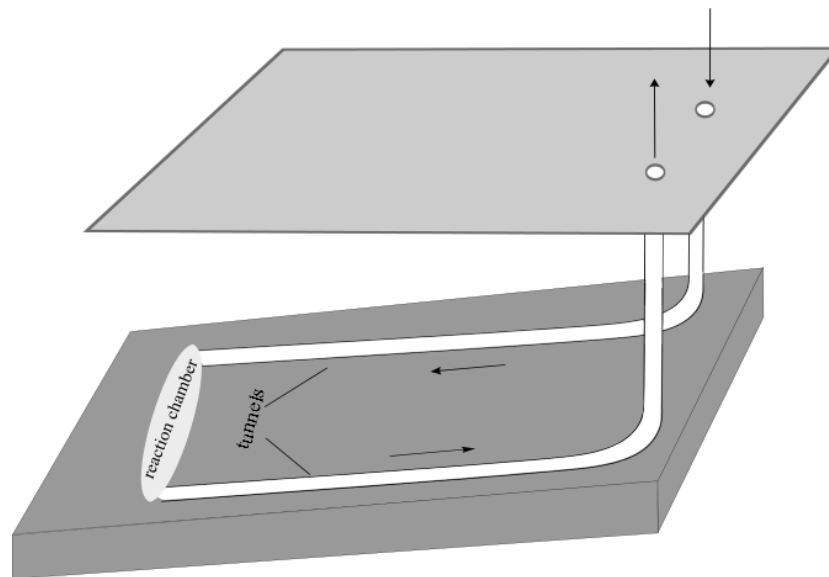


Figure 2-4: Long tunnel configuration in China (Couch (2009))

2.1.5.4 India

In recent years, India has shown a great interest in UCG. Khadse et al. (2007) published a detailed feasibility study of UCG with respect to Indian coal seams and concluded that UCG in India should target the low-rank coals at depth of 300-1200 m. Based on the knowledge developed worldwide by the previous trials, Gujarat, Rajasthan and Tamil Nadu were proposed to be best candidates for UCG operations.

2.2 Review of experiments related to UCG

2.2.1 Pilot-scale experiments

Along with the UCG field trials in US, LLNL performed an extensive pilot project in Tono Basin, Washington. It consisted of five medium-scale operations

based on WIDCO coal mines with a depth of 20-30 metres which were referred to as Large Block Experiments (LBK) and were designed to investigate cavity growth and shape in a medium-scale block (Hill and Thorsness, 1982). These experiments were also used to study the effect of steam/oxygen ratio and injection flow on the product gas composition and cavity growth. A mixture of propane/silane was used in these experiments to ignite the coal seam.

After finishing the experiments, approximately 59000 yards of overburden was removed to expose the cavities. Totally 15 cross-sections of cavities were studied in these experiment. Cavity was defined as a region in which coal has been thermally altered (Dried, pyrolysed or combusted) during the process. Based on this definition, the reported cavity shapes were attributed to the early stages of UCG process, since only a small amount of coal was consumed. The characteristics of the cavity shapes were found to be generally similar and cavity shape seems to be insensitive to the injection flow rate and composition. A schematic figure of the cavity cross section is shown in Figure 2-5. The findings of these series of well-defined experiments are summarized as follows:

- a. Cavity cross-sections are roughly oval.
- b. Height of the cavity is more than its width. Height/width is greatest at center of cavity and a significant void is formed on the top.
- c. Cavity bottom is bowl-shaped.
- d. Most of the cavity volume was filled with rubble with a mean diameter of 1cm. Ash and slag were found at the bottom of cavity, especially in the vicinity of the injection well.

- e. A void space appeared below the roof of the cavity with a thin layer of char at roof. Void space diminishes towards the upstream and downstream edges of the cavity.
- f. A thin annulus (10-14 cm) exists on the side and bottom of the cavity where a transition occur from coal to ash.

In all five tests, resistance of system to flow increased with time. Link blockage by the accumulation of coal particles, char and ash rubble was suggested as a possible reason.

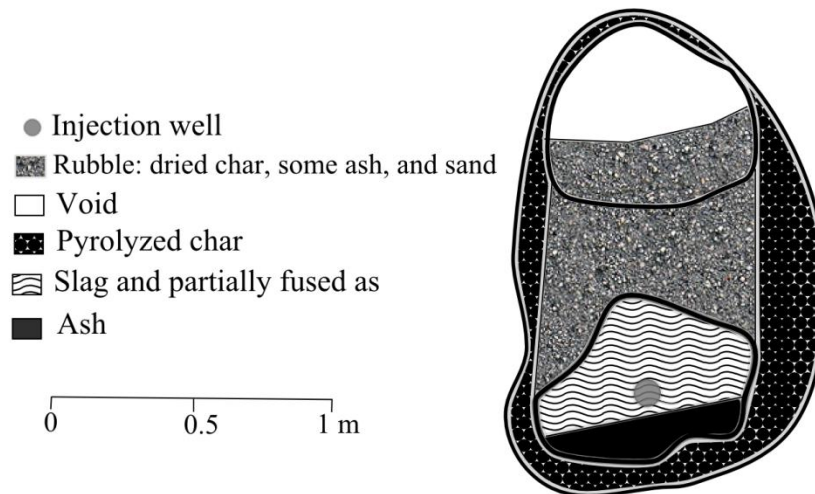


Figure 2-5: Typical cross-section of cavity in LBK experiments (Modified from Hill and Thorsness (1982))

China also conducted series of pilot projects to investigate the feasibility of UCG in steep abandoned coal mines (Yang et al., 2007, 2008). Researches adopted concept of two-phase gasification for to produce a hydrogen-rich syngas. They

have used Radon tracers to measure the size and velocity of the gasification front in the cavity. Velocity of the reaction front was found to be 0.204 m/day for two-phase gasification and 0.487 m/day for continuous air injection. Syngas heating value was calculated to be 11.00 MJ/m³ and 4.18 MJ/m³ for cyclic switch and continuous air injection, respectively, which shows a considerable increase by the former approach.

2.2.2 Coal block experiments

Due to differences between uncontrolled UCG cavity and controlled gasifiers atmosphere, the experimental results based on gasifier might not be directly applicable for UCG trials. Thus, relevant UCG experiments should be performed in different sizes coal blocks. Generalizing data from these experiments should still be done with extreme care since the whole process may not be properly represented in lab-scale experiments. Table 2-3 represents major laboratory studies on UCG.

Table 2-3: Major UCG experiments on coal blocks

Researchers	Coal Type	Dimensions of seam (Length*Width*Height)	Major Observations
Yeary and Riggs	Lignite- Sub-bituminous	25 cm * 5 cm * 25 cm	Lateral cavity growth
Park and Edgar	Lignite	9 cm* 2.5 cm	Lateral cavity growth
Daggupati et al.	Lignite	30-38 cm*20cm*25cm	Cavity growth and shape
Yang	High-volatile bituminous	6.8 m*0.25 m*1.1 m (68°) 7.5 m*2 m*1 m (65°)	Two-phase UCG in inclined abandoned coal mines
Prabu and Jaynati	Camphor, Wood, Lignite	24 cm*8-10 cm*10-12 cm	Cavity shape
Stanczyk et al.	Lignite- Hard Coal	2.5m*0.7m*0.7m	Two-phase UCG in lignite

Initial UCG experiments were conducted in US from 1975 to 1989 as a part of LLNL's research and development on UCG. These experiments were mostly concerned with lateral cavity growth and its mechanism. Yeary and Riggs (1987) calculated the growth for lignite and sub-bituminous coal. Recession rate of cavity sidewall has been shown to have a strong dependence on the flow rate and temperature of the injected gas. Lignite recession rate has been reported to be generally lower compared to sub-bituminous, while having a higher spalling rate (Yeary and Riggs, 1987). These observations are consistent with weak mechanical properties of lignite and high reactivity of sub-bituminous coal. Also, ash has remained intact in the sidewall for lignite coal, which can be attributed to higher ash content and stronger ash structure in lignite sample.

Numerous experiments were conducted under supervision of Park and Edgar at the University of Texas, Austin, on the combustion of consolidated lignite blocks. Their results (Park and Edgar, 1985, 1986) indicated that shrinkage of coal due to pyrolysis and drying plays an important role in cavity growth perpendicular to the bedding plane. The function of the gasification reactions was mostly to widen the developed cracks. Similar to LBK experiments, downward growth of cavity was limited by the presence of ash layer. The coal burn rate was shown to have a linear relationship with the oxygen content in the injected gas. Combustion front was observed to be located at char surface.

A series of experiments have been conducted in European Union, mostly Poland, to investigate the UCG behaviour in lignite coal seams. The main objective of this ongoing project is to study the effect of various parameters on hydrogen

concentration in syngas. Experiments were conducted in a 2.5*0.7*0.7 m coal block with a 10 cm link bored in the block. Three distinct stages for the UCG process were observable in all of these experiments: ignition, combustion, and gasification with steam. As reported by Stańczyk et al. (2010), only 1 hr of stable steam gasification was achieved in their first experiments and further gasification was impossible due to low temperature of the coal block and fast drop in temperature due to high moisture content of the experimented lignite (53%). To compensate this, the experiment was continued with high injection rates of oxygen. Replacing oxygen with air was unfeasible due to rapid decrease in temperature and termination of reactions (Stańczyk et al., 2011). Thus, oxygen-rich air was used and optimum oxygen/air ratios for lignite and hard coal UCG were proposed accordingly. Shorter ignition and combustion periods, higher temperatures and lower oxygen/air ratios were found to be attainable for hard coal due to its higher carbon content compared to lignite. In order to increase the extent of steam-gasification injection of pure oxygen was continued until high temperature of about 1100 to 1200 °C was reached in the reaction front (Stańczyk et al., 2012). Then, the inlet gas was switched to steam and the heating value of the product syngas increased to around 11.5 MJ/m³ as the injection gas is changed to steam. The inlet gas was changed to oxygen whenever temperature dropped to 700-800 °C in the reaction front. Instead of cutting through the block, the geo-radar technique which is based on the difference in dielectric properties was used in these experiments to identify various zones in the reacted coal. Three zones of free-space cavity, partially gasified lignite, and un-reacted dry coal were detected.

In the experiments performed in IIT Bombay, India, the cavity growth, cavity shape, and product gas composition with respect to various operating conditions were studied (Daggupati et al., 2010). These experiments were undertaken in a 30*20*25 cm lignite coal block. A 3 mm-diameter link was drilled to connect the injection and production wells. In first series of experiment, cavity growth and final shape of cavity is of major concern. Ignition has been initiated using LPG for 5 minutes and gas is switched to pure oxygen to combust the coal. Experiments were continued for a maximum of 8 hours with different injection rates and well distances. After termination of experiments, coal block was opened to expose and study the cavity shape. Similar to the field trials, the cavity was found to be teardrop shape and symmetric around the injection point. Cavity growth in upstream of injection point is less than width and height of the cavity. Common cavity temperature is around 950 to 1000 °C (Daggupati et al., 2010). Increasing flow rate resulted in linear increase in cavity volume in all dimensions. This increase is attributable to the effect of increased flow rate on decreasing the mass transfer limitation by removing the ash at coal surface. The forward and backward growth and volume of the cavity was found to decrease with increasing the distance between the wells, while cavity width and height increase. When the cavity reaches the production well, considerable bypass of oxygen terminates the process. Stable operation of similar experiments with a mixture of steam and oxygen found to be possible only by the injection of high temperature steam (600-700 °C) in a cyclic manner (Daggupati et al., 2011). Cavity shape was the same but larger in case of steam/oxygen injection. Coal particles of 1-2 cm in diameter

were also observed at the bottom of cavity in this case, while only ash was found in combustion. Therefore, it can be concluded that coal spalling is increased in gasification. The best syngas heating value was achieved by a steam/oxygen ratio of 2.5.

Prabu and Jaynati (2011) investigated the cavity formation in blocks of wood, coal, and camphor and compared the results. In all these cases, teardrop-shape cavities were formed with a more bulbous shape at lower flow rates.

One of the major challenges for applicability of UCG in steep coal seams is low heating value of produced gas. Yang et al. (2003) studied the UCG in a 6.8 m*0.25 m*1.1 m coal block with a dip angle of 65° with pure oxygen or mixture of oxygen and steam as injection gases. In the case of oxygen/steam mixture, the flow rate of the produced gases decreased after 41 hours and injecting the gases close to reaction front was required to sustain the process. An auxiliary well between injection and production well was used to supply the gas for the reaction front. A steam/oxygen ratio of 2 was found to give the best syngas heating value. Using multiple injection points increased the duration of the gasification stage, while shortened the oxidation phase.

Hongato et al. (2011) have studied two-stage gasification in lignite coal blocks and investigated effect of oxygen concentration in oxidation stage of process. They have concluded that higher concentrations of oxygen in inlet will shorten oxidation stage and extend the time of second stage.

2.3 Summary of trials and experiments

The, worldwide consumption of coal by UCG is listed below:

- a. Soviet Union: 1500 Ktonnes since 1950 (Cost: US\$10 billion)
- b. USA: 50 Ktonnes since 1970 (Cost: US\$ 300 million)
- c. Europe: less than 10 Ktonnes since 1950 (Cost: US\$1.. million)
- d. Australia: over 32 Ktonnes between 200-2002 (Cost: US\$5 million)

Australian operation in Chinchilla has been considered to be the most successful UCG operation in terms of performance and cost.

UCG trials have been performed over a 50 years period and in different geological settings and various coal ranks. The knowledge developed based on these activities can be used to select the appropriate seam and design an effective procedure. Following results can be concluded from the trials:

- Depth of the seam dictates the operating pressure which is one of the most important parameters in UCG process. Considerable leaks (Up to 20-30 percent of gas) have been reported in shallower seams.
- Lower rank coals were generally found to be more appropriate for UCG due probably to non-swelling property and high reactivity of these coals.
- The UCG cavity should be kept at pressures lower than hydrostatic pressure of the surrounding environment to ensure that products would not leak into surrounding seam and also a steady water influx which reduces the water consumption of the process is supplied.

- Heating value of the produced gas can be increased drastically, by using oxygen-enriched air.
- Syngases produced from CRIP technology generally have a higher heating value.

It should be noted that these experiments reviewed here have only studied short-term and early behaviour of UCG reactor and the results may or may not be representative of a long-term UCG operation.

2.4 Review of UCG Modeling Efforts

Since conducting UCG trials and data extraction is costly and difficult, modeling have been an important part of UCG study to predict the effect of various physical and operating parameters on the performance of the process. There has been a huge effort in modelling of the UCG process along with the trials. As mentioned earlier, UCG involves various mechanisms that happen simultaneously over a range of time and length scale and a full model that describes all of these the mechanisms would typically include a number of following sub-models:

- Injection/production linkage sub-model
- UCG reactor sub-model
- Ground water hydrology
- Ground subsidence model
- Surface facility models

Combining all these sub-models would theoretically give an exact description of the process; however building such a model is a cumbersome task. Therefore all previous models have focused on studying these aspects separately though several simplifying assumptions. In the following section, a brief overview of more important models would be given and their approach is discussed.

2.4.1 Packed bed models

Earliest models of UCG in literature include models that describe process as a packed bed reactor. These models would consider coal seam as a highly permeable porous media, in which bed properties change with reactions. At a work funded by LLNL, Winslow (1976) modelled the process in a 1D domain with reactions happening in char particles of 1cm size. In his model, the fluid flow is described by Darcy equation, in which permeability is set to change with extent of reactions. Permeability is assumed to reach a constant value for porosity larger than 0.25. Heat and mass transfer is modelled in gas and solid phase, with only convection terms in equations. Heat transfer between phases is described through experimental correlations. Results were generally in accordance with experiments; however a sensitivity analysis was not conducted to investigate effect of coal particle diameter, porosity and other parameters in the model.

Thorsness and Kang (1985) extended the packed model of Winslow (1976) by including homogenous reactions, diffusion effects, wall transport, and also by

modifying char reaction rates based on Ash Segregation (AS) and Shell Progressive (SP) reaction models.

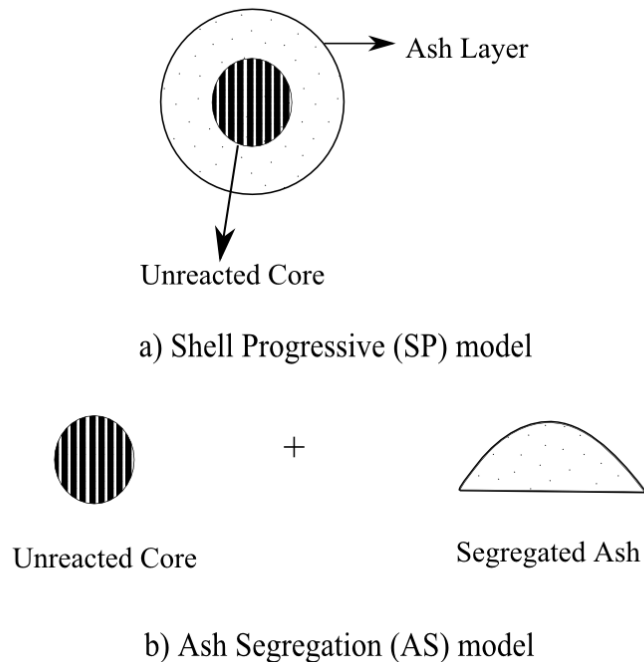


Figure 2-6: Different reaction regimes in packed-bed model

Recently, Khadse et al. (2006) developed a simple 1D model describing a UCG process at char-rubble zone in a cylinder with a diameter of 15 cm and length of 1 m filled with coal particles of 1 cm. They used a pseudo-steady approach, as there is a large difference between solid and gas characteristic time-scale. It is assumed that gas reaches steady state before any change happens in solid. Initial porosity of the bed is 0.2. Results were found to be only in a qualitative agreement with the experiments of Thorsness et al. (1985). Simplicity of the model has enabled authors to investigate effect of various parameters such as O_2 concentration, Steam/ O_2 ratio, and inlet pressure in their model. They found that increasing both

oxygen and steam fraction in feed increases the propagation rate of reaction front. Pressure was found to have no effect on the process. In all the cases, a steady flow rate and composition in outlet was reached after 5000 seconds of process.

Packed bed model has been validated with laboratory experiments; however extension of these models to field trials is infeasible, since other cavity growth mechanisms such as thermo-mechanical failure could not be incorporated into model. Also, as pointed out by Winslow (1976), this method requires fine grid at vicinity of reaction front that limits its applicability to field scale trials.

2.4.2 Coal Slab models

Some models have tried to describe the UCG coal seam as a coal slab. These models describe the process by governing the movement of various defined regions in a coal slab. These sections include: gas film, ash layer, char region, dried coal, and virgin coal. There is an influx of injection gases toward the cavity wall, while there is a counter flux of steam and pyrolysis products from the wall to the cavity. The general framework of these models is shown in Figure 2-7.

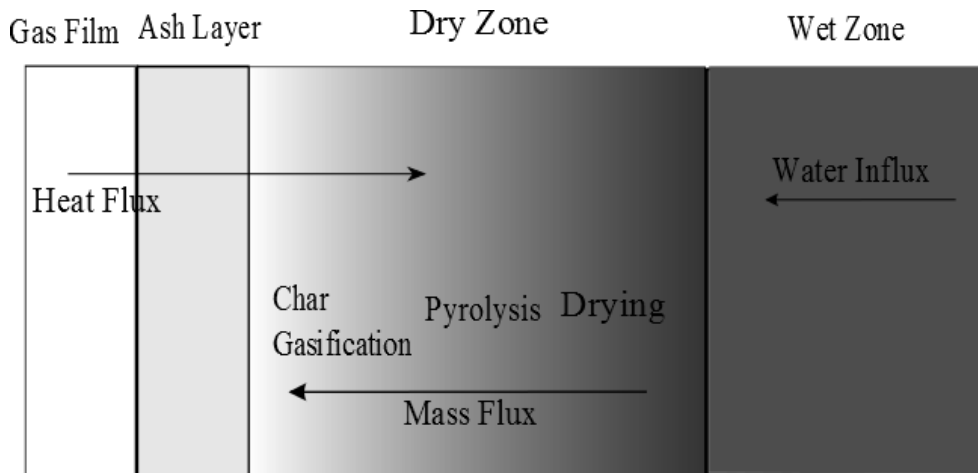


Figure 2-7: Scheme of Coal Block models (Modified from Perkins and Sahajwalla (2005))

Tsang (1980) was the first to use this approach and developed a 1D unsteady UCG model. Coal slab was divided into two regions: wet zone, and dry zone. In wet zone, heat conduction and liquid transfer is solved. It has been assumed that all drying happens in one moving point (Stefan model). In this model, movement of drying front is described using the following equation:

$$\varepsilon \rho_w \Delta H_v \frac{\partial \bar{x}}{\partial t} = (K_e \frac{\partial T}{\partial n})_+ - (K_e \frac{\partial T}{\partial n})_- \quad (\text{Eq. 1})$$

$$T = T_{vap} \quad @ \quad x = \bar{x}$$

where ΔH_v is heat of evaporation of water, \bar{x} is location of drying front, ε is porosity, and K_e is thermal conductivity of solid. This model neglects effects of steam convection and assumes drying process is dominated by conduction

In dry region, pseudo-steady state assumption was adopted to solve mass balance, heat transfer and gas-flux. Pyrolysis reactions are modeled as simultaneous

independent reactions with kinetic parameters obtained from works of Campbell (1978). Porosity and permeability is set to change with extent of reactions with correlations obtained from oil well acidization. The experimental results of Forrester (1979) were used for model validation. This model neglects the combustion and provides the heat by setting a high temperature at boundary.

Massaquoi and Riggs (1983) extended Tsnag's model by inclusion of combustion of char and volatiles at the boundary; while solving for a steady state case. They also included three zones outside the coal slab: ash zone with a constant thickness, gas film, and the bulk gas. The developed model was used to describe simultaneous combustion and drying of a wet Texas lignite coal. A criterion was defined for transition from heterogeneous to homogenous combustion. Their results indicated that homogenous combustion of coal happen at lower surface temperature than reported for char particles. Also, they have concluded that burn rate would decrease with increase in concentration of oxygen, when flame front is located in char face and increase when the flame is located in gas film.

Park and Edgar (1987) developed an unsteady 1D model with a moving burning front based on the work of Massaquoi and Riggs (1983) to describe lateral cavity growth in UCG (with flow perpendicular to coal surface). They also included coal shrinkage due to drying and pyrolysis, as well as steam and CO₂ gasification. They validated their results with the experimental data from Poon (1986). They have concluded that movement of the cavity wall due to shrinkage is only important in lab-scale processes and can be neglected in larger scale process. Their results indicate that cavity growth is controlled by the rate of oxygen

transfer to the cavity wall, when flame is located at char surface. If flame is in the gas film, CO_2 and steam gasification determine the cavity growth rate. When flame is at the char surface, overall process is controlled by mass transfer of the gas to the coal surface, therefore thickness of ash layer and oxygen concentration is important in determining the burn rate.

Abdel-Hadi and Hsu (1987) extended previous coal block models by developing pseudo-2D geometry with a moving burn front. A rectangular domain with length of 1.5 m and width of 1 m was used in their model. They have verified their model with the laboratory results reported by Thorsness et al. (1976). Perkins and Sahajwalla (2005, 2006) used FLUENT to describe UCG process in a 1D coal block and investigated the effect of various parameters on the process performance and cavity growth rate. This model is an extension of Tsang's study (Tsang, 1980) by including multi-component diffusion and random pore model to account for change of heterogeneous reaction rates with conversion. They have proposed that cavity growth occurs at reducing conditions, therefore only heterogeneous gasification reactions are solved and required heat is provided by defining a constant temperature at the char surface. They assumed that solid and gas phases are in thermal equilibrium and bulk gas has a fixed composition that is representative of the product gas. Various experiments of pyrolysis and drying of large coal particles are used for model verification and an excellent agreement were reported. However, applicability of the model is limited and cannot be used to predict performance of UCG process because of unphysical assumptions such as constant temperature at and fixed gas composition at boundary. Results of their

parametric study indicate that temperature of the coal surface, water influx and coal composition have the highest impact on cavity growth rate.

Recently, Nourizadeh et al. (2010) developed a 3D model using CMG-STARs, a reservoir simulation software based on finite-difference method, and discretized domain into coarse cubic meshes of 25-50 cm, typical to reservoir solvers. Their computational domain was similar to proposed field trials in Alberta (15 m* 5 m*9 m). They have introduced an arbitrary clay layer in the seam to investigate effect of inert layers on the process; however thermo-mechanical failure of this layer is not included in the model. They included chemical reactions and conduction/convection of heat and species in their model. Their results show a large degree of grid dependence. They did not present any validation for their model. They have extended their modelling to simulate CRIP with successive ignition points (Seifi et al., 2011). Again no validation or comparison with experimental data was reported.

2.4.3 Channel models

In this approach the UCG process is represented by an expanding channel when two distinct zones of rubble/char and open channel exist. Channel regime could dominate the process at later stages of process.

Figure 2-8 shows basic concept and physics behind this approach. “Air or oxygen flows down the central channel and is transported by turbulent flow to the boundary layer along the channel wall. The oxygen diffuses through the boundary

layer to the solid surface and reacts. The hot combustion gases diffuse back through the boundary layer to the channel” (Gunn and Krantz, 1987).

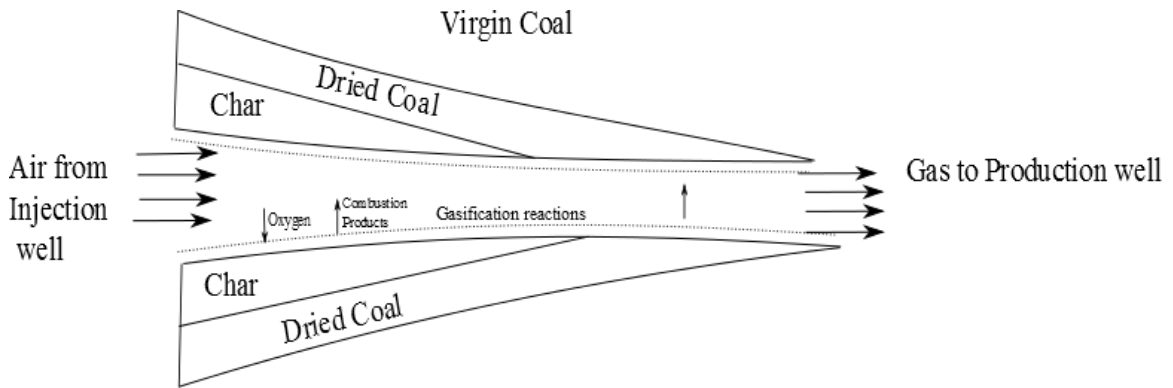


Figure 2-8: Reactions and Transport phenomena in channel model

Dinsmor et al. (1978) developed a steady-state 2D model to describe processes in an UCG channel. He assumed that gasifier is a cylindrical channel with reactions happening at walls. Mass transfer correlations were calculated based on turbulent flow in pipes. He concluded that operation of UCG in channel regime is undesirable and would lead to decrease in gas heating value due to bypass of oxygen. In his model, larger channels would lead to lower velocity and Reynolds number, which in turn decreases the mass-transfer by forced convection. Calculated growth rates were lower than earlier field trials and highlighted the importance of natural convection in channels, which increases mass and heat transfer.

Eddy and Shwartz (1983) were the first to consider the effect of natural convection in cavity growth. They developed a 2D model and described the evolution of cavity based on movement of cavity wall. All reactions are assumed

to happen at wall in a constant temperature. Flow is treated as an entrance region of pipe as the calculated entrance length is much larger than vertical well distance.

Entrance length is calculated using following equation:

$$\frac{L_e}{d} = 0.0288 \text{Re}_d \quad (\text{Eq. 2})$$

where L_e is entrance length and d is pipe diameter. Minimum Reynolds number in system is 4000 which results in entrance length of 48.8 m. The entrance length increases as the cavity diameter grows. They considered mixing of fresh flow and blast gas based on number of circulation in cavity. Transport of heat and species inside the cavity is governed by empirical correlations for turbulent transport phenomena in enclosures. Their results indicated that natural convection is several orders of magnitude higher than forced convection in these conditions. The model was able to reproduce results of Hanna II and Pricetown field trials qualitatively. Recently, Luo et al. (2009) at Linc Energy extended this model by including heat transfer and more coal wall reactions. Flow inside the cavity is solved based on irrotational fluid flow inside an enclosure, which describes velocity potential based on geometric features of the enclosure. The geometry is shown in Figure 2-9. Velocity potential is calculated using Eq. 3.

$$\phi = \frac{m^{\circ}}{4\pi r} + Ur \cos(\pi - \theta) \quad (\text{Eq. 3})$$

where U is velocity of uniform stream and m° is mass flow rate. Pressure distribution in cavity is found based on Bernouli's equation:

$$p + \frac{1}{2} \rho u^2 = p_\infty + \frac{1}{2} \rho U^2 \quad (\text{Eq. 4})$$

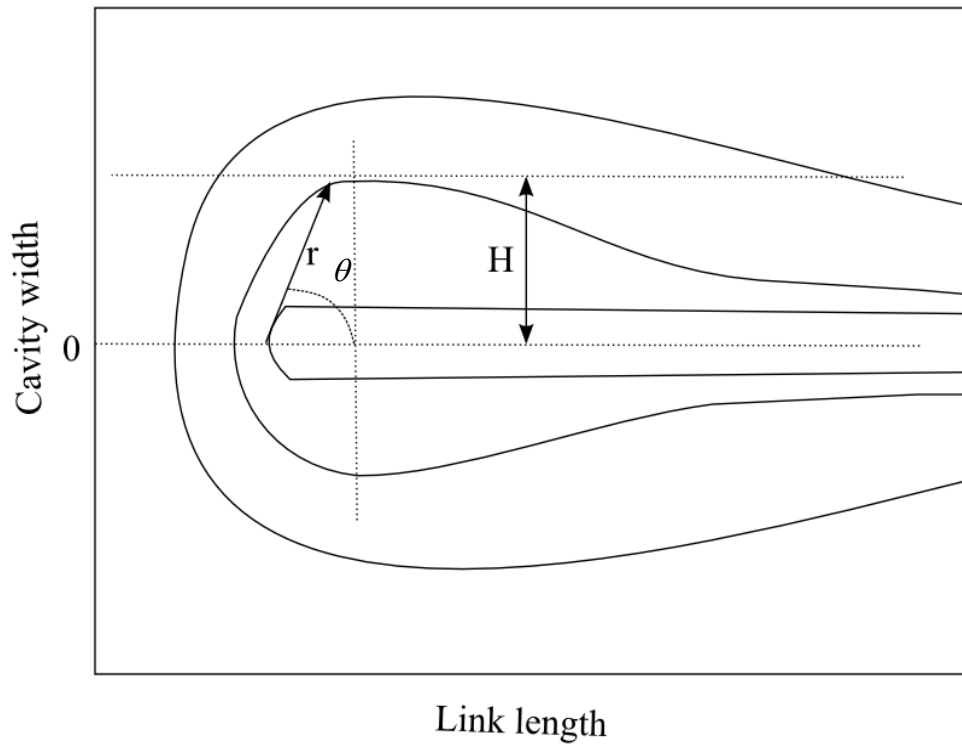


Figure 2-9: UCG cavity defined in the work of Luo et al. (2009)

They used FLUENT to predict the cavity shape in different times based on heterogeneous reaction rates at cavity wall. Their model has been validated with Chinchilla and Hanna II results (Luo et al., 2009). This model predicts a hemispherical shape for cavity geometry and is limited since heat and mass transfer characteristics of cavity are unknown. Also, coupling of this model with mechanical failure of coal would be cumbersome, since the accumulated rubble in cavity changes transport phenomena inside cavity.

At thin seams, failure of overburden has a major effect on the process. Such a failure would create open channels; as shown in Figure 1-7. Various models have been developed in Europe to describe the process in these channels.

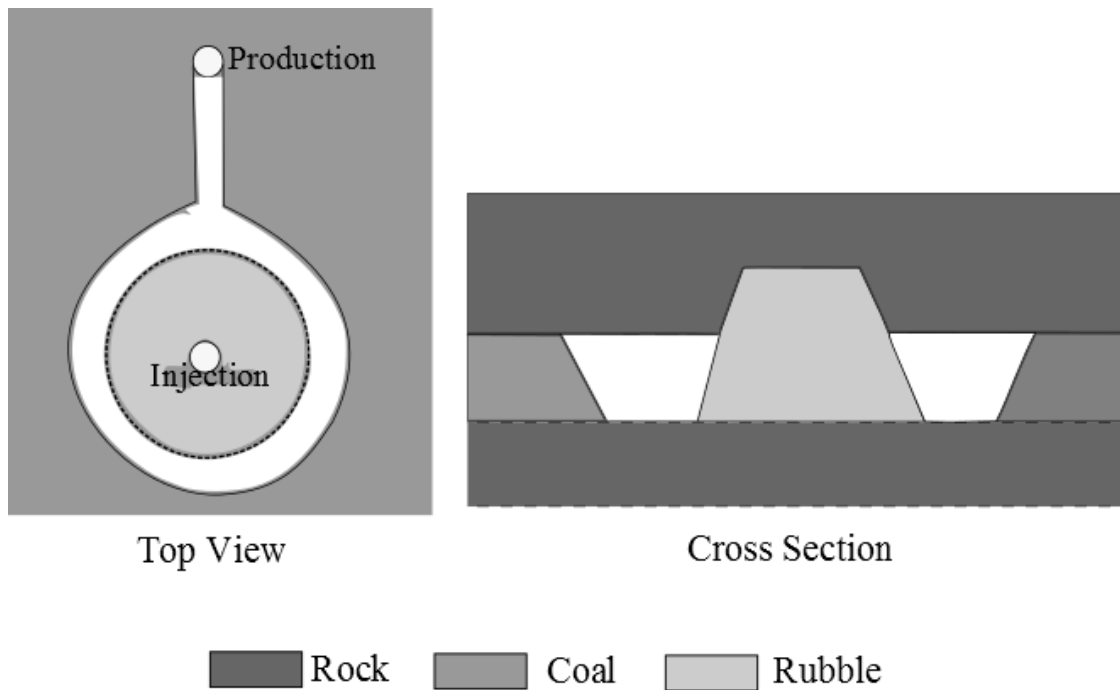


Figure 2-10: Channel formation in thin seams (Modified from Kuyper (1995))

As part of German-Belguian consortium for UCG trial in Thulin, Pirlot et al. (1993, 1994, and 1998) developed a 1D steady-state channel model with two distinct zones: high permeability rubble and low permeability rubble. Mass and heat transfer in channel is modelled by empirical correlations for packed bed. Reaction rates of gas phase are written for an ideal plug flow. Coal consumption rate is calculated on channel wall. Model has been extended to 2D to simulate the cavity growth and shape.

Batenburg et al. (1994) also developed a steady 2D model for UCG in open channels. Reaction rates were calculated based on resistances in the system including boundary layer, pore diffusion, surface phenomena and chemical kinetics. Heat transfer is modelled by radiation between walls of channel. They have also included the effect of natural convection due to temperature difference. Their results indicate that natural and forced convection transfer coefficients are in the same order of magnitude and both of them are important. Kuyper (1994, 1996) developed a 2D model to describe UCG process in a cross-section of an open channel. The $k - \varepsilon$ turbulence model was used to describe fluid flow due to large gradients of density and concentration in the channel. Radiation and convection were assumed to be the major heat transfer mechanisms in channel. Model results showed that oxygen is consumed far from coal wall by combustible gases. Double-diffusive natural convection in channel would cause periodic generation and collapse of CO₂ bubbles. Also, mass transfer is reported to be the controlling mechanism for reduction reactions at coal wall. They also studied the effect of CO₂ injection into the coal seam and reported that CO₂ injection have similar effect as adding steam; although to a lesser extent.

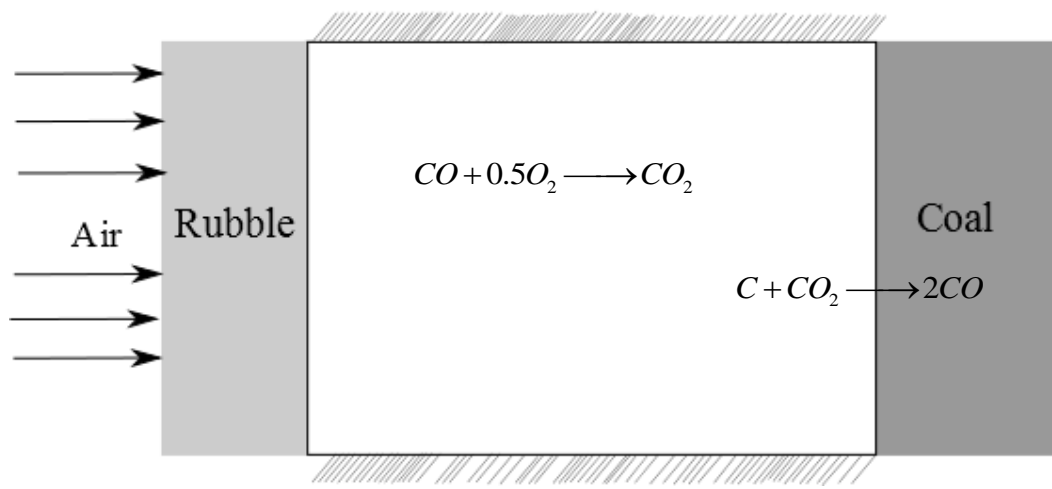


Figure 2-11: Channel geometry in Kuyper's model (1996)

Perkins and Sahajwalla (2007) expanded Kuyper's model by including an ash layer at lower part of the channel. The 2D axi-symmetric model is used to investigate natural convection along with relevant reactions in a partially filled cavity. Flow was assumed to be laminar in ash zone and turbulent in void space. Model is verified with Biezen's experiments (1996) for double-diffusive natural convection in a trapezoidal channel. They concluded that oxygen should be injected at the bottom of the channel, otherwise, valuable gasification products would be oxidized leading to low heating value of the production gas.

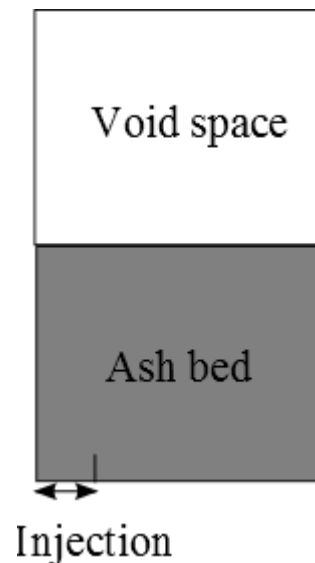


Figure 2-12: Channel geometry in Perkins and Sahajwalla (2007)

2.4.4 Other approaches for UCG modeling

2.4.4.1 Reactor models

Over the years, there have been a few studies in which UCG process is described as a series of ideal reactors. Such models can be used to predict product gas composition without considering complex phenomena occurring underground.

Change et al. (1985) used this approach to predict the resource recovery during UCG process. In this model, the domain is divided into cylindrical elements, where each element consists of two distinct zones: rubble and void. It is assumed that rubble zone acts as an ideal Plug Flow Reactor (PFR), while void space is assumed to be perfectly mixed modeled as a CSTR. Each element is allowed to change based on coal consumption. The fraction of flow in each zone is changed

to match results of the field trials. The spalling and water influx is calculated based on empirical correlations. Their modelling results highlight the importance of turbulence in field trials. Therefore, they have concluded that small laboratory scale experiments could not be scaled to field trials.

Some researchers have used the response of tracer material to characterize different zones in the underground cavity and track cavity growth. Based on the residence time of tracer elements, cavity is modeled as an arrangement of ideal reactors.

Debelle et al. (1992) used various chemical engineering reaction models to fit the quasi-exponential decay of tracer response. Various stages of the process such as reverse combustion linking and forward gasification were represented regression models. For gasification period, it was concluded that cavity offers a high level of back-mixing, resembling a well-mixed reactor with a small dead zone.

Thorsness (1980) performed tracer experiments in a UCG field test at the Hoe Creek trial (No. 3). Their goal was to investigate the extent of water influx and steam injection requirements. Tracer response curve was regressed with a series of CSTRs in two parallel paths. Pirard et al. (2000) used helium tracer in El Tremedal trial in Spain and concluded that cavity behaves almost like a small number of CSTRs in series with high level of back mixing.

Recently, Daggupati et al. (2011) used CFD to describe cavity as series of ideal reactors. Residence Time Distribution (RTD) of gases is calculated based on CFD results. This approach has been validated by laboratory-scale tracer experiments. Based on RTD and velocity distribution, cavity is simulated as a network of ideal

reactors. Proposed arrangement of reactors consists of a series of five CSTRs and a side stream of five small CSTRs, followed by a PFR. They have concluded that as the cavity size increases, cavity behaviour changes from PFR to CSTR. They have implemented their reactor model in ASPEN PLUS and compared the results with CFD predictions.

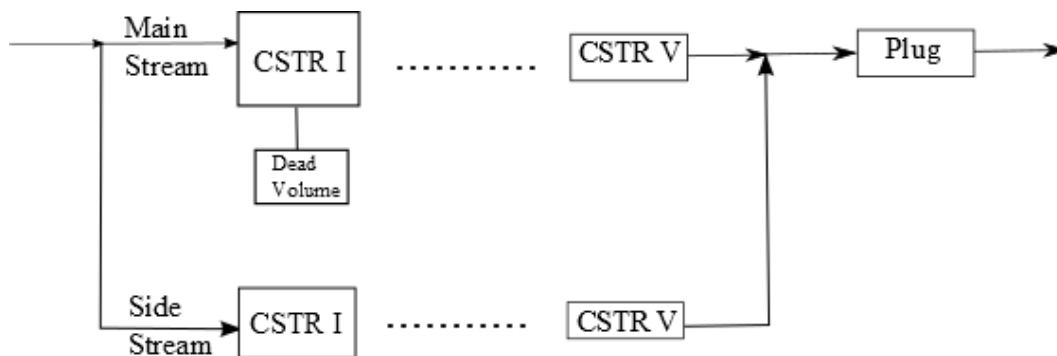


Figure 2-13: Proposed reactor arrangement for cavity in works of Daggupati et al. (2011)

2.4.4.2 Probabilistic simulation

In a unique approach to model UCG process, Batenburg and Bruining (1993) adapted probabilistic simulation to describe forward gasification phase in a 2D UCG geometry. The model uses stream function on the grid blocks. The derivative of the stream function along ash-char interface is interpreted as the possibility that interface is moving in a certain block. This model is very limited; as the temperature of the gases and composition are constant in each region.

At the same research group, Biezen et al. (1994) extended the concept of probabilistic simulation by including movement of several interfaces including ash-void, ash-coal, void-coal, and void-rock. The model consists of two modules: one module solves flow in the entire domain and the other selects a block of

coal/rock for gasification or spalling. A single streamline is selected randomly and based on the interface located on the streamline, relevant physical phenomena proceeds. For example, in void-coal interface surface gasification reactions occur and corresponding amount of ash is accumulated at the bottom of cavity. They later extended their model to simulate cavity evolution in a 3D domain (Biezen, 1995). This model is intended to simulate development of gasifier from early times (gasification in a permeable bed) to a developed stage (gasification in a channel). Application of this model is limited due to its complexity and unphysical assumptions such as constant temperature at each domain.

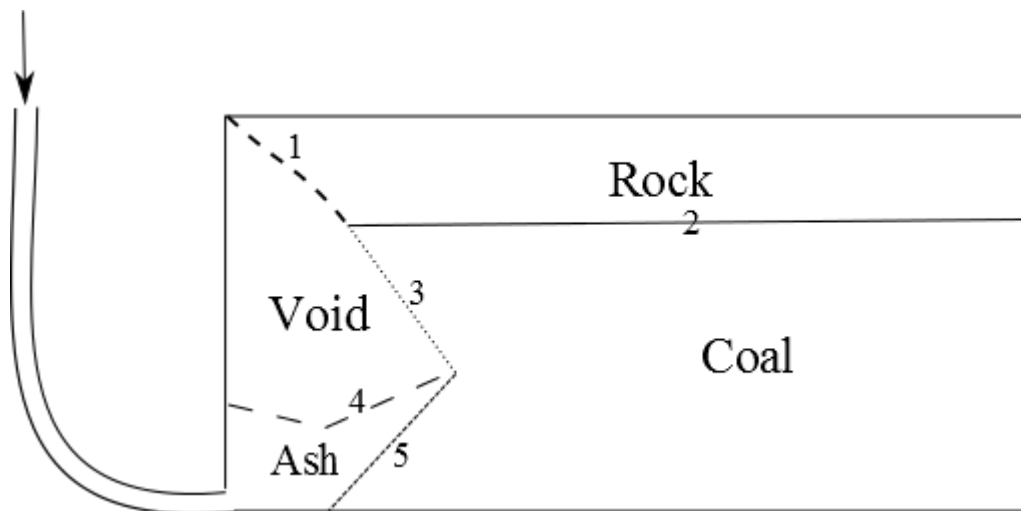


Figure 2-14: Probabilistic simulation of UCG process by possibility of movement of following interfaces: 1.Void-Rock; 2. Coal-Rock; 3. Void-Coal; 4.Void-Ash; 5. Ash-Void. (Biezen et al. (1995))

2.4.4.3 Process models

All of these reviewed modelling efforts so far have the deficiency of focusing on some aspect of the UCG process, while neglecting others. During UCG trials in

US, LLNL funded many modelling studies for UCG process. Several 1D models were developed and validated with certain series of data from field trials. These segregated models were later combined together to form the CAVISM process model that represents 15 years of continuous UCG research and development in US (Thorsness, 1989). The model is applicable for predicting lateral cavity growth of thick and shrinking coal seams in which oxygen is injected at the bottom of the coal seam. The model is based on some major assumptions such as: cavity is axisymmetric around injection; thermal radiation is the main heat transfer mechanism in well-mixed void space; cavity growth is dominated by thermo-mechanical failure of wall and a packed bed of char and rubble forms over a thin layer of ash. Various sub-models were incorporated into this model to quantify major phenomena in UCG such as water influx, flow dispersion through a rubble bed, sidewall growth of cavity due to reactions, and spalling of cavity roof into the domain. This model has reproduced results of some of field trials in US by tuning several parameters that are introduced in the model. Therefore, the model could not be used for predicting UCG behaviour in other seams, as these parameters are not known prior to process.

2.5 Summary of modeling review

Although several models with varying levels of complexity have been published over the past years, applicability of these models is limited to specific and isolated cases and the models could hardly be used to predict the performance of UCG

trials. Furthermore, most of these models are in 1D or 2D, while the field trials reveal a 3D non-regular cavity shape. Also, as mentioned earlier fluid flow is laminar in early stages of process while changes to turbulent in a developed channel. Turbulence would arise from natural convection due to temperature and concentration gradients in the cavity. Developed models are meant to simulate one of these stages and could not be used in these two conditions.

Chapter Three: Modeling

In this chapter, the mathematical formulation and governing equations of the developed UCG model are presented and discussed in detail. The details include cavity growth mechanisms, transfer properties in coal seam and effect of various parameters on process efficiency. As mentioned in Chapter 1, two models have been developed in this study using COMSOL Multiphysics and ANSYS FLUENT. A brief description of numerical methods, geometry, and model implementation in each software is discussed here. The model is applicable for shrinking coals, in which porosity and permeability increase upon heating. These types of coal are of prime interest for further application of the UCG process.

3.1 Governing equations

3.1.1 Conservation equations

The flow in porous medium is implemented in ANSYS FLUENT by adding a source term into the original Navier-Stokes equation. This equation is as follows:

$$\frac{\partial}{\partial t}(\rho_g \vec{v}) + \nabla \cdot (\rho_g \vec{v} \vec{v}) = \mu \nabla^2 \vec{v} - \nabla p + \rho_g \vec{g} - \left(\frac{\mu}{\alpha} \vec{v} + \frac{C_2}{2} \rho |\vec{v}| \vec{v} \right) \quad (\text{Eq. 5})$$

where ρ_s is density of fluid, \vec{v} is velocity vector, μ is viscosity of fluid and p is pressure.

The source term that is the last term on the right side of the equation includes two parts: a viscous loss (Darcy) $\frac{\mu}{\alpha} \vec{v}$, and an inertial loss term $(\frac{C_2}{2} \rho |\nu| \vec{v})$, where α is permeability and C_2 is the inertial resistance factor.

COMSOL Multiphysics uses the Brinkman model to describe flow in porous medium:

$$\left(\frac{\rho_g}{\phi} \right) \frac{\partial \vec{v}}{\partial t} + \left(\frac{\mu}{\alpha} + Q \right) \vec{v} = -\nabla p + \frac{\mu}{\phi} \nabla^2 \vec{v} + F \quad (\text{Eq. 6})$$

where Q is mass source term and F is volume force. This equation is similar to Navier-Stokes except that inertia term $(\nabla \cdot (\rho_g \vec{v} \vec{v}))$ has been neglected.

In the model, it has been assumed that gas and solids that form the porous media are in thermal equilibrium in each cell; therefore one energy equation is used to describe heat transport in system. The energy equation for the combination of gas and solids can be written as follow:

$$\frac{\partial}{\partial t} (\rho_g C_{p_g} \phi + \rho_s C_{p_s} (1-\phi)) + \rho_g C_{p_g} (\vec{v} \cdot \nabla T) = \nabla \cdot [k_{eff} \nabla T] + \sum rate_i \Delta H_i \quad (\text{Eq. 7})$$

where k_{eff} is effective conductivity of cell which is calculated based on volume percent of solid and gas in each cell, ϕ is porosity, ρ_s is solid density, C_{p_g} and k_g are specific heat and heat conductivity of gas, C_{p_s} and k_s are specific heat and heat conductivity of solid, and ΔH is heat of reaction.

Transport of species in gas phase is described by convection-diffusion equation.

$$\frac{\partial}{\partial t} (\rho_g Y_i \phi) + \rho_g (\vec{v} \cdot \nabla Y_i) = \nabla \cdot [\rho_g D_i \nabla Y_i] + \sum rate_i \quad (\text{Eq. 8})$$

where Y_i is mass fraction of species in gas phase and D_i is diffusion coefficient of gas species.

As described above, the fluid-phase equations are modified in FLUENT and COMSOL to account for the presence of solids and find the effective fluid flow in porous media. Thus, no real solid-phase is introduced to take part in fluid/solid reactions. As discussed in the previous chapters, the reactions between gas and solid coals are the major source of cavity growth in UCG. In order to implement the gas/solid reactions in FLUENT and COMSOL and at the same time take advantage of the built-in porous media formulation, a virtual solid phase is defined and a series of equations were written to track the consumption of solid components due to chemical reactions. These equations have the following general form:

$$\frac{\partial}{\partial t}(\rho_s Y_s (1-\phi)) = S_s \quad (\text{Eq. 9})$$

where Y_s is mass fraction of solid components and S_s is source term due to reactions in solid.

These equations are solved along with the continuity equation in gas phase written as follows:

$$\frac{\partial}{\partial t}(\rho_g \phi) = S_m \quad (\text{Eq. 10})$$

where S_m is gas-phase mass source due to chemical reactions.

In this model, the cavity development is tracked by the increase of porosity due to chemical reactions and thermal effects. Porosity increases as the solid components

are being consumed by reactions or species transfer from solid phase to gas phase due to thermal effects.

$$\frac{\partial}{\partial t}(\varphi) = S_{\varphi} \quad (\text{Eq. 11})$$

where S_{φ} is source term for porosity which is calculated based on reactions in coal.

It has been assumed that after consumption of coal, the ash content of the coal segregates and there is no ash layer between the gases and coal (Yoon et al., 1978). This assumption is verified by several experiments and field trials where ash was observed at the bottom of the cavity (Daggaputti et al., 2011; Hills and Thorsness, 1982).

The permeability of the porous media is a function of its porosity. Various empirical correlations are proposed to describe this relationship. In this study, Eq. 12 is used:

$$k = k_0 \exp(\sigma(\varphi - \varphi_0)) \quad (\text{Eq. 12})$$

where k_0 is initial permeability and φ_0 is initial porosity of coal. σ is calculated based on experiments. Thorsness et al. (1978) has measured this parameter for subbituminous coal and reported value of 12 for σ .

3.1.2 Chemical reactions

A combination of ten heterogeneous and homogeneous reactions, including drying, pyrolysis are considered to take place in the UCG model developed in this

work. The list of these reactions and corresponding heat released by these reactions are summarized in Table 3-1.

Table 3-1: Main reactions in a gasification process

No.	Reaction	Representation	Heat of reaction (kJ/mol)
1	Drying	Coal \rightarrow Dry Coal+ H ₂ O	+40
2	Pyrolysis	Dry Coal \rightarrow Char + Volatiles	0
3	Coal combustion	C + O ₂ \rightarrow CO ₂	-393
4	CO ₂ gasification	C + CO ₂ \rightarrow 2CO	+172
5	Steam gasification	C + H ₂ O \rightarrow CO+ H ₂	+131
6	Methanation	C + 2 H ₂ \rightarrow CH ₄	-75
7	Water-gas shift	CO + H ₂ O \leftrightarrow CO ₂ + H ₂	-41
8	Gas phase oxidations	CO + 0.5O ₂ \rightarrow CO ₂	-111
		H ₂ + 0.5O ₂ \rightarrow H ₂ O	-242
		CH ₄ + 2O ₂ \rightarrow CO ₂ +2H ₂ O	-802

Reactions involved in UCG are not fundamentally different from the reactions of coal and char in the surface gasifiers. In gasification reactions, combustion of coal and volatiles provide the necessary heat for endothermic gasification reactions. Water-gas shift reaction would determine the ratio of carbon monoxide and hydrogen in syngas.

3.1.2.1 Drying

The moisture content of coal varies between 5-40 wt% in different coal ranks. This moisture can be divided into three categories based on how they are resided in coal's structure as unbound, weakly-bound, and chemically-bound. The unbound moisture is released at evaporation temperature of water; while weakly-bound water is released at higher temperatures as it has been absorbed in

capillaries. The chemically-bound moisture would release at much higher temperatures around 200-400 °C (Lyckowski and Chao, 1984). Most of the previous UCG models assumed that drying occurs at a front layer in which temperature is kept constant equal to the water evaporation temperature. Thus, the release of weakly-bound and chemically-bound moistures at higher temperatures is not correctly governed in these models. In the present model, drying is assumed to be governed by an Arrhenius-type reaction expression:

$$-\frac{dM}{dt} = -rate_{drying} = k(M^* - M) \quad (\text{Eq. 13})$$

where M is moisture content of coal at any moment and M^* is moisture content of coal from proximate analysis.

3.1.2.2 Pyrolysis

Upon further heating of coal, at the coal pyrolysis reactions begin at temperatures around 350-400 °C (Anthony and Howard, 1976). Coal is an organic polymer complex with different atoms in structure that decomposes with heating. As the temperature increases, weaker bonds rupture releasing volatile matter. The releasing of the volatiles occurs in the following order: chemically bound H₂O, CO₂, CO, CH₄, tars and H₂ (Perkins, 2005). Due to high residence time of gas and high pressure in underground coal gasification process, tar would likely undergo secondary reactions such as cracking and tar yield would be lower compared to surface gasifiers (Perkins and Sahajwalla, 2005). Therefore, in this model tar is

assumed to break down to smaller molecules. Pyrolysis of coal is represented by the following reaction:



Stoichiometric coefficients of this reaction in this study are based on the work of Suuberg et al. (1978). The overall pyrolysis reaction is calculated using a first-order reaction rate as follows:

$$-\frac{dVM}{dt} = -rate_{\text{pyrolysis}} = k(\text{VM}^* - \text{VM}) \quad (\text{Eq. 15})$$

where VM is volatile matter content at any moment and VM^* is effective volatile matter content of coal. VM^* is assumed to be the same as volatile matter from proximate analysis. Some models use the same reaction expression with different reaction constants to describe evolution of different species during pyrolysis (Campbell, 1977). In this model, release of all species is represented by one activation energy and pre-exponential factor (Syamlal, 1992).

3.1.2.3 Heterogeneous reactions (Combustion and Gasification)

After pyrolysis reaction, coal has been converted to a highly porous carbonaceous solid which is called char. Char would participate in heterogeneous reactions with different components of the gas phase. The rate constant of these reactions are given in Table 3-2.

Table 3-2: Approximate relative rates of heterogeneous reactions of coal (800 C, 0.1 atm)

Reaction	Rate constant (1/s)
$C + O_2 \rightarrow CO_2$	1E+5
$C + H_2O \rightarrow CO + H_2$	3
$C + CO_2 \rightarrow 2CO$	1
$C + 2 H_2 \rightarrow CH_4$	3E-3

A general kinetic expression for gasification reactions can be written in following form:

$$\frac{dX}{dt} = f(P_i, T_p)g(X) \quad (\text{Eq. 16})$$

where $f(P_i, T_p)$ is intrinsic surface reaction rate as a function of partial pressure and particle temperature and $g(X)$ describes evolution of reactive sites as a function of char conversion (X). Bhatia and Perlmutter (1980; 1981) developed a random-pore model based on nucleation of crystals to characterize development of pores and changes in surface area with conversion of char.

$$g(X) = \frac{S_0}{1 - \phi_0} (1 - X) \sqrt{1 - \psi \ln(1 - X)} \quad (\text{Eq. 17})$$

where ψ is related to structure of initial pores. Figure 3-1 shows $g(x)/S_0$ for different values of ψ . Surface area increases at lower conversion of char and decreases at higher conversion, as observed in experiments (Bhatia and Perlmutter (1980)). Therefore ψ is set to 5 in this study to represent the changes of surface during gasification (Liu et al., 2000).

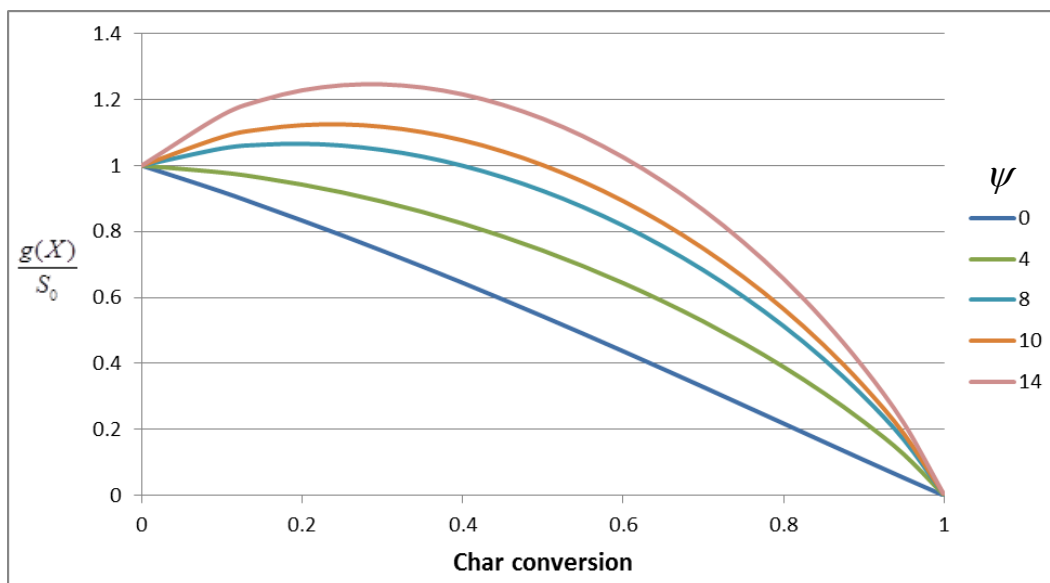


Figure 3-1: Surface area vs. conversion for different values of ψ

Eq. 14 is used to describe temperature and pressure dependence of reactions based on works of Roberts and Harris (2000) and Tomita et al. (1977). These rates are shown to be valid for pressures up to 30 atm.

$$f(P_i, T) = k \exp\left(\frac{-E}{RT}\right) P_i^n \quad (\text{Eq. 18})$$

A simpler rate expression is used for studies at low pressure based on works of Ye et al. (1998) and Di Blasi et al. (1999).

$$\frac{dX}{dt} = k \exp\left(-\frac{E}{RT}\right) (1-X) P_i^n \quad (\text{Eq. 19})$$

This rate expression indicates a monotonous decrease in available surface area, the same as $\psi = 0$ in Eq. 13. Table 3-3 summarizes the reaction parameters as used in this model.

Table 3-3: Kinetic constants for reactions in coal

Reaction	E (kJ/mol)	k	n	Reference
Drying	78.24	5.1e+4	NA	Syamlal (1992)
Pyrolysis	78.24	5.1e+4	NA	Syamlal (1992)
Combustion	100.4	3.07e+5	1	Di Blasi et al.(1999)
CO ₂ gasification	91	22.11	0	Ye et al.(1998)
H ₂ O gasification	131	4.35e+3	0	Ye et al.(1998)
HP CO ₂ gasification ¹	211	3	0.5	Roberts and Harris (2000)
HP H ₂ O gasification ¹	231	30	0.5	Roberts and Harris (2000)
HP H ₂ gasification ¹	150	2.8e-4	1	Tomita (1977)

1. These reaction rates are used for studies at high pressure and are based on Eqs. 10, 11, and 12.

3.1.2.4 Homogenous reactions

Most of the experiments on coal blocks have indicated that oxygen is consumed by homogeneous combustion of the pyrolysis and gasification products in gas phase (Massaquoi and Riggs, 1983). Water-gas shift reaction is another important gas-phase reaction that would determine the ratio of CO/H₂ in the syngas. Reaction expressions and their kinetics are summarized in Table 3.4.

Table 3-4: Rate expressions and kinetic data for homogenous reactions

Reaction	Rate expression	A	E (kJ/mol)	Reference
CO combustion	$k[CO][O_2]^{0.25}$	2.24E+12	107	FLUENT database
H ₂ combustion	$k[H_2][O_2]$	9.87E+8	31	FLUENT database
CH ₄ combustion	$k[CH_4]^{0.2}[O_2]^{1.3}$	2.12E+11	203	FLUENT database
Water-gas shift reaction	$k[CO][H_2O]$	2.78E+6	12.5	Biba et al.(1978)

$$k = A \exp\left(-\frac{E}{RT}\right)$$

3.2 Implementation in COMSOL Multiphysics

At first year of this study a 2D model was developed in COMSOL to describe UCG process in commercial scale. The geometry was based on CRIP trial in El-Tremedal, Spain (Couch, 2009).

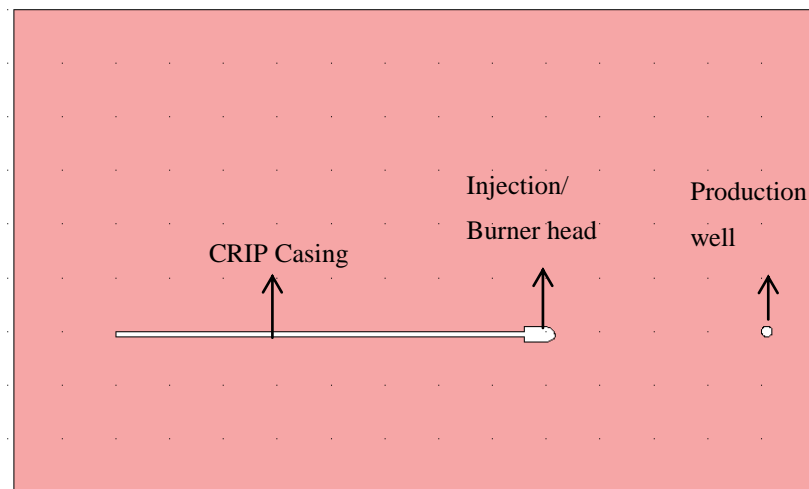


Figure 3-2: CRIP configuration for modeling UCG in COMOSL

As mentioned earlier, three variables are introduced to track solid components, as COMSOL does not allow the solid part of porous media to participate in reactions. General equation has the following form:

$$\int_{\Omega} \text{weak } \partial v = 0 \quad (\text{Eq. 20})$$

Weak term is replaced with proper expressions to represent solid consumption due to reactions based on Eq. 5.

3.2.1 Numerical methods

COMSOL uses the finite-element method to solve set of equations. It converts the equation into weak form, which is derived by multiplying the PDE with a test function and then integrating it over the domain. A generalized weak form equation for a diffusion equation of a scalar is as follows:

$$\underbrace{\int_{\Omega} \mathcal{G} \frac{\partial \phi}{\partial t} d\Omega}_{\text{Time dependent term}} = \underbrace{\int_{\partial\Omega} \mathcal{G} n \cdot (\Gamma \nabla \phi) d\partial\Omega}_{\text{Boundar Fluxes}} - \underbrace{\int_{\Omega} \Gamma \nabla \mathcal{G} \nabla \phi d\Omega}_{\text{Diffusive flux}} + \underbrace{\int_{\Omega} \mathcal{G} R d\Omega}_{\text{Source term}} \quad (\text{Eq. 21})$$

where \mathcal{G} is test/shape function, a function by which solution is approximated in each grid in finite element analysis. The solution is described as:

$$\phi = \sum \phi_i \mathcal{G}_i \quad (\text{Eq. 22})$$

where ϕ_i is scalar values at node point i and \mathcal{G}_i is shape function at the element consisting node i . In this study, quadratic Lagrange function was used as shape function, as recommended by COMSOL.

Time-Dependent Segregated Solver is used in which variables are split into sub-steps. Variables are grouped and divided into four sub-steps. These groups include: velocity components and pressure; Temperature; Concentration of gas species and Concentration of solid species. This technique would accelerate convergence, as in each subsection only the relevant equation is linearized and solved.

Numerical solutions of transport equations would exhibit numerical instabilities when Peclet number is larger than 1.

$$Pe = \frac{\|\vec{v}\| h}{2\Gamma} \quad (\text{Eq. 23})$$

where h is the mesh element size. Peclet number indicates relative importance of convection to diffusion. As indicated in Eq. 23, Peclet number could be reduced by refining a mesh; however, this method is not practical as it requires a very dense mesh. COMSOL has implemented various stabilization techniques that add an artificial diffusion to damp the instability. In this study, isotropic diffusion is used as stabilization method, in which following term is added to transport equation:

$$\Gamma_{artificial} = \delta_{id} h \|\vec{v}\| \quad (\text{Eq. 24})$$

where δ_{id} is a tuning parameter set to 0.5. The new Peclet number is expressed as following:

$$Pe = \frac{h \|\vec{v}\|}{2(\Gamma + \Gamma_{artificial})} = \frac{h \|\vec{v}\|}{2\Gamma + h \|\vec{v}\|} \quad (\text{Eq. 25})$$

as $\|\vec{v}\|$ approaches infinity, Pe approaches 1, but never exceeds it, which makes the numerical solution stable.

The geometry should be discretized into grids prior to solution. In this study, triangular mesh is used for mesh generation with minimum quality of 0.75.

3.3 Implementation in ANSYS FLUENT

Figure 3-3 shows the developed geometry for modelling the UCG process in ANSYS. This geometry is based on the work of Daggupati et al. (2010) and includes following zones: injection pipe, burner, link, production pipe, and coal block.

Since the process is the same on left and right side of injection, a symmetry plane has been introduced at $z=0$ to reduce the computational expenses. This assumption is verified by results of Hanna field trials (Yeary, 1989).

In this geometry, burner provides the essential heat for ignition of coal at start of the process and link provides the permeable path between the injection and production wells.

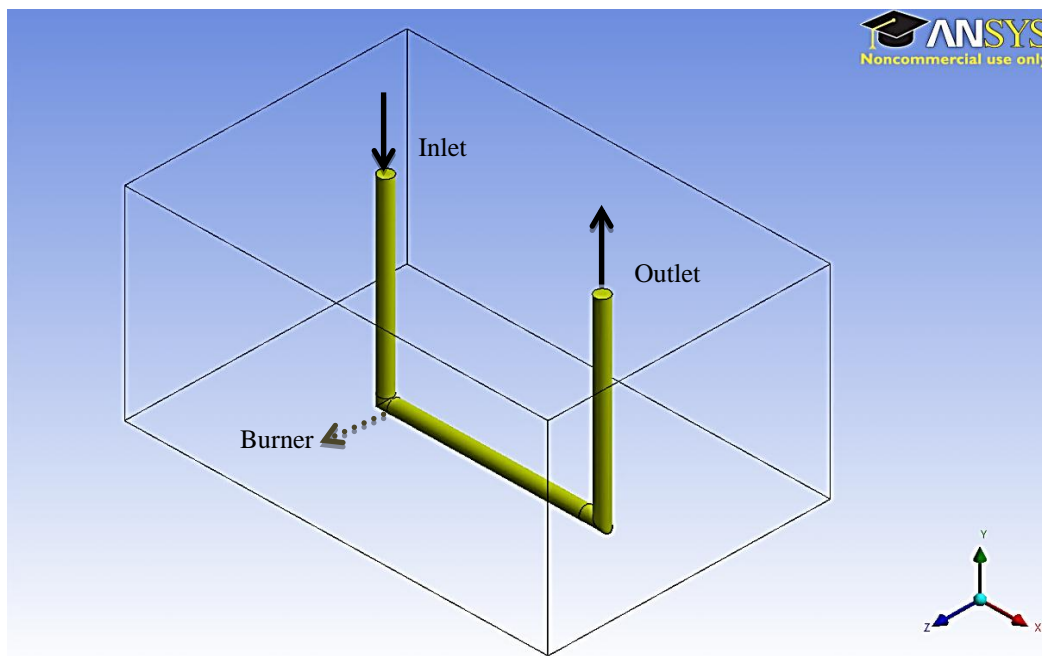


Figure 3-3: Geometry for UCG modelling in FLUENT

Coal block is considered to be a porous medium with a defined initial porosity and permeability. As discussed earlier, the porous media model in FLUENT does not allow for solid to participate in reactions, therefore User-Defined Scalars (UDS) are defined to track solid components. Three scalar equations calculate the consumption of moisture, volatile matter and fixed carbon based on reactions described in section 3.1.2. A general form of UDS equations in FLUENT is as follows:

$$\frac{\partial}{\partial t}(\rho_g \phi \gamma) + \frac{\partial}{\partial x_i}(\rho_g v_i \phi - \Gamma \frac{\partial \phi}{\partial x_i}) = S_\phi \quad (\text{Eq. 26})$$

where ϕ is User-Defined Scalar. Γ is diffusion coefficient, γ is porosity, and S_ϕ is the source term. .

Eq. 26 is modified to represent the conservation of solid components as described by Eq. 5. Corresponding expressions are defined to describe heat and species mass sources due to these reactions. These source terms are written as User-Defined Functions (UDF) and are incorporated into the model. The program codes for different UDFs used in this study are presented in Appendix A.

A number of 5 User-Defined Memories (UDM) have also been defined to track the dynamic distribution and occurrence of different reactions in the process. UDMs for post-processing purposes.

3.3.1 Numerical methods

ANSYS FLUENT 13.0 is used to solve the set of equations discussed earlier. FLUENT is based on the finite volume approach in which the integral form of the discretized equations is solved in each computational cell. General form of the discretized equation for an arbitrary control volume is as follows (ANSYS FLUENT theory guide, 2010):

$$\int_V \frac{\partial}{\partial t} (\rho\phi) dV + \oint \rho\phi\vec{v} \cdot d\vec{A} = \oint \Gamma_\phi \nabla\phi \cdot d\vec{A} + \int_V S_\phi dV \quad (\text{Eq. 27})$$

where ϕ is scalar variable. Γ_ϕ is diffusion coefficient, and \vec{A} is surface area vector.

Equation 27 is linearized and solved using Gauss-Seidel linear equation solver implemented in FLUENT.

3.3.2 Spatial discretization

Solution of Eq. 27 results in values of scalar at each computational node. To calculate convection terms in Eq. 27, scalar values are required at cell surfaces which must be interpolated from cell-centroid values (nodes). Various interpolation schemes are available in FLUENT including: First-Order Upwind, Second-Order Upwind, Power-Law, Quadratic Upwind Interpolation (QUICK), and Third-Order MUSCL.

First-Order Upwinding assumes the value of the variable throughout the cell and at the face to be the same as the centroid value. This method would lead to faster convergence; however, introduces false numerical diffusion (Patankar, 1980).

Second-Order Upwinding calculates face values based on multi-dimensional expansion of Taylor series around the cell-centroid, using following expression:

$$\phi_f = \phi + \nabla \phi \cdot \vec{r} \quad (\text{Eq. 28})$$

Higher order interpolation schemes are believed to minimize false numerical diffusion (Patankar, 1980).

3.3.3 Pressure-velocity coupling

In incompressible flow formulation, continuity equation is a constraint on velocity field and not a dynamic equation. In other words, there are four equations for four independent variables: u, v, w, and p, but no independent transport equation for pressure. To change the pressure dynamically, pressure field could be constructed based on velocity field using different coupling methods. Constructed pressure must conserve the continuity equation. ANSYS FLUENT provides five pressure-velocity coupling methods: SIMPLE, SIMPLEC, PISO, Coupled, and Fractional Step (FSM). SIMPLE acronym for Semi-Implicit for Pressure-Linkage Equations is the most popular pressure-velocity coupling and widely used in different cases due to its simplicity and robustness. In this method, an iterative procedure is used to link pressure and velocity. The algorithm starts with an initial guess for variables in the system. Momentum equations are solved and pressure is corrected using a pressure correction equation. In the next step, all the other transport equations are solved and residuals are checked. If the solution is not converged, the current results would be used as an initial guess for the next iteration. This

loop will continue until a converged solution is obtained. SIMPLEC and PISO also use the same algorithm with modified pressure correction equation for special cases.

3.3.4 Under-relaxation factor

The following equation is used during each iteration to calculate new value of the variable in each cell based on its old value.

$$\phi = \phi_{old} + \alpha \Delta \phi \quad (\text{Eq. 29})$$

α is the under-relaxation factor and its value control the change of variables in each iteration. Due to the nonlinearity of the equations, it is essential to reduce the change of variables in each time step; otherwise the solution becomes unstable and diverges. There is no recommended value for α and the optimum value is found based on experience.

3.3.5 Convergence criteria

For any transport equation, the discretized form of the equation has the following form:

$$a_p \phi_p = \sum a_{nb} \phi_{nb} + b_p \quad (\text{Eq. 30})$$

where a_p and a_{nb} are central and neighbouring coefficients respectively. Imbalance of this equation is called residual and can be expressed as

$$R_p = \sum a_{nb} \phi_{nb} + b_p - a_p \phi_p \quad (\text{Eq. 31})$$

This equation will be scaled based on summation of residual in all computational cells. Scaled residuals are used in CFD studies to monitor the behaviour of numerical solution. . Usually, when the scaled residuals drop by three orders of magnitude, a qualitative convergence has been obtained. For species and energy equations stricter criteria is required to achieve convergence. In this study, default values of tolerance (1E-3) are used for pressure and velocity components, while tolerance of gas and solid components are set to 1E-5, and energy equation to 1E-6. Similar values have been used by others (Tu et al., 2008).

3.3.6 Meshing

Prior to solving the model, geometry is discretized into grids. Since finite-volume is based on control volumes and not the grid intersection, any type of grid can be used. Using unstructured cells provides greater flexibility for resolving complex features of the geometry. In this model, ANSYS Meshing software is used to generate required grids. Meshing parameters are changed to generate a high quality mesh, with average skewness of 0.24 and maximum of 0.86. Based on ANSYS guidelines, a mesh with these properties are categorized as a high quality grid (ANSYS meshing tutorial, 2010). A detailed study on the effect of grid size on solution and optimum mesh size is presented in next section.

Chapter Four: Results and Discussion

This chapter is divided into two parts. At first, a brief discussion is presented on the assumptions and results of developed model in COMSOL Multiphysics. The shortcomings of this model are discussed in detail. The justification of transferring to ANSYS FLUENT for further development of the model is presented afterwards. In the next part, a detailed study of developed model in FLUENT is presented and a sensitivity analysis is performed to investigate effect of various parameters on process performance.

4.1 Results of developed model in COMSOL

In the developed model in COMSOL, it has been assumed that most of the cavity growth is occurring in the absence of oxygen (Perkins and Sahajwalla, 2005). Oxygen has been depleted by combusting pyrolysis gases. Therefore, essential heat source for the initiation of the endothermic reactions in the system is provided by setting a high temperature at burner head. This temperature should be regarded as one of modeling parameters and its effect on results should be investigated. Also, gas composition is fixed at boundary representing produced syngas. These assumptions are justified by experimental observations as described in Chapter 2. The experimental results of Forrester (1979) in which a cylinder coal block was heated from walls with pre-defined heating rate between 0.05-3 K/s, is used to validate the predictions of the present model. The proximate

analysis of the coal used in their experiments is shown in Table 4-2. Table 4-1 summarizes the model parameters and their values used here:

Table 4-1: Model parameters used for simulation of experiments of Forrester (1979)

Parameter Name	Value
Solid density	1230 kg/m ³
Initial porosity	0.05
Operating pressure	1 atm
Initial temperature	300 K

Table 4-2: Proximate analysis of coal used in experiments of Forrester (1979)

	wt %
Moisture	21.7
Volatile matter	35.23
Fixed carbon	36.89
Ash	6.18

Figure 4-1 shows results of model, as reproduced from Perkins and Sahajwalla (2005).

Developed model was used to simulate UCG process in geometry shown in Figure 3-2. The specifications of the simulated geometry are provided in Table 4-3. These dimensions represent the proposed CRIP pilot project for Alberta coal reservoirs (Nourozieh et al., 2010). Targeted coal in this pilot is subbituminous with following proximate analysis:

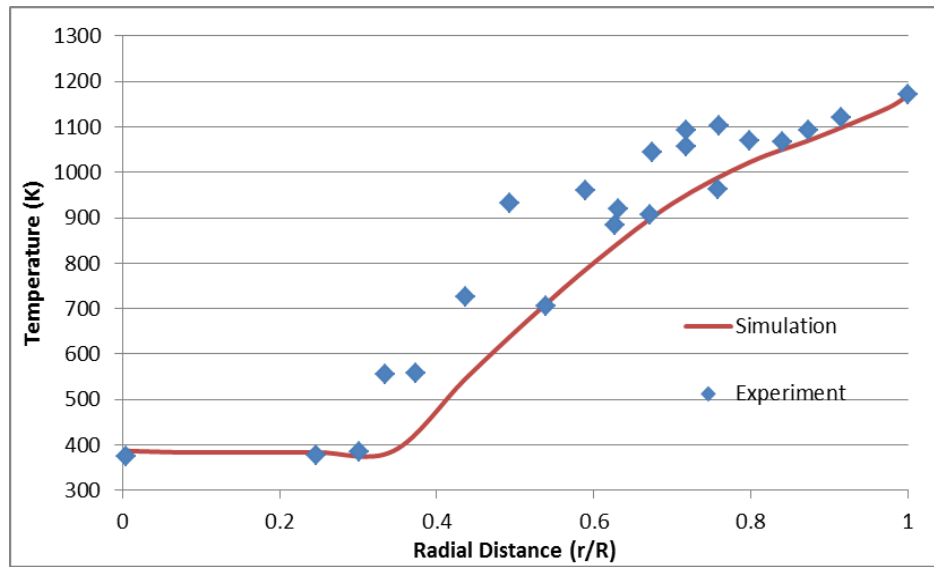


Figure 4-1: Comparison of temperature distribution of simulation and experiments with gas temperature 1173 K. (Reproduced from Perkins (2005))

Table 4-3: Dimensions of modeled geometry in COMSOL

Distance	Value (m)
Length of seam	15
Height of seam	9
Injection-Production well distance	4
Injection/Production diameter	0.2
Process casing diameter	0.1

Table 4-4: Proximate analysis of Alberta coal reservoir

	wt %
Moisture	5
Volatile matter	30.2
Fixed carbon	55.6
Ash	9.2

Model parameters are summarized in Table 4-5.

Table 4-5: Parameters used for simulation of UCG in Alberta coal reservoir

Parameter Name	Value
Solid density	1325 kg/m ³
Surface are	1.2E+7 m ² /m ³
Operating pressure	115 atm
Initial temperature	335 K
Initial Permeability	1E-15 m ²
Initial porosity	0.08
Burner Temperature	1000-1500 K

As discussed earlier, a fixed gas composition is set at boundary, which represents the produced gas.

Table 4-6: Bulk gas composition assumed for simulation of UCG (Perkins and Sahajwalla 2005)

Gas	mol %.
CO	13
CO ₂	20
H ₂	27
H ₂ O	33
CH ₄	7

Figure 4-2 shows the cavity after 4 days of process time. Cavity is symmetric around injection well and has a tear-drop shape similar to reported shapes of cavity in field trials and experiments (Prabu and Jaynati (2011), Daggupati (2010), Yeary (1989)). Rate of cavity growth along the axis of seam is around 80 cm/day which is comparable to reported values of 35-110 cm/day as reported in various field trials (Perkins and Sahajwalla, 2006).

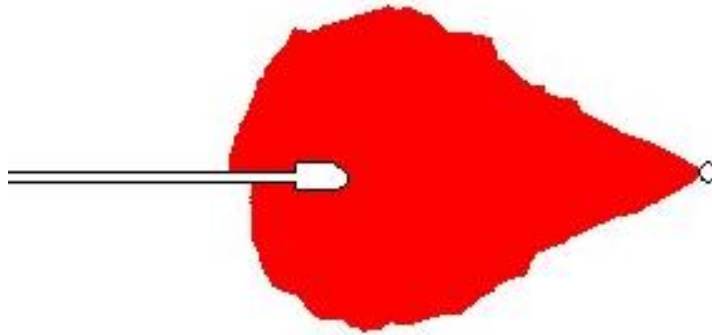


Figure 4-2: Cavity shape after 5 days of process

Figure 4-3 shows rate of evolution of steam from coal. As expected, the rate has two peaks, one at lower temperature related to evaporation of free water, and one at higher temperature corresponding to release of chemically bound water.

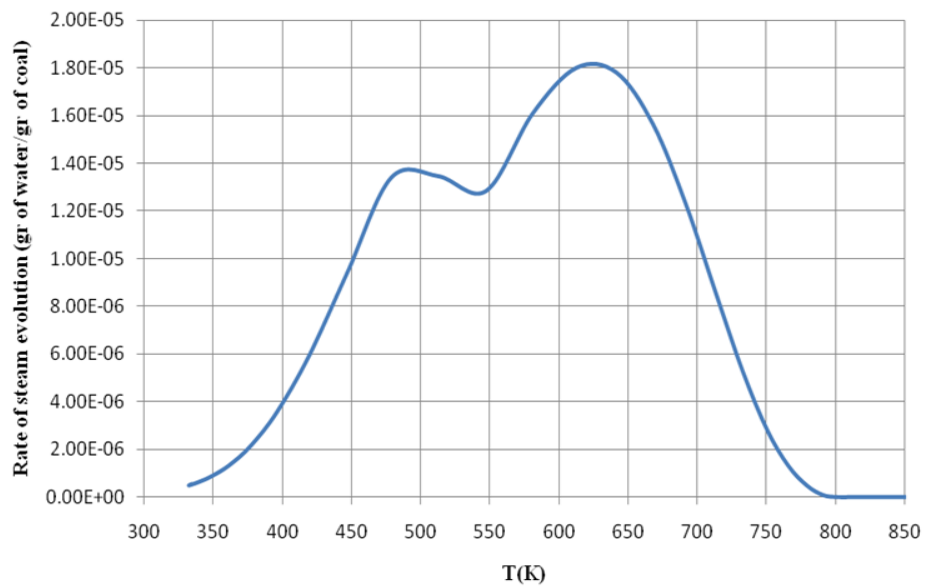


Figure 4-3: Rate of evolution of steam vs. temperature in a probe point in seam

As post-processing tools are limited in COMSOL, a MATLAB code was written to track the area of cavity. Figure 4-4 shows area of the cavity with respect to time. As seen in the graph, after 3-4 hours of process, the area of cavity increases with a constant rate. This linear coal consumption is shown to be the case for field trials. Also, it indicates that process reaches a pseudo-steady state after initial transient behaviour of the system.

Although the simulation is in 2D, it can be extended to 3D by assuming the same shape for a cavity in side view. However, this extrusion will lead to cavity below injection point, which is limited due to presence of ash layer at bottom of cavity. Therefore, lower half of cavity in side view should be disregarded. This approach has been successfully implemented in Linc Energy's model for prediction of cavity shapes at Chinchilla field trial (Luo et al., 2009).

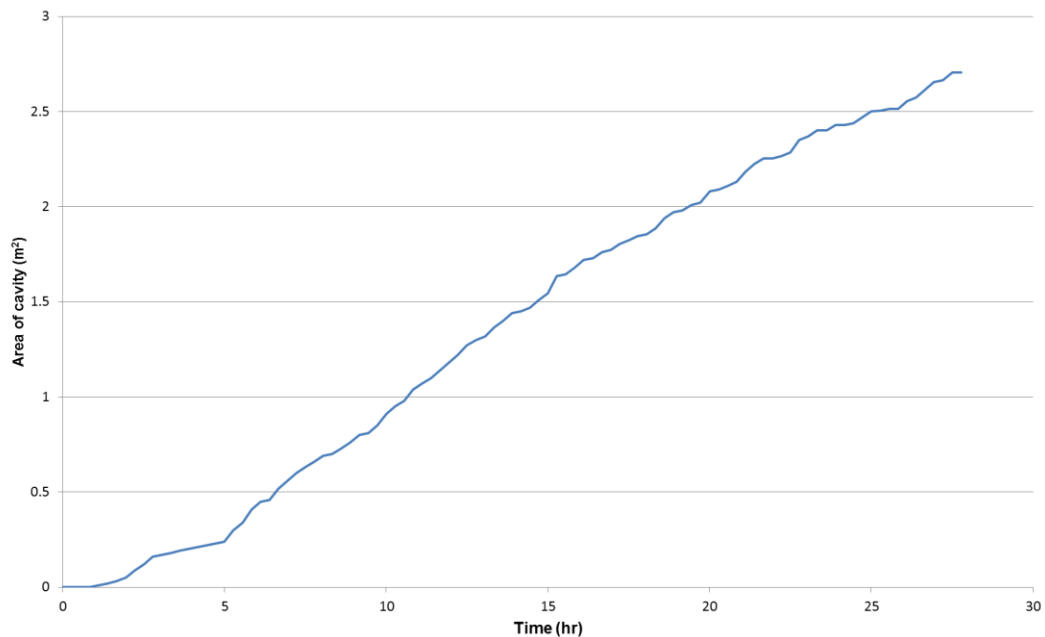


Figure 4-4: Area of cavity vs. time

4.1.1 Shortcomings of developed model in COMSOL.

The developed model in COMSOL yields a mesh-independent solution for predicting cavity shape at different stages of process. However, some assumptions limit its applicability. These assumptions are as follows:

- **Two-dimensional geometry:** The developed model is in a 2D geometry, which can be extruded to 3D as discussed earlier. However, the cavity shape in the real process is irregular 3D shape. Therefore, the complete model should be developed in 3D. Solver in COMSOL 3.5 has limited applicability for 3D geometries and solving the simplest case of fluid flow in porous media was cumbersome and led to unphysical results.
- **Constant temperature/gas composition at boundary:** In this model, the required heat for endothermic reactions are provided by setting a high temperature at burner, and combustion of gases/char is neglected. Also, gas composition is fixed at boundary. Although these assumptions have been verified with experiments, they can only be used for tracking the growth of cavity and local values of concentration and temperature might not be correct. Exact values of temperature and steam in cavity and seam are required for calculation of thermal stresses and mechanical failure of coal. Also, the combustion rate is five orders of magnitude larger than gasification rates. Implementing this source term in COMSOL model would make the solution unstable and the solver would diverge.

In order to overcome these shortcomings, it was proposed to develop the model in ANSYS FLUENT, which provides a relatively robust solver for 3D geometries,

combustion modelling and turbulent simulation. In the next section, the developed model in FLUENT is described in detail. Also, a sensitivity analysis is performed to identify most influential factors in performance of UCG.

4.2 Results of developed model in ANSYS FLUENT

Developed model in ANSYS FLUENT is based on laboratory experiments of Daggaputti et al. (2010). The geometry is shown in Figure 3-3. The specifications of the modelled geometry are as given in Table 4.7. The geometry was intentionally scaled down to decrease the computational expenses. Unlike the model developed in COMSOL, all of the heterogeneous and homogenous reactions are implemented in this model. Proximate analysis of primary coal in this study is given in Table 4.8.

Table 4-7: Dimensions of developed model in FLUENT

Distance	Value (cm)
Length of seam	3
Height of seam	1.5
Width of seam	2
Injection-Production well distance	1.2
Injection/Production diameter	0.1
Link diameter	0.1

Table 4-8: Primary coal used in developed model in FLUENT

	wt %
Moisture	10
Volatile matter	35.6
Fixed carbon	40.7
Ash	13.7

Table 4-9: Model parameters as used in FLUENT

Parameter Name	Value
Solid density	1200 kg/m ³
Surface area	1.2E+7 m ² /m ³
Operating pressure	1-20 atm
Initial temperature	300 K
Initial permeability	1E-15-1E-13 m ²
Initial porosity	0.05

Table 4-10: Boundary conditions for developed model in FLUENT

Injection gas	O ₂
Mass flux at inlet	0.05-0.3 kg/(m ² .s)
Burner temperature	1500 K
Inlet temperature	300-700 K
Outlet Pressure	1 atm

UCG process is initiated by using a burner that provides initial heat for coal combustion. In this study, a fixed temperature of 1500 K is set at burner, which represents the flame temperature at commercial propane burners. Fixed temperature at burner is removed when the coal combustion has reached a stage that can provide essential heat for continuation of the process. When oxygen concentration at outlet decreases considerably, it can be concluded that combustion has initiated.

4.2.1 Grid sensitivity analysis

A grid sensitivity analysis was done to select the optimum mesh size for this study and to ensure mesh independency of numerical solution. As recommended by Tu et al. (2008), number of cell counts is doubled in each mesh case and selected

variables are studied in each case. Table 4-11 summarizes the data for these studies:

Table 4-11: Selected variables after 8500 seconds of process for various mesh cases

Min cell size	2 mm	1 mm	0.7mm	0.5 mm
No. of volume cells	4802	9904	24072	38742
Outlet flow (mg/s)	0.271	0.273	0.276	0.277
Outlet temperature (K)	511.1	534.1	534.3	534.5
Composition of outlet (wt %)				
- O ₂	8.42	7.69	7.94	7.92
- CO ₂	21.38	21.51	21.85	21.98
- CO	13.56	13.44	13.77	13.59
- H ₂ O	50.91	51.67	50.74	50.85
- H ₂	0.76	0.72	0.74	0.73
- CH ₄	4.93	4.96	4.96	4.93
Volume of affected coal* (m ³)	6.891E-8	1.453E-7	2.825E-7	2.834E-7

* Affected coal is defined where coal has been dried and pyrolyzed and 10% of fixed carbon has been consumed

As indicated in Table 4-11, the composition of the outlet gas has changed around 10%, while the volume of the affected coal changes 5 times with the finer mesh. It can be concluded that finer mesh is required for prediction of a realistic cavity volume and shape, while coarse mesh could be used for prediction of gas composition. Further refinement of mesh from 0.7 mm does not yield in significant change in any of the characteristics, and hence this mesh was chosen for further analysis of various cases in this study.

4.2.2 Base case simulation

In this section, results of a base case simulation are discussed in detail. Operating pressure is 1 atm with inlet flow of 0.1 kg/(m² s) with an initial permeability of 1 mD. Figure 4-5 shows ratio of outlet flow to inlet flow. Outlet flow increases linearly as moisture and volatile matter is being released. However, after that the

drying and pyrolysis are finished all over the seam, outlet flow decreases significantly as steam and volatile matter are not released anymore. Note that almost 50wt% of the coal is moisture and volatile matter. The outlet flow is still higher than inlet flow after termination of drying and pyrolysis, due to gases released by the heterogeneous reactions of coal. While the cavity is growing, injected oxygen needs to travel in a longer distance to reach the cavity walls. This leads to lower rates of heterogeneous reactions, and reduced outlet gas flow rate

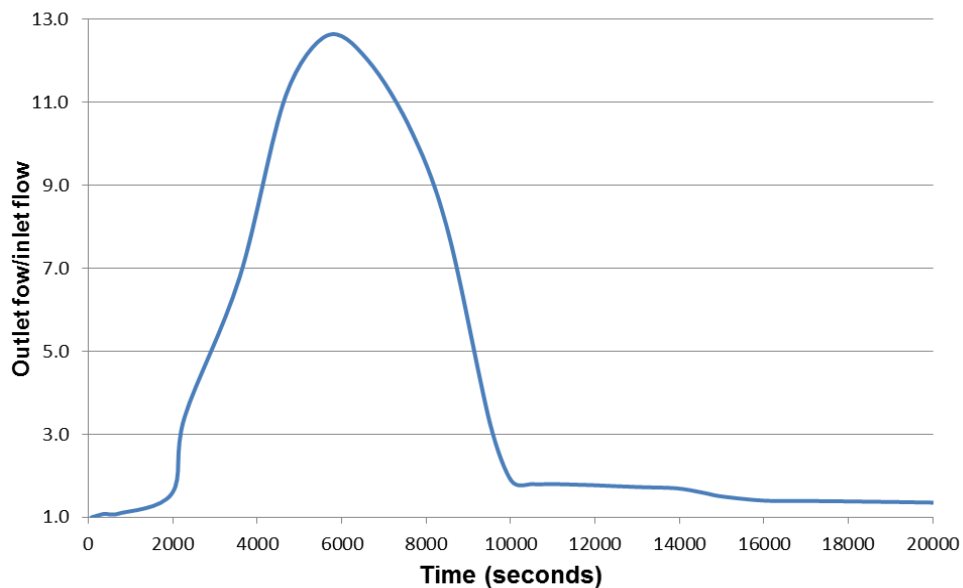


Figure 4-5: Outlet flow/Inlet flow for base case simulation

Figure 4-6 shows the composition of three major components of the outlet gas across the reaction period. After initial increase in composition of the oxygen in outlet, it decreases when coal and volatile matter combustion initiated. The oxygen concentration levels-off after 4200 seconds of the process. Then, for about 5000 seconds syngas with steady flow and composition is produced at production well. This steady state condition would remain the whole coal dries. After all the

moisture and volatile matter of coal is driven out (around 9500 seconds of process) composition changes significantly and reaches a new steady condition.

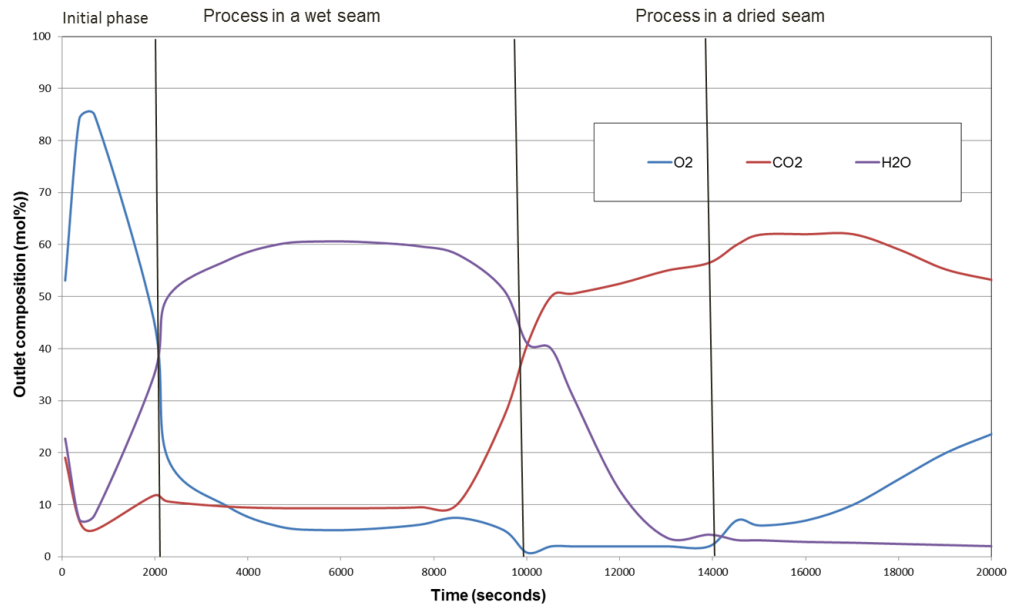


Figure 4-6: Composition of produced gas in base case simulation

The new steady condition after termination of pyrolysis and drying of whole seam shows a significant increase in CO₂ content and decrease in all other gases. This could be attributed to the lower temperature at cavity due to turning off of the burner. When burner is turned off, the only heat source in the system is from combustion reactions, thus the temperature inside the cavity drops to around 1000 K. This lower temperature will lead to the domination of combustion reaction as the CO₂ gasification would be slow at this temperature. Moreover, as there is no steam left in the system, steam gasification reaction is not happening which will lead to a lower content of CO and H₂ in the generated syngas.

Figure 4-7 shows the outlet temperature and heating value of the produced syngas with time. As the figure shows, at first 3000 seconds of the process, outlet temperature increases due to the presence of burner. After that, combustion is the main heat source and outlet temperature increases with a lower rate. At around 9500 seconds, drying of the seam is almost completed thus temperature increases with a higher rate until it reaches a plateau at about 715 K. Temperature would drop gradually as some of the oxygen would come out without reacting with coal.

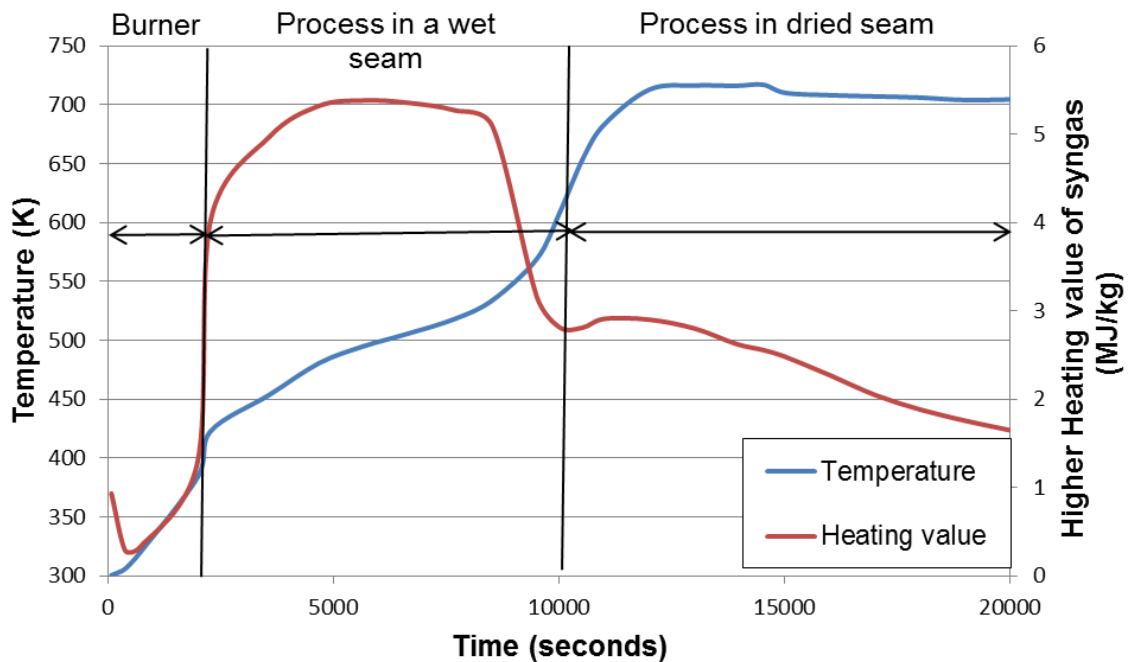


Figure 4-7: Outlet temperature vs. time for base case simulation

Heating value of produced gas also follows the same trend. It increases at first 3000 seconds of the process until it reaches a steady value of 5.6 MJ/kg. This value is comparable with field trials and experiments (Couch, 2009). After drying of the whole seam, the heating value drops significantly as there is no steam left

in the seam and the combustible gases will be consumed by the combustion reactions. Therefore, it can be concluded that presence of steam is essential for successful operation of UCG.

Figure 4-8 shows the temperature distribution in coal seam after 9000 seconds of process. It should be noted that local temperature in the coal seam is higher than the outlet temperature. This might be attributed to gas heat loss to surrounding environment. Figure 4-9 shows the reaction fronts inside the seam.

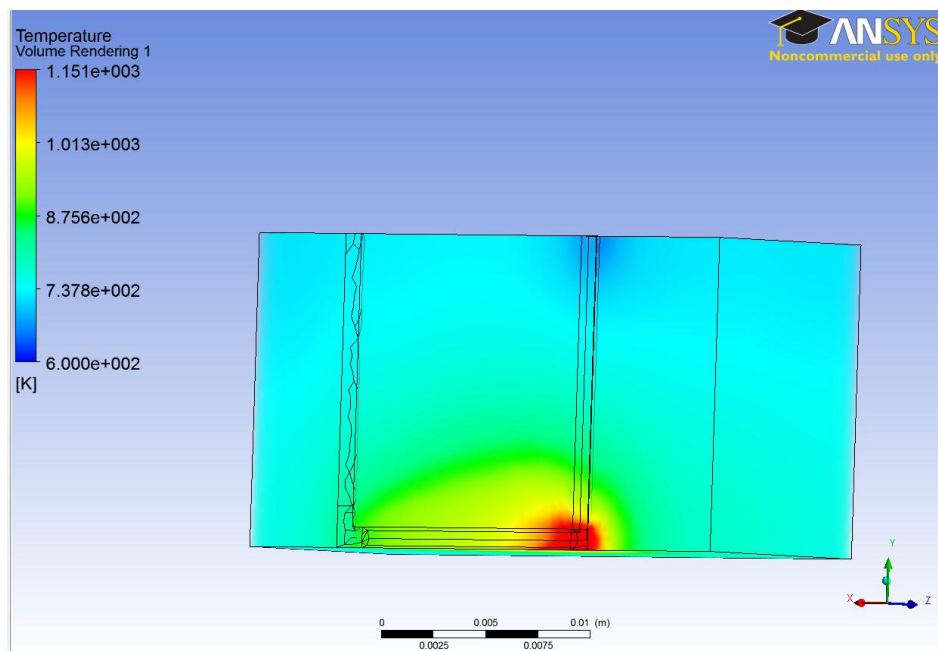


Figure 4-8: Temperature distribution in coal seam after 9000 seconds of process

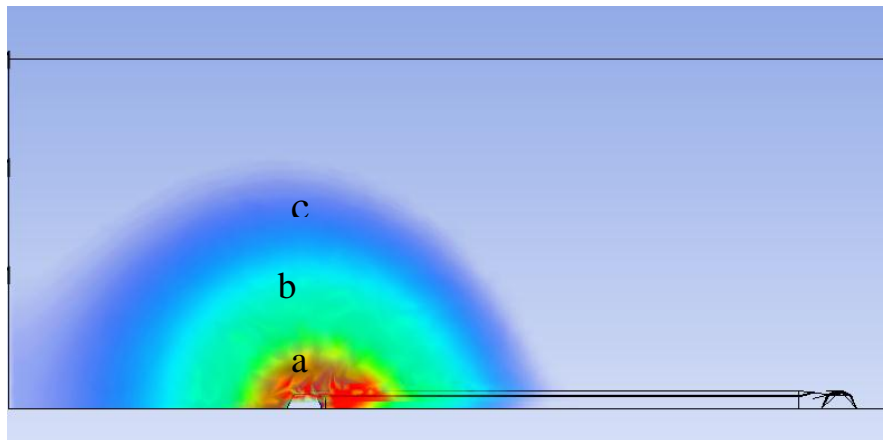


Figure 4-9: Reaction fronts in system after 4500 seconds of process: (a) combustion front, (b) pyrolysis front, (c) drying front

Figure 4-10 shows a typical cavity shape formed in the process. The color scheme represents the porosity of the seam.

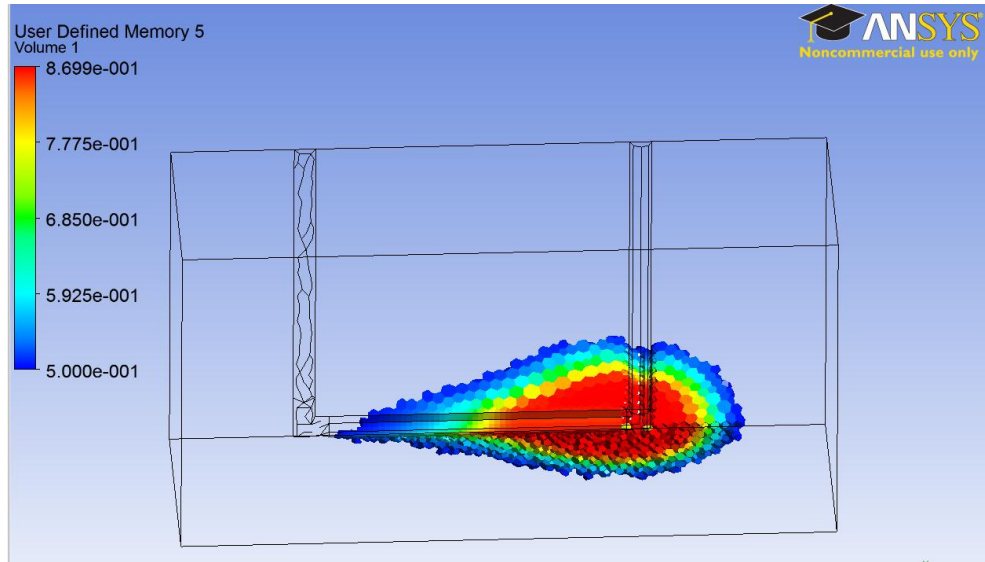


Figure 4-10: Cavity shape after 9000 seconds of process in base case simulation

As can be seen in Figure 4-10, the cavity has a tear-drop shape, which could be characterized based on its width, height, forward and backward length of the

cavity as shown in Figure 4-11. The cavity shape is compared with available data on literature in Table 4-13. Dimensions are normalized with respect to the distance between wells in each case to provide a better comparison. As shown in Table 4-12, cavity has the same geometric features as experiments. The major difference between model and experiment is the height of cavity which can be attributed to the anisotropic nature of the seam. It can be concluded that the coal in experiment has had higher permeability in y direction, which has led to faster growth in this direction.

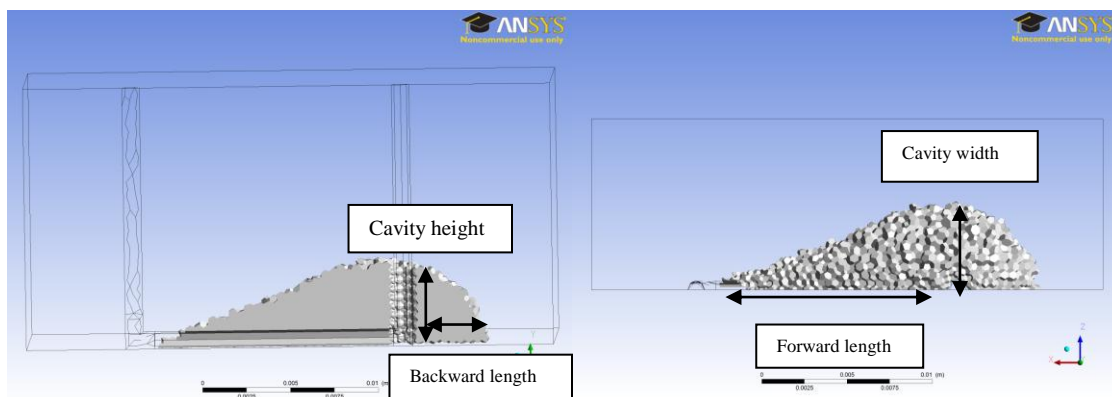


Figure 4-11: Definition of characteristic dimension of cavity

Table 4-12: Comparison of scaled dimensions of cavity with experiments

Dimension	Model	Experiment (Daggupati et al., 2010)
Forward length	1	1
Backward length	0.429	0.433
Height	0.399	0.517
Width	0.404	0.425

In field trials, seam is much larger and the cavity reaches the production well before drying of the seam is completed. Therefore, only the results for the period before completion of the drying have been used for the sensitivity analyses here.

4.2.3 Effect of discretization scheme

As mentioned in section 3.3.2, discretization scheme refers to the method of interpolation of variables in grids. In this study, second-order upwinding is used as a base case for modeling to minimize numerical false-diffusion. A sensitivity analysis was performed to study the effect of various interpolation schemes on the solution. As shown in Table 4-14, the gas composition is not affected by the method of discretization, while using the first-order upwinding has increased the volume of affected area by 100%. Diffusion is major mechanism for heat and species transfer in the seam. Using the first-order upwinding scheme increases the diffusive flux by introducing extra diffusion into the solution. Higher heat and mass transfer rate would lead to faster rate of cavity growth. As expected, decreasing the grid size would decrease the effect of false-diffusion on the results.

Table 4-13: Effect of discretization scheme after 8500 seconds of process

Min cell size	2 mm	2 mm	1 mm	1 mm
Discretization scheme	Second-order	First-order	Second-order	First-order
Outlet flow (mg/s)	0.270	0.244	0.273	0.247
Outlet temperature (K)	511.1	523.7	534.1	538.7
Composition of outlet (wt %)				
- O ₂	8.42	8.32	7.69	7.77
- CO ₂	21.38	21.66	21.51	21.06
- CO	13.56	13.95	13.44	13.95
- H ₂ O	50.91	50.49	51.67	51.62
- H ₂	0.76	0.73	0.72	0.73
- CH ₄	4.93	4.86	4.96	4.87
Volume of affected coal (m ³)	6.891E-8	1.471E-7	1.453E-7	2.106 E-7

4.2.4 Effect of operating pressure

To control the inflow of water into and outflow of gases from the cavity, the operating pressure in UCG cavity should be in equilibrium with the hydrostatic pressure of the surrounding areas. Therefore, operating pressure depends on the depth of the seam and increases with the rate of 0.01 MPa/m.

As discussed earlier, the rates of the combustion reactions which are the dominant reactions in UCG depend on the partial pressure of oxygen. Increasing the pressure from 1 to 10 atm increases the rate of combustion and thus the cavity growth rate. This increase of pressure also leads to 20% increase in CO₂ concentration in the product syngas, 40°C increase of the outlet temperature and lower bypass of oxygen.

Table 4-14: Effect of operating pressure on UCG process after 6500 seconds of process

Operating Pressure (atm)	1	5	10
Outlet flow (mg/s)	0.385	0.415	0.473
Outlet temperature (K)	491.1	530.5	535.2
Dry composition of outlet (wt %)			
- O ₂	18.09	3.05	1.40
- CO ₂	40.85	59.34	58.75
- CO	29.45	25.79	28.56
- H ₂	1.47	1.71	1.49
- CH ₄	10.16	10.12	9.79
Affected volume of coal (m ³)	4.35E-8	4.79E-7	5.38E-7

4.2.5 Effect of inlet temperature

In a few studies, researchers conducted UCG experiments with injection of a high temperature steam and reported the improved syngas quality (Daggupati et al., 2011). A sensitivity analysis was performed to study the effect of temperature of

the injected oxygen on the process. The results showed that this parameter is only effective on the cavity volume and the effect on other characteristics of the process is almost negligible. **Error! Reference source not found.** shows the cavity volume for different inlet gas temperatures which indicates an increase of less than 10% in cavity growth rate due to the increase of inlet temperature. The difference increases towards the end of the drying the whole seam, as the case with a higher temperature in inlet dries faster.

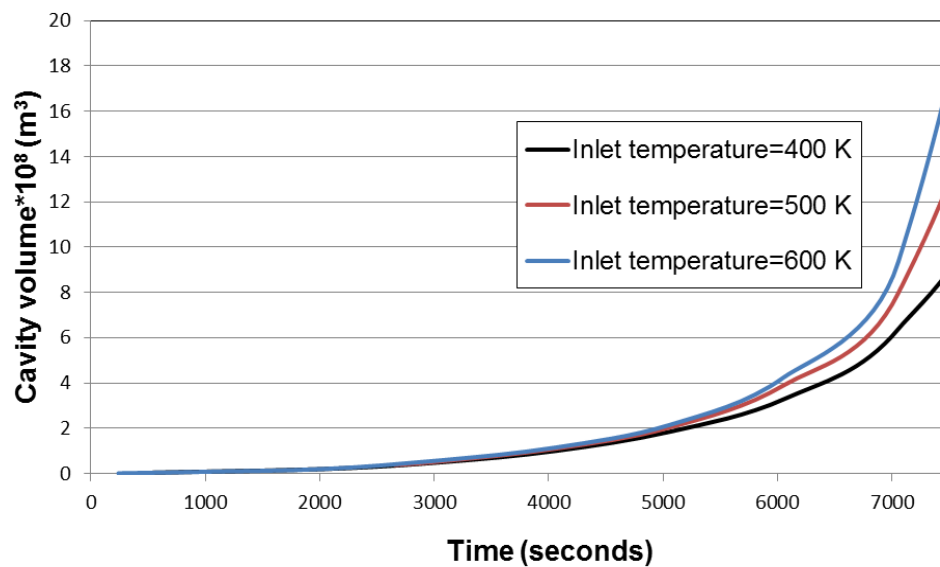


Figure 4-12: Effect of inlet temperature on the cavity growth rate

4.2.6 Effect of inlet flux

The inlet flux is optimized based on process conditions in each trial. Generally, it should be high enough to provide necessary heat for endothermic gasification reactions but not too low to lower the heating value of the generated syngas by diluting the generated syngas and combusting the valuable gases with oxygen. Inlet flow may also be optimized to produce the desirable syngas quality. Higher

injection rate also increases the gas velocity in the link and cavity and as a result increases the mass transfer by convection, which would lead to faster rates of combustion, drying and cavity growth.

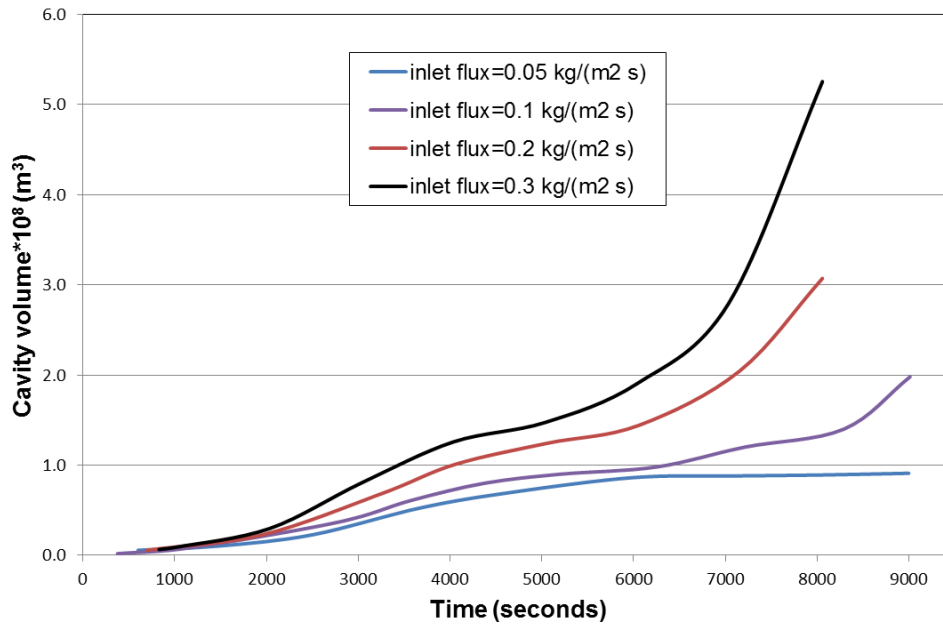


Figure 4-13: Cavity volume vs. time for different inlet flow rates

Figure 4-14 shows the heating value of the produced gas. As the inlet flow of oxygen increases, valuable gases are combusted with oxygen which leads to 5-10% decrease in heating value of produced gas. It should be noted that in case of lower influx of oxygen, turning off the burner would cease the cavity growth as the heat of combustion is not high enough.

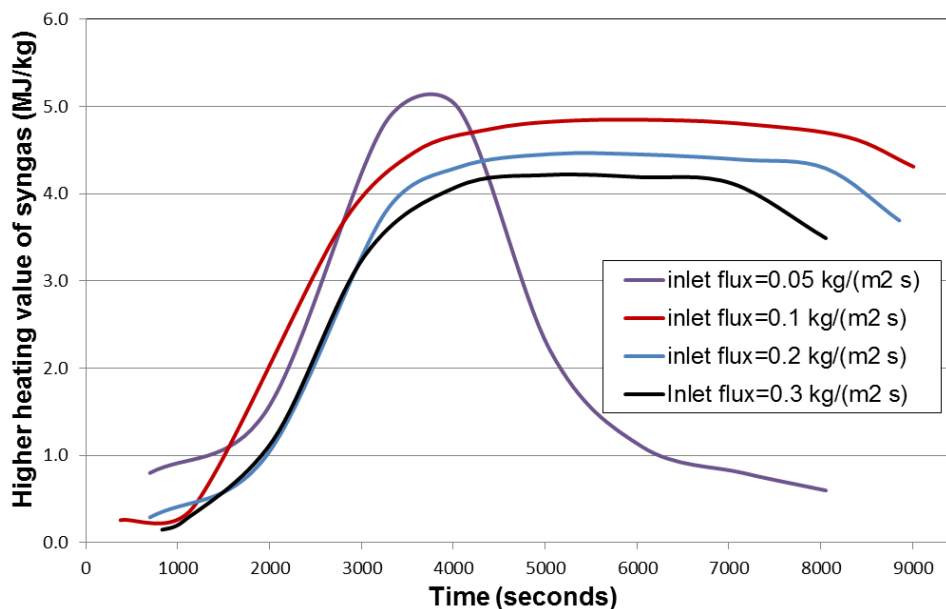


Figure 4-14: Heating value of syngas for various injection rates

Also, at lower flow rates cavity is more bulbous; while at higher flow rates cavity would be more elongated in the direction of the production well. Table 4-16 compares the dimensions of cavity after 8000 seconds of process for three different inlet gas flow rate.

Table 4-15: Dimensions of the cavity for different injection rates

Inlet flux(kg/m ² s)	0.05	0.1	0.2	0.3
Forward length	4.7 mm	+65%	+103%	+163%
Height	2.28 mm	+22.8%	+28%	+33.7%
Backward length	2.07 mm	+15%	+31%	+57.9%
Width	2.35 mm	+8%	+25.1%	+42.8%

4.2.7 Effect of permeability

Permeability is one of the major properties of seam affecting UCG process. Initial permeability of the seam is low, and therefore establishment of a permeable link is necessary for starting and continuing the process, as discussed in Chapter 2.

Tsang (1980) reported initial permeabilities of different coal seams as follow: 8 Darcy for Texas lignite, 1.7 Darcy for Gillette lignite, 0.13 Darcy for Hanna-subbituminous, and 0.017 for Pricetown bituminous. The permeability decreases with increasing the rank of coal. It should be noted that the in-situ permeability also depends on the overburden pressure. The dependency of coal permeability with overburden pressure is correlated as (Su et al., 1978):

$$\frac{\alpha}{\alpha_{ref}} = \left(\frac{P}{P_{ref}} \right)^{-0.8} \quad (\text{Eq. 32})$$

where α is in-situ permeability with overburden pressure of P.

In this study, initial permeability of seam was changed between 0.01 to 100 md to investigate the effect of permeability in UCG process. As shown in Figure 4-15, the cavity grows faster in the seam with higher permeability, as it has less resistance for flow of gas, and gases can permeate more easily. This is facilitated transfer of reactants in the bed and rate of cavity growth increases.

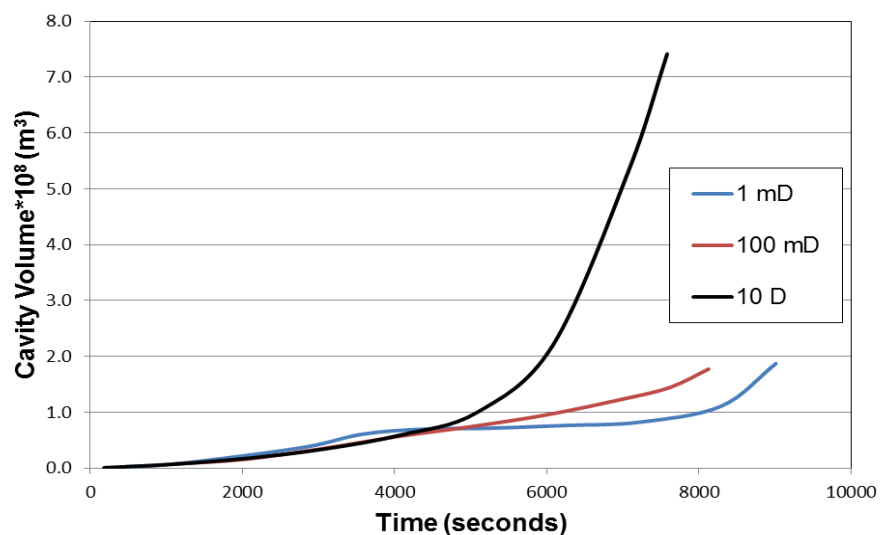


Figure 4-15: Cavity volume for seams with different initial permeability

Initial permeability of coal has a pronounced effect on shape of the cavity as illustrated in Figure 4-16. Higher permeability of coal will lead to a bulbous cavity, while lower permeability causes the cavity to grow along the permeable channel. This could also be attributed to easier permeation of the reactants in seam at higher permeabilities. In the seam with low permeability, gas flow is mostly confined within the permeable channel and therefore cavity grows around the link.

4.2.8 Effect of varying thermal properties of coal

Thermal properties of coal change with temperature as well as reactions that change the composition of coal such as evaporation, devolatilization and char reactions.

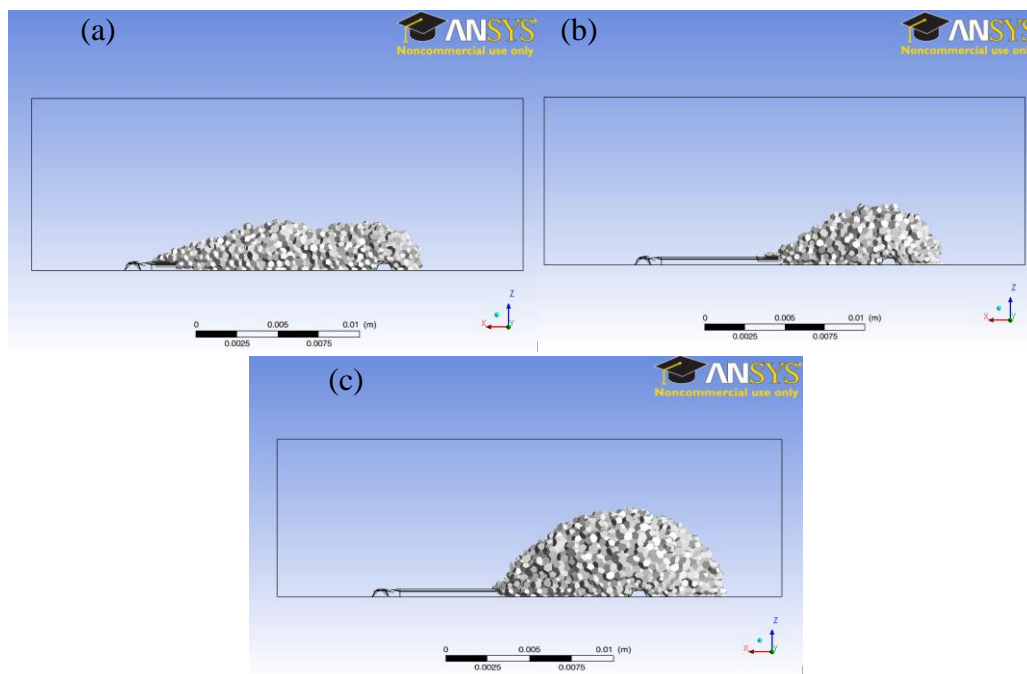


Figure 4-16: Cavity shape for cases with different initial permeabilities

(a) 1mD (b) 100 mD (c) 10 D

heat capacity of the coal in base case studied here was considered to be 0.3 W/(m K) (Herin and Deming, 1996) and 1300 J/(kg K), respectively. To show the effect of varying thermal properties of coal on the process, two studies were performed. In each study, one of the thermal properties was changed based on an appropriate correlation in literature.

Park and Edgar (1987) proposed the following functionality for conductivity of subbituminous coals vs. temperature:

$$k_c = \begin{cases} 0.37 & T < 673 \\ 0.25 + 0.0002 * (T - 673) & T \geq 673 \end{cases} \quad (\text{Eq. 33})$$

Heat capacity of coal increases with temperature initially and decreases afterwards due to decomposition of coal (Merrik, 1983). In this study, this dependency is described using the correlations of Massaquoi and Riggs (1983).

$$\begin{aligned} C_p &= Y_{ash} C_{p_{ash}} + (1 - Y_{ash}) C_{p_{daf}} \\ C_{p_{ash}} &= 600 \\ C_{p_{daf}} &= \begin{cases} 1297 + 1.415 * (T - 546) & T < 598 \\ 1757 - 0.65 * (T - 871) & T < 598 \end{cases} \end{aligned} \quad (\text{Eq. 34})$$

Figure 4-17 shows the variation of heat capacity and thermal conductivity based on the Eqs. 33 and 34.

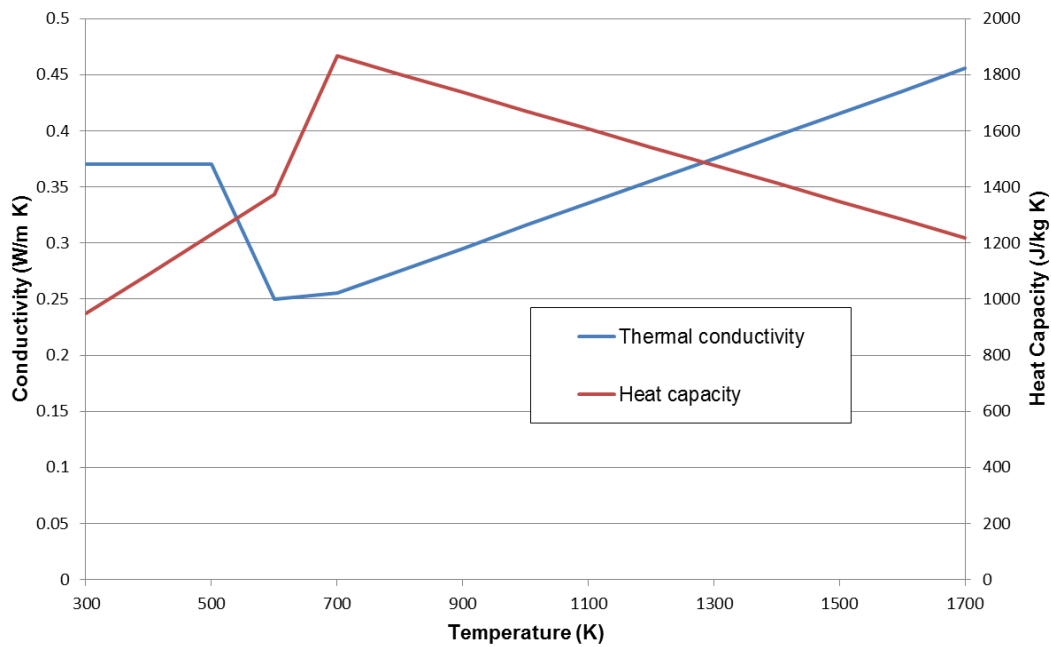


Figure 4-17: Thermal properties of coal as a function of temperature

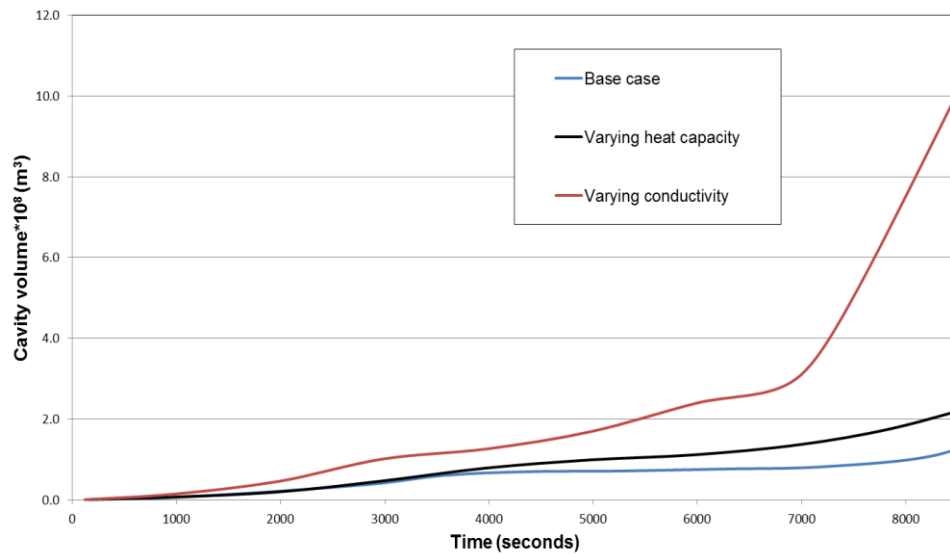


Figure 4-18: Cavity volume for cases with temperature-dependant thermal properties

Figure 4-16 shows the cavity volume vs. time. As illustrated in Figure 4-18, temperature-dependent heat capacity increases the cavity volume by 30%, while using varying heat conductivity makes the rate of cavity growth two times faster.

4.2.9 Effect of moisture content

Moisture content of the seam is one of the critical parameters in the assessment of suitability of UCG. In this study, three coals with moisture content of 5, 10, and 20 percent were studied. Other components have scaled to have the same ratio as the initial sample, as indicated in Table 4-8. The results of this study are presented in Figure 4-19 and Figure 4-20. The higher the moisture is the more energy is required for its evaporation. Therefore, as moisture content of coal increases from 5wt% to 20wt%, cavity growth rate decreases by 50%. Also, H₂O content of syngas increases by 20% as a result of this increase in moisture content. Thus, it can be concluded that the operation of UCG in coal seams with high moisture such as lignite is more challenging and requires special methods that have been described in Chapter 2.

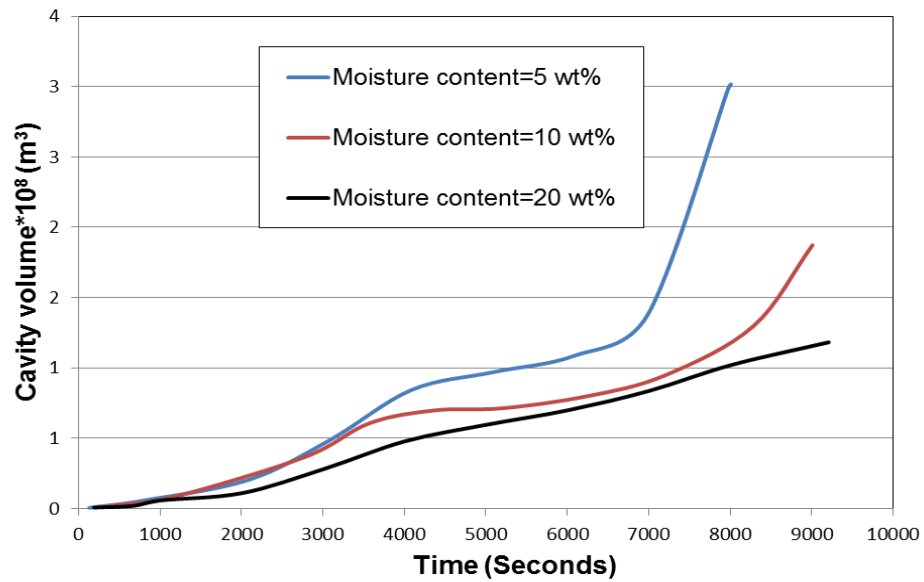


Figure 4-19: Cavity volume for cases with different initial moisture

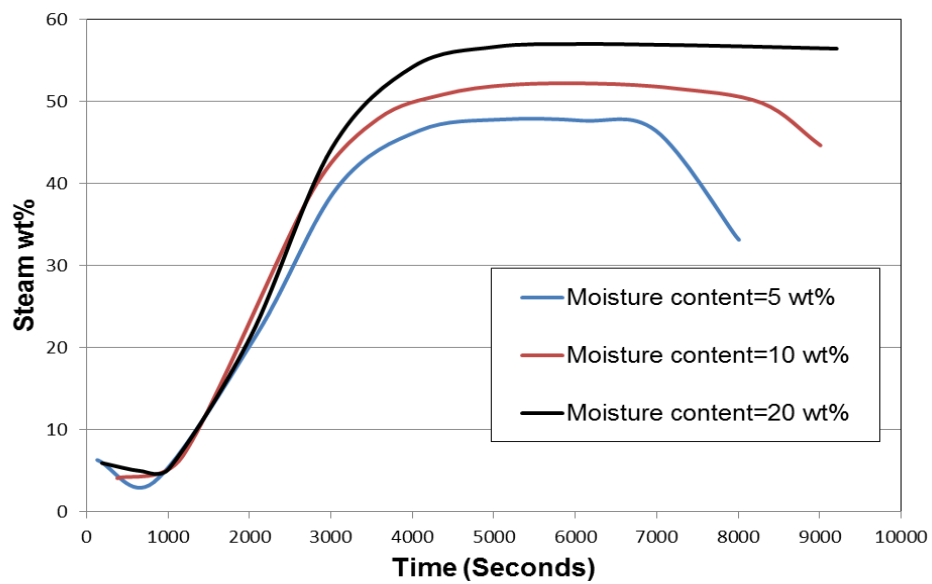


Figure 4-20: Weight percent of steam in outlet

Chapter Five: Conclusions and Recommendations

5.1 Conclusions

In this study, CFD models have been developed to predict the performance of the UCG process. The simplified 2D model in COMSOL is capable of predicting the trends for growth of cavity; however its simplistic assumption in neglecting combustion and its 2D geometry would limit its applicability for prediction of local values of temperature and concentration of gas species. Therefore, a comprehensive was later developed in ANSYS FLUENT to overcome these shortcomings. This model based on a scaled-down geometry was used to study various aspects of the process. The model results were compared with available data from experiments and previous field trials. Grid sensitivity analysis indicated that a finer mesh is required to achieve a grid-independent CFD model of the system, while coarse mesh may be used for the prediction of outlet gas composition with satisfactory accuracy. The model results show that the process reaches a steady state condition in 300-400 seconds after the initiation of the combustion reactions. This steady-state condition implies that the composition of the produced gas remains almost constant and the coal is being consumed at a constant rate. This condition remains steady until the whole seam is dried and pyrolysed. After this period, cavity growth rate and outlet temperature increases with a higher rate. Because the heating value of the produced syngas drops

significantly after termination of drying, presence of steam is necessary to guaranty the production of high quality syngas.

A detailed sensitivity analysis has been performed to investigate the effect of various parameters on the UCG process. The results indicated that variation of the coal seam properties with temperature especially the thermal conductivity has a major effect on the process. Initial permeability of seam was also found to be highly effective as such the higher permeability of seam would lead to a faster growth and a much wider cavity. It has been shown that increasing pressure would lead to higher rate of cavity growth; while it does not affect the shape of the cavity. Lower inlet gas flow rates led to a cavity shape that was more bulbous; while at higher flow rates cavity was more elongated in the direction of the production well. It was also found that increasing the inlet flow beyond a certain value, would lead to a lower concentration of CO and H₂ in outlet, as these gases will be combusted with oxygen.

5.2 Recommendations for future work

A CFD model with all relevant physics and reactions is developed in FLUENT, which was used for modeling the UCG process in small coal seam geometry. Since the actual process is conducted in a much larger scale, the current geometry needs to be scaled up to be comparable with experimental works. Thus, the next step would be to develop a model to predict the performance of UCG in the field trials.

The results indicated sensitivity of the process to the properties of seam and change of these properties with temperature. It is recommended to conduct experiments for a certain Albertan coal and formulate these dependencies for these specific seams, which will provide a great input for the UCG modeling.

As the results of the current model and some field trials show, after an initial transient state the process reaches a pseudo-steady state in which coal is consumed at a constant rate. A much simpler pseudo-steady model could be developed for this period which facilitates the coupling of the model with geotechnical models for prediction of the coal spalling and overburden failure.

References

- Abdel-Hadi, Eed A. A., and T. R. Hsu. 1987. "Computer Modeling of Fixed Bed Underground Coal Gasification Using the Permeation Method." *Journal of Energy Resources Technology* 109 (1): 11.
- Adams D.M.B., Carpenter A.M., Collot A., Couch G., Fernando R., Henderson C., Kristiansen A., Mitchell S.C., MoreeaTaha R., Nilsson P., Rousaki K., Scott D.H. 2009. "Gasification fundamentals and processes". IEA Clean Coal Centre.
- Aiman, W. R.,Thorsness, C. B.,Hill, R. W., Stephens, D. R. 1980. "An Underground Coal Gasification Experiment: Hoe.Creek II." *Combustion Science and Technology*, 21(3): 97.
- Batenburg, W.D, Biezen N.J, Bruining J. 1994. "A New Channel Model for Underground Coal Gasification of Thin, Deep Coal Seams", *In Situ*, 18(4):491.
- Batenburg, W.D., Bruining J. 1993. "The Efficiency of Filtration Gasification." *In Situ*, 17(4): 413.
- Beath A., Davis B. 2006. UCG History. In: *Proceedings of the Underground Coal Gasification Workshop*.Kolkata, India, 12- 15 Nov 2006.
- Beath A, Mallett C. (2006). UCG Modelling. In: *Proceedings of the Underground Coal Gasification Workshop*. Kolkata, India, 12-15 Nov 2006.
- Biba V, Macak J, Klose E, Malecha J.(1978). Mathematical model for the gasification of coal under pressure. *Ind Eng Chem Process Des Dev*. 92-98
- Biezen E N J, Bruining J, Molenaar J (1995) An Integrated 3D Model for Underground Coal Gasification. In: *Proceedings of the annual technical conference of the Society of Petroleum Engineers*.Dallas, TX, USA, 22-25 Oct. 1995.
- Biezen, E. N., Bruining, J., & Molenaar, J. (1994). An Integrated Model for Underground Coal Gasification. In: *Proceedings of the annual technical conference of the Society of Petroleum Engineers*. New Orleans, LA, USA, 25-28 Sep. 1994.
- Britten, J. A., Thorsness, C. B. (1989). A Model for Cavity Growth and Resource Recovery during Underground Coal Gasification. *In Situ*, 13, 1–53.

- Burton E, Friedmann J, Upadhye R (2006) Best practices in Underground Coal Gasification. Draft.US DOE contract no W-7405-Eng-48, Lawrence Livermore National Laboratory, Berkley, CA.
- Campbell, J. H. (1978). Pyrolysis of Subbituminous Coal in Relation to In-Situ Coal Gasification. *Fuel*, 57, 217 - 224.
- Carbon Energy website, www.carbonenergy.com.au
- Chang, H. L., Himmelblau, D. M.,Edgar, T. F. (1985).A Sweep Efficiency Model for Underground Coal Gasification. *In Situ*, 9 (2), 185 – 221.
- Coeme, A., Pirard, J. P., Mostade, M. (1993). Modeling of the Chemical Processes in a Longwall Face Underground Gasifier at Great Depth. *In Situ*, 17(1), 83–104.
- Cooke S.D., Oliver L.R. (1983). Ground water quality at the Hanna Underground Coal Gasification experimental sites, Hanna, Wyoming: Database and Summary, Western Research Institute of the University of Wyoming Research Corporation.
- Couch, G. R. (2009). Underground Coal Gasification. *Science* (New York, N.Y.) (Vol. 183, p. 129). IEA Clean Coal Centre.
- Daggupati, S., Mandapati, R. N., Mahajani, S. M., Ganesh, A., Pal, a. K., Sharma, R. K., Aghalayam, P. (2011). Compartment Modeling for Flow Characterization of Underground Coal Gasification Cavity. *Industrial & Engineering Chemistry Research*, 50(1), 277-290.
- Daggupati, S., Mandapati, R. N., Mahajani, S. M., Ganesh, A., Sapru, R. K., Sharma, R. K., & Aghalayam, P. (2011). Laboratory Studies on Cavity Growth and Product Gas Composition in the Context of Underground Coal Gasification. *Energy*, 36(3), 1776-1784.
- Daggupati, S., Mandapati, R. N., Mahajani, S. M., Ganesh, A., Mathur, D. K., Sharma, R. K., & Aghalayam, P. (2010). Laboratory Studies on Combustion Cavity Growth in Lignite Coal Blocks in The Context of Underground Coal Gasification. *Energy*, 35(6), 2374-2386.
- Davis B.E., Ahner F.P., Gulf Research and Development Co. (1982). Underground Coal Gasification of Steeply Dipping beds: A Second Generation Synthetic Fuels Process. SPE Annual Technical Conference and Exhibition, 26-29 September 1982, New Orleans, Louisiana.
- Debelle B., Malmendier M., Mostade M., Pirard J. P. (1992). Modelling of Flow at Thulin Underground Coal Gasification Experiments, *Fuel*, 71, 95-106
- Dennis S. D. (2006). Rocky Mountain 1- Underground Coal Gasification test project: Final Technical Report for the period 1986 to 2006. U.S. Department of Energy.

- Dinsmoor, B., Galland, J. M., Edgar, T. F. (1978). The Modeling of Cavity Formation during Underground Coal Gasification. *Journal of Petroleum Technology*, 30(5), 695-704.
- DTI (2005). Directional drilling in coal. DTI/Pub URN 05/657. Technology status report TSR024.
- Di Blasi C., Buonanno F., Branca C. (1999) Reactivities of some biomass chars in air. *Carbon*, 37, 1227-1238
- Didcot, Oxford, UK, Department of Trade and Industry Cleaner Fossil Fuels Programme.
- Dufaux A, Gaveau B, Letolle R, Mostade M, Noel M, Pirard J P (1990) Modelling of the Underground Coal Gasification Process at Thulin on The Basis of Thermodynamic Equilibria and Isotopic Measurements. *Fuel*, 69, 624-632.
- Forrester, R. C. (1979). Two-Dimensional Studies of Coal Pyrolysis Preliminary Results. In *Proceedings of the 5th Annual Underground Coal Conversion Symposium*; U.S. Department of Energy: Washington, DC, 402 - 410.
- Gas Tech. Inc. (2007). Viability of Underground Coal Gasification in the deep coals of Powder River Basin, Wyoming.
- Gunn R.D, Krantz W.B. (1987). Underground Coal Gasification: Development of Theory, Laboratory Experimentation, Interpretation and Correlation with the Hanna Field Tests, Department of Energy, US.
- Gregg D.W., Edgar T.F. (1978). Underground Coal Gasification. *AIChE Journal*, 1978, 24(5) , 753–781.
- Gregg, D.W., Hill, R.W., Olness, D.U. (1976). An overview of the Soviet Effort in Underground Coal Gasification, UCRL-52004, Lawrence Livermore National Laboratory (LLNL) Report, Berkeley, CA.
- Eddy, T. L., Schwartz, S. H. (1983). A Side Wall Burn Model for Cavity Growth in Underground Coal Gasification. *Journal of Energy Resources Technology*, 105(2), 145-156.
- Hattingh, L. (2008). Underground Coal Gasification. Sasol Mining Ltd.
- Hill, R. W., Thorsness, C. B. (1982). Summary Report on Large Block Experiments in Underground Coal Gasification, Tono Basin, Washington: Vol. 1. Experimental description and data analysis. UCRL-53305, Lawrence Livermore National Laboratory (LLNL) Report, Berkeley, CA.

Hongtao L., Feng C., Xia P., Kai Y., Shuqin L. (2011). Method of oxygen-enriched two-stage underground coal gasification, *Mining Science and Technology (China)*, 21(2), 191-196.

Kapusta, K., Stańczyk, K. (2011). Pollution of Water during Underground Coal Gasification of Hard Coal and Lignite, *Fuel*, 90(5), 1927-1934.

Khadse, A. N., Qayyumi, M., Mahajani, S., Aghalayam, P. (2007). Underground coal gasification: A new clean coal utilization technique for India. *Energy*, 32(11), 2061-2071.

Khadse, A. N., Qayyumi, M., Mahajani, S., Aghalayam, P. (2006). Model for the Underground Coal Gasification (UCG) Channel Reactor Model for the Underground Coal Gasification (UCG) Channel, *International Journal of Chemical Reactor Engineering*, 4, 1-25.

Kuyper, R. A., van der Meer, T. H., Bruining, J. (1996). Simulation of Underground Gasification of Thin Coal Seams. *In Situ*, 20, 311–346.

Kuyper, R. A., van der Meer, T. H., Hoogendoorn, C. J. (1994). Turbulent Natural Convection Flow due to Combined Buoyancy Forces during Underground Coal Gasification of Thin Seams. *Chemical Engineering Science*, 49, 851–861.

Laurus Energy website, laurusenergy.com

Lyczkowski, RW, and YT Chao. 1984. "Comparasion of Stefan Model with Two-Phase Model of Coal Drying." *International journal of heat and mass transfer* 27 (8).

Luo, Y., Coertzen, M., Dumble, S. (2009). Comparison of UCG Cavity Growth with CFD model predictions, Seventh International Conference on CFD in the Minerals and Process Industries CSIRO, Melbourne, Australia (December), 9-11 December 2009.

Mathy, B., Pirlot, P., Pirard, J. P., Coeme, A., Mostade, M., DeRo, P. (1994). Flow Modeling in an Underground Gasifier at Great Depth by the Boundary Element Method. *In Situ*, 18(4), 399–418

Massaquoi, J. G. M., Riggs, J. B. (1983). Mathematical Modeling of Combustion and Gasification of a Wet Coal Slab—II: Mode of Combustion, Steady State Multiplicities and Extinction. *Chem. Eng. Sci.*, 38(10), 1757 – 1766.

Massaquoi, J. G. M., Riggs, J. B. (1983). Mathematical Modeling of Combustion and Gasification of a Wet Coal Slab—I: Model Development and Verification. *Chem. Eng. Sci.* 1983, 38 (10), 1747 – 1756.

Massaquoi, M., Riggs, J. B. (1983). One-Dimensional Model of the Physico- Chemical Processes Occurring Inside a Burning Coal Surface, 29(6), 975-981.

- Mai, M.C., Park, K.Y., Edgar, T.F. (1985). Analysis of Early Cavity Growth in Underground Coal Gasification, *In Situ*, 9(2), 119-147(1985)
- Nourozieh, H., Kariznovi, M., Chen, Z., Abedi, J. (2010). Simulation Study of Underground Coal Gasification in Alberta Reservoirs: Geological Structure and Process Modeling. *Energy & Fuels*, 24(6), 3540-3550.
- Pana, C. (2009). Review of Underground Coal Gasification with Reference to Alberta's Potential Review of Underground Coal Gasification with Reference to Alberta's Potential. *Energy* (p. 63).
- Park K.Y., Edgar, T. F. (1987). Modeling of Early Cavity Growth for Underground Coal Gasification. *Ind. Eng. Chem. Res.*, 6(2), 237-246.
- Perkins, G., Sahajwalla, V. (2008). Steady-State Model for Estimating Gas Production from Underground Coal Gasification. *Energy & Fuels*, 22(6), 3902-3914.
- Perkins, G., Sahajwalla, V. (2007). Modelling of Heat and Mass Transport Phenomena and Chemical Reaction in Underground Coal Gasification. *Chemical Engineering Research and Design*, 85(3), 329-343.
- Perkins, G., Sahajwalla, V. (2006). A Numerical Study of the Effects of Operating Conditions and Coal Properties on Cavity Growth in Underground Coal Gasification. *Energy*, (12), 596-608.
- Perkins, G., Sahajwalla, V. (2005). A Mathematical Model for the Chemical Reaction of a Semi-infinite Block of Coal in Underground Coal Gasification. *Energy & Fuels*, 19(4), 1679-1692.
- Patankar, Suhas V., 1980 Numerical heat transfer and fluid flow / Suhas V. Patankar Hemisphere Pub. Corp. ; McGraw-Hill, Washington : New York :
- Poon, S.S.M, Edgar, T.F., Park, K.Y. (1986). The Combustion Rates of Texas Lignite Cores, *In Situ*, 10(2), 109-143.
- Pirard, J. P., Basseur, A., Coeme, A., Mostade, M., Pirlot, P. (2000). Results of the Tracer Tests during the El Tremedal Underground Coal Gasification at Great Depth. *Fuel*, 79, 471-478.
- Pirlot, P., Pirard, J. P., Coeme, A., Mostade, M. (1998). A Coupling of Chemical Processes and Flow in View of the Cavity Growth Simulation of an Underground Coal Gasifier at Great Depth. *In Situ*, 22(2), 141-156.
- Prabu, V., Jaynati, S. (2011). Simulation of Cavity Formation in Underground Coal Gasification using Borehole Combustion. *Energy*, 36, 5854-5864.

Roberts, D. G.; Harris, D. J. (2000). Char Gasification with O₂, CO₂ and H₂O: Effects of Pressure on Intrinsic Reaction Kinetics. *Energy & Fuels*, 14, 483-489.

Sasol website, sasol.com

Seifi, M., Chen, Z., Abedi, J. (2011). Numerical Simulation of Underground Coal Gasification using the CRIP method. *The Canadian Journal of Chemical Engineering*, 89(6), 1528-1535.

Shafirovich, E., Varma, A. (2009). Underground Coal Gasification: A Brief Review of Current Status. *Industrial & Engineering Chemistry Research*, 48(1), 7865-7875.

Stańczyk, K., Smoliński, A., Kapusta, K., Wiatowski, M., Świądrowski, J., Kotyrba, A., & Rogut, J. (2012). Experimental Simulation of Hard Coal Underground Gasification for Hydrogen Production. *Fuel*, 91(1), 40.

Stańczyk K., Howaniec N., Smoliński A., Świądrowski J., Kapusta K., Wiatowski M., Grabowski J., Rogut J., (2011). Gasification of Lignite and Hard Coal with Air and Oxygen Enriched Air in A Pilot scale Ex Situ Reactor for Underground Gasification, *Fuel*, 90(5), 1953-1962

Stańczyk, K., Smoliński, A., Kapusta, K., Wiatowski, M., Świądrowski, J., Kotyrba, A., & Rogut, J. (2010). Dynamic Experimental Simulation of Hydrogen Oriented Underground Gasification of Lignite. *Fuel*, 89(11), 3307-3314.

Syamlal, M., Bissett L.A. (1992). METC Gasifier Advanced Simulation (MGAS) Model. U.S. Department of Energy, Morgantown Energy Technology Center, Morgantown, West Virginia, US.

Suuberg, E., Otake, Y. & Yun, Y., (1993). Role of moisture in coal structure and the effects of drying upon the accessibility of coal structure. *Energy & Fuels*, 33(2), pp.384-392.

The Future of Coal, Options for a carbon-constrained world. (2007). MIT Publications.

Tu, Jiyuan; Yeoh, Guan Heng; Liu, Chaoqun (2008). *Computational Fluid Dynamics - A Practical Approach*. Elsevier.

Thorsness, C. B. (1980). Steam Tracer Experiment at the Hoe Creek No.3 Underground Coal Gasification Field Test, Report UCRL-53082, Lawrence Livermore National Laboratory: Livermore, CA.

Thorsness, C. B., Cena, R. J. (1983). An Underground Coal Gasification Cavity Simulator with Solid Motion. UCRL-89084, Lawrence Livermore National Laboratory (LLNL) Report, Berkeley, CA.

- Thorsness, C. B., Creighton, J.R. (1983). Review of Underground Coal Gasification field experiments at Hoe Creek. AIChE Symposium Series, 226(79), 15-43.
- Thorsness, C.B., Hill, R.W. (1981). Coal Block Gasification: Laboratory Results and Field Plans. Report no. UCRL-85906. U.S. DOE, Livermore, CA: Lawrence Livermore National Laboratory.
- Thorsness, C. B., Kang, S. W. (1985). Further development of a general-purpose Packed Bed Mode For Analysis Of UCG Process. Report no. UCRL-92489, Lawrence Livermore National Laboratory (LLNL) Report, Berkeley, CA.
- Tomita, A.; Mahajan, O. P.; Walker Jr., P. L. (1977). Reactivity of Heat-Treated Coals in Hydrogen. Fuel, 56, 137 - 144.
- Tsang, T. H. T. (1980). Modeling of Heat and Mass Transfer during Coal Block Gasification, Ph.D. Thesis, University of Texas at Austin, Austin, TX.
- Upstream news website, <http://www.upstreamonline.com/live/article222165.ece>
- USRMA website, <http://www.usmra.com/chinatable.htm>
- Walker, L.K., Blinderman, M.S., Brun, K. (2001). An IGCC Project at Chinchilla, Australia based on Underground Coal Gasification (UCG). Gasification Technologies Conference, San Francisco, October 8-10, 2001.
- Winslow, A. M. (1976). Numerical model of Coal Gasification in A Packed Bed. UCRL-77627, Lawrence Livermore National Laboratory (LLNL) report, Berkeley, CA.
- Yang L., Zhang X., Liu S., Yu L., Zhang W. (2008). Field test of large-scale Hydrogen manufacturing from Underground Coal Gasification (UCG), International Journal of Hydrogen Energy, 33(4), 1275-1285
- Yang, L., Liu, S., Yu, L., Liang, J. (2007). Experimental study of Shaftless Underground Gasification in Thin High-Angle Coal Seams. Energy & Fuels, 21(4), 2390-2397.
- Yang, L. (2004). Study on the Model Experiment and Numerical Simulation for Underground Coal Gasification. Fuel, 83(4-5), 573-584.
- Yang, L. (2003) Study on the Method of Two-Phase Underground Coal Gasification with Unfixed Pumping Points. Energy Sources, 25, (9), 917-930.
- Ye, D. P. Agnew J. B., Zhang D. K., (1998). Gasification of a South Australian low-rank coal with carbon dioxide and steam: kinetics and reactivity studies. Fuel, 77, 1209-1219.
- Yearly D.L, Riggs (1987). Study of Small-scale Cavity Growth Mechanisms for Underground Coal Gasification, In Situ, 11(4), 305-327.

Yeary D.L. (1987). Experimental Study of Lateral Cavity Growth Mechanisms in Underground Coal Gasification, MSc. Thesis, Texas Tech University, Lubbock, TX.

Appendix A: User-Defined Functions

```

/*****
User-Defined Memories are used to store reactions of solid phase
C_UDMI(c,t,0): Drying
C_UDMI(c,t,1): Pyrolysis
C_UDMI(c,t,2): Combustion
C_UDMI(c,t,3): CO2 Gasification
C_UDMI(c,t,4): H2O Gasification
Also a UDM has been defined to keep the value of porosity :
C_UDMI(c,t,5): Porosity
*****/
#include "udf.h"
/*****
*****/
UDF for specifying user-defined scalar time derivatives
*****/
DEFINE_UDS_UNSTEADY(my_uds_unsteady,c,t,i,apu,su)
{
    real physical_dt, vol, rho, phi_old;
    physical_dt = RP_Get_Real("physical-time-step");
    vol = C_VOLUME(c,t);

    rho = C_R_M1(c,t);
    *apu = -rho*vol / physical_dt; /*implicit part*/
    phi_old = C_STORAGE_R(c,t,SV_UDSI_M1(i));
    *su = rho*vol*phi_old/physical_dt; /*explicit part*/
}

/*****
*****/

```

Porosity as scalar

```
*****
****/
```

```
DEFINE_PROFILE(porosity_UDS, t, nv)
```

```
{
cell_t c;
begin_c_loop(c,t)
/*****
Porosity in terms of moisture, VM and FC content of coal
*****/
C_PROFILE(c,t,nv) = 0.05+(C_UDSI(c,t,0)+C_UDSI(c,t,1)+C_UDSI(c,t,2));
C_UDMI(c,t,5)=0.05+(C_UDSI(c,t,0)+C_UDSI(c,t,1)+C_UDSI(c,t,2));
end_c_loop(c,t)
}
```

```
*****/
****
```

Porous Resistance Direction Vector Profile that utilizes C_PROFILE

```
*****/
****
```

```
DEFINE_PROFILE(resistance_function, t, nv)
```

```
{
cell_t c;
real porosity;
porosity= 0.05+(C_UDSI(c,t,0)+C_UDSI(c,t,1)+C_UDSI(c,t,2)) ;
begin_c_loop(c,t)
C_PROFILE(c,t,nv) = 1e+15/exp(12*(porosity-0.05)) ;
end_c_loop(c,t)
}
*****/
****
```

UDF for temperature dependant heat conductivity

```
*****/
****
```

```
DEFINE_PROPERTY(coal_conductivity,c,t)
```

```
{
real cond;
real porosity, ym;
porosity= 0.05+(C_UDSI(c,t,0)+C_UDSI(c,t,1)+C_UDSI(c,t,2)) ;
ym=(0.095-C_UDSI(c,t,0))/(1-porosity);
cond = 0.6*ym+(1-ym)*pow((1230/4511),3.5)*pow(C_T(c,t),0.5);
return cond;
}
```

```

/*****
****
UDF for temperature dependant heat capacity

****/
DEFINE_SPECIFIC_HEAT(coal_cp, T, Tref, h, yi)
{
  real cps;
/*
  heat capacity based on Merric
  real g;
  real ym, ydaf, porosity, yash;
  Thread *t;
  cell_t c;
  porosity= 0.05+(C_UDSI(c,t,0)+C_UDSI(c,t,1)+C_UDSI(c,t,2)) ;
  ym=(0.095-C_UDSI(c,t,0))/(1-porosity);
  ydaf=(0.72485-C_UDSI(c,t,1)-C_UDSI(c,t,2))/(1-porosity);
  yash = 1-ym-ydaf;
  g =
exp(1200/C_T(c,t))*pow((1200/C_T(c,t),2)/pow((exp(1200/C_T(c,t))-1),2);
  cps = 1300*ym+(754+0.586*C_T(c,t))*yash+ydaf*3*8.3*0.1*1000*g;*/
  if (T<598)
      cps= (0.31+3.38e-4*(T-546))*4184;
  else
      cps= (0.42-1.548e-4*(T-871))*4184;

  *h = cps*(T-Tref);
  return cps;
}

/*****
****
UDF for specifying a source for drying
Drying: Virigin Coal ==> Dry Coal + Heat
Kinetics:
METC Gasifier Advanced Simulation (MGAS) model, Syamlal, M.
C_UDSI(c,t,0): Moisture content of coal at each moment
moistureinf : Moisture content of coal from proximate analysis
****/
DEFINE_SOURCE(solid_h2op_source,c,t,dS,eqn)
{
  real source;

```

```

real tem = C_T(c,t);
real k;
real moistureinf = 0.1;

if (C_UDSI(c,t,0)>moistureinf*0.95 )
  k = 0.;
else
  k = 51000*exp(-78240/(8.3*tem));
  source=k*(moistureinf*0.95-C_UDSI(c,t,0))*C_R(c,t);
  C_UDMI(c,t,0)=k*(moistureinf*0.95-C_UDSI(c,t,0))*C_R(c,t);
return source;
}

/*****
*****/
UDF for specifying a h2o mass source source for drying
*****/
DEFINE_SOURCE(mass_source_h2o,c,t,dS,eqn)
{
real source;
real tem = C_T(c,t);
real k;
real moistureinf = 0.1;
real porosity;
porosity= 0.05+(C_UDSI(c,t,0)+C_UDSI(c,t,1)+C_UDSI(c,t,2)) ;

if (C_UDSI(c,t,0)>moistureinf*0.95)
  k = 0.;
else
  k = 51000*exp(-78240/(8.3*tem));
  source=k*(moistureinf*0.95-C_UDSI(c,t,0))*1200;
return source;
}

/*****
*****/
UDF for specifying a heat source for drying
H(drying)=40 KJ/mool
*****/
DEFINE_SOURCE(heat_source_drying,c,t,dS,eqn)
{
real source;
real tem = C_T(c,t);

```

```

real k;
real moistureinf = 0.1;
real porosity;
porosity= 0.05+(C_UDSI(c,t,0)+C_UDSI(c,t,1)+C_UDSI(c,t,2)) ;
if (C_UDSI(c,t,0)>moistureinf*0.95 )
    k = 0.;
else
    k = 51000*exp(-78240/(8.3*tem));
    source=-k*(moistureinf*0.95-C_UDSI(c,t,0))*1200*40000/0.018;
return source;
}

```

```

/*****
****

```

UDF for specifying a source for VM release

Kinetics:

METC Gasifier Advanced Simulation (MGAS) model, Syamlal, M.

```

****/

```

```

DEFINE_SOURCE(solid_vm_release,c,t,dS,eqn)

```

```

{
real source;
real tem = C_T(c,t);
real k;

if (C_UDSI(c,t,1)>0.356*0.95)
    k = 0.;
else
    k = 51000*exp(-78240/(8.3*tem));
    C_UDMI(c,t,1)=k*(0.356*0.95-C_UDSI(c,t,1))*C_R(c,t);
    source=k*(0.356*0.95-C_UDSI(c,t,1))*C_R(c,t);
return source;
}

```

```

/*****
****

```

UDF for specifying vm mass source from pyrolysis

```

****/

```

```

DEFINE_SOURCE(mass_source_vm_pyrolysis,c,t,dS,eqn)

```

```

{
real source;
real tem = C_T(c,t);
real k;
real porosity;

```

```

porosity= 0.05+(C_UDSI(c,t,0)+C_UDSI(c,t,1)+C_UDSI(c,t,2)) ;
if (C_UDSI(c,t,1)>0.356*0.95)
  k = 0.0;
else
  k = 51000.0*exp(-78240/(8.3*tem));
  source=k*(0.356*0.95-C_UDSI(c,t,1))*1200.0;
return source;
}

```

```

/*****
****

```

UDF for specifying H2O mass source from pyrolysis

```

*****

```

```

****/

```

```

DEFINE_SOURCE(mass_source_h2o_pyrolysis,c,t,dS,eqn)

```

```

{
real source;
real tem = C_T(c,t);
real k;
real porosity;
porosity= 0.05+(C_UDSI(c,t,0)+C_UDSI(c,t,1)+C_UDSI(c,t,2)) ;
if (C_UDSI(c,t,1)>0.356*0.95)
  k = 0.0;
else
  k = 51000.0*exp(-78240/(8.3*tem));
  source=0.45*k*(0.356*0.95-C_UDSI(c,t,1))*1200.0;
return source;
}

```

```

/*****
****

```

UDF for specifying H2 mass source from pyrolysis

```

*****

```

```

****/

```

```

DEFINE_SOURCE(mass_source_h2_pyrolysis,c,t,dS,eqn)

```

```

{
real source;
real tem = C_T(c,t);
real k;
real porosity;
porosity= 0.05+(C_UDSI(c,t,0)+C_UDSI(c,t,1)+C_UDSI(c,t,2)) ;
if (C_UDSI(c,t,1)>0.356*0.95 )
  k = 0.;
else

```

```

k = 51000*exp(-78240/(8.3*tem));
source=0.01*k*(0.356*0.95-C_UDSI(c,t,1))*1200.0;
return source;
}

```

```

/*****
****
UDF for specifying CO mass source from pyrolysis
****/

```

```

DEFINE_SOURCE(mass_source_co_pyrolysis,c,t,dS,eqn)
{
real source;
real tem = C_T(c,t);
real k;
real porosity;
porosity= 0.05+(C_UDSI(c,t,0)+C_UDSI(c,t,1)+C_UDSI(c,t,2)) ;
if (C_UDSI(c,t,1)>0.356*0.95 )
k = 0.;
else
k = 51000*exp(-78240/(8.3*tem));
source=0.205*k*(0.356*0.95-C_UDSI(c,t,1))*1200.0;
return source;
}

```

```

/*****
****
UDF for specifying CO2 mass source from pyrolysis
****/

```

```

DEFINE_SOURCE(mass_source_co2_pyrolysis,c,t,dS,eqn)
{
real source;
real tem = C_T(c,t);
real k;
real porosity;
porosity= 0.05+(C_UDSI(c,t,0)+C_UDSI(c,t,1)+C_UDSI(c,t,2)) ;
if (C_UDSI(c,t,1)>0.356*0.95 )
k = 0.;
else
k = 51000*exp(-78240/(8.3*tem));
source=0.27*k*(0.356*0.95-C_UDSI(c,t,1))*1200.0;
return source;
}

```

```

/*****
****
UDF for specifying CH4 mass source from pyrolysis
*****/
DEFINE_SOURCE(mass_source_ch4_pyrolysis,c,t,dS,eqn)
{
real source;
real tem = C_T(c,t);
real k;
real porosity;
porosity= 0.05+(C_UDSI(c,t,0)+C_UDSI(c,t,1)+C_UDSI(c,t,2)) ;
if (C_UDSI(c,t,1)>0.356*0.95 )
    k = 0.;
else
    k = 51000*exp(-78240/(8.3*tem));
    source=0.07*k*(0.356*0.95-C_UDSI(c,t,1))*1200.0;
return source;
}
/*****
****
UDF for specifying FixedCarbon combustion
C+ O2 ==> CO2
Kinetics:      C. Di Blasi, F. Buonanno, C. Branca
Reactivities of some biomass chars in air
Carbon 37 (1999) 1227-1238
(Table 4, Pine wood)
*****/
DEFINE_SOURCE(solid_FC_combustion_source,c,t,dS,eqn)
{
real source;
real tem = C_T(c,t);
real k, Mtot,yo2;

Mtot=C_YI(c,t,0)/32.0+C_YI(c,t,1)/44.0+C_YI(c,t,2)/28.0+C_YI(c,t,3)/16.0+C_YI(c,t,4)/18.0+C_YI(c,t,5)/2.0+C_YI(c,t,6)/28.0;
yo2= C_YI(c,t,0)/Mtot/32.;
if (C_UDSI(c,t,2)>0.407*0.95 || C_UDSI(c,t,0)<0.09*0.95)
    k = 0.;
else
    k = 3.07e5*exp(-100400/(8.3*tem));
    C_UDMI(c,t,2)=k*(C_P(c,t)+101325)*yo2*(0.407*0.95-C_UDSI(c,t,2))/101325*C_R(c,t);
}

```

```

    source=k*(C_P(c,t)+101325)*yo2*(0.407*0.95-
C_UDSI(c,t,2))/101325*C_R(c,t);
    return source;
}
/*****
****
UDF for specifying O2 consumption due to combustion
C+ O2 ==> CO2
****/

DEFINE_SOURCE(mass_source_o2_FC_combustion,c,t,dS,eqn)
{
    real source;
    real tem = C_T(c,t);
    real k, Mtot,yo2;
    real porosity;
    porosity= 0.05+(C_UDSI(c,t,0)+C_UDSI(c,t,1)+C_UDSI(c,t,2)) ;
    Mtot=C_YI(c,t,0)/32.0+C_YI(c,t,1)/44.0+C_YI(c,t,2)/28.0+C_YI(c,t,3)/16.0+C_
    YI(c,t,4)/18.0+C_YI(c,t,5)/2.0+C_YI(c,t,6)/28.0;
    yo2= C_YI(c,t,0)/Mtot/32;

    if (C_UDSI(c,t,2)>0.407*0.95 || C_UDSI(c,t,0)<0.09*0.95)
        k = 0.;
    else
        k = 3.07e5*exp(-100400/(8.3*tem));
        source=-k*(C_P(c,t)+101325)*yo2*1200*(0.407*0.95-
C_UDSI(c,t,2))*0.032/101325/0.012;
    return source;
}

/*****
****
UDF for specifying mass source from combustion of FC
****/

DEFINE_SOURCE(mass_source_net_combustion,c,t,dS,eqn)
{
    real source;
    real tem = C_T(c,t);
    real k, Mtot,yo2;
    real porosity;
    porosity= 0.05+(C_UDSI(c,t,0)+C_UDSI(c,t,1)+C_UDSI(c,t,2)) ;

```

```

Mtot=C_YI(c,t,0)/32.0+C_YI(c,t,1)/44.0+C_YI(c,t,2)/28.0+C_YI(c,t,3)/16.0+C_
YI(c,t,4)/18.0+C_YI(c,t,5)/2.0+C_YI(c,t,6)/28.0;
yo2= C_YI(c,t,0)/Mtot/32;
if (C_UDSI(c,t,2)>0.407*0.95 || C_UDSI(c,t,0)<0.09*0.95)
    k = 0.;
else
    k = 3.07e5*exp(-100400/(8.3*tem));
    source=k*(C_P(c,t)+101325)*yo2*1200*(0.407*0.95-C_UDSI(c,t,2))*(0.044-
0.032)/101325/0.012;
    return source;
}

/*****
****
UDF for specifying a co2 mass source from combustion of FC
*****/

DEFINE_SOURCE(mass_source_co2_FC_combustion,c,t,dS,eqn)
{
    real source;
    real tem = C_T(c,t);
    real k, Mtot,yo2;
    real porosity;
    porosity= 0.05+(C_UDSI(c,t,0)+C_UDSI(c,t,1)+C_UDSI(c,t,2)) ;
    Mtot=C_YI(c,t,0)/32.0+C_YI(c,t,1)/44.0+C_YI(c,t,2)/28.0+C_YI(c,t,3)/16.0+C_
YI(c,t,4)/18.0+C_YI(c,t,5)/2.0+C_YI(c,t,6)/28.0;
    yo2= C_YI(c,t,0)/Mtot/32;
    if (C_UDSI(c,t,2)>0.407*0.95 || C_UDSI(c,t,0)<0.09*0.95)
        k = 0.;
    else
        k = 3.07e5*exp(-100400/(8.3*tem));
        source=k*(C_P(c,t)+101325)*yo2*1200*(0.407*0.95-
C_UDSI(c,t,2))*0.044/101325/0.012;
    return source;
}

/*****
****
UDF for specifying heat source in FC combustion
H(combustion)=-393 KJ/mol
*****/

DEFINE_SOURCE(heat_source_FC_combustion,c,t,dS,eqn)

```

```

{
real source;
real tem = C_T(c,t);
real k, Mtot,yo2;
real porosity;
porosity= 0.05+0.95*(C_UDSI(c,t,0)+C_UDSI(c,t,1)+C_UDSI(c,t,2)) ;
Mtot=C_YI(c,t,0)/32.0+C_YI(c,t,1)/44.0+C_YI(c,t,2)/28.0+C_YI(c,t,3)/16.0+C_
YI(c,t,4)/18.0+C_YI(c,t,5)/2.0+C_YI(c,t,6)/28.0;
yo2= C_YI(c,t,0)/Mtot/32;

if (C_UDSI(c,t,2)>0.407*0.95 || C_UDSI(c,t,0)<0.09*0.95)
  k = 0.;
else
  k = 3.07e5*exp(-100400/(8.3*tem));
  source=k*(C_P(c,t)+101325)*yo2*1200*(0.407*0.95-
C_UDSI(c,t,2))*393000/101325/0.012;
return source;
}

/*****
****
UDF for specifying solid consumption due to C-CO2 gasification
C+ CO2 ==> 2CO          dH= 171 KJ/mol
!      D. P. Ye, J. B. Agnew and D. K. Zhang
!      Gasification of a South Australian low-rank coal with carbon dioxide and
steam: kinetics and reactivity studies
!      Fuel 77(1998) 1209-1219
*****/
DEFINE_SOURCE(solid_FC_co2gasification,c,t,dS,eqn)
{
real source;
real tem = C_T(c,t);
real k, Mtot,yco2;
real porosity;
porosity= 0.05+0.95*(C_UDSI(c,t,0)+C_UDSI(c,t,1)+C_UDSI(c,t,2)) ;
Mtot=C_YI(c,t,0)/32.0+C_YI(c,t,1)/44.0+C_YI(c,t,2)/28.0+C_YI(c,t,3)/16.0+C_
YI(c,t,4)/18.0+C_YI(c,t,5)/2.0+C_YI(c,t,6)/28.0;
yco2= C_YI(c,t,1)/Mtot/44;

if (C_UDSI(c,t,2)>0.407*0.95 || C_UDSI(c,t,0)<0.09*0.95 || yco2<1e-3)
  k = 0.;
else
  k = 1327.0/60.0*exp(-91000/(8.3*tem));
  C_UDMI(c,t,3)=k*(0.407*0.95-C_UDSI(c,t,2))*C_R(c,t);

```

```

    source=k*(0.407*0.95-C_UDSI(c,t,2))*C_R(c,t);
return source;
}

/*****
****
UDF for specifying net mass generation due to C-CO2 gasification
C+ CO2 ==>2CO
****/
DEFINE_SOURCE(mass_source_net_co2gasification,c,t,dS,eqn)
{
real source;
real tem = C_T(c,t);
real k, Mtot,yco2;
real porosity;
porosity= 0.05+0.95*(C_UDSI(c,t,0)+C_UDSI(c,t,1)+C_UDSI(c,t,2)) ;
Mtot=C_YI(c,t,0)/32.0+C_YI(c,t,1)/44.0+C_YI(c,t,2)/28.0+C_YI(c,t,3)/16.0+C_
YI(c,t,4)/18.0+C_YI(c,t,5)/2.0+C_YI(c,t,6)/28.0;
yco2= C_YI(c,t,1)/Mtot/44;

if (C_UDSI(c,t,2)>0.407*0.95 || C_UDSI(c,t,0)<0.09*0.95 || yco2<1e-3)
    k = 0.;
else
    k = 1327.0/60.0*exp(-91000/(8.3*tem));
    source=k*(0.407*0.95-C_UDSI(c,t,2))*1200*(2*0.028-0.044)/0.012;
return source;
}

/*****
****
UDF for specifying CO2 consumption due to C-CO2 gasification
C+ CO2 ==>2CO
****/
DEFINE_SOURCE(mass_source_co2_co2gasification,c,t,dS,eqn)
{
real source;
real tem = C_T(c,t);
real k, Mtot,yco2;
real porosity;
porosity= 0.05+0.95*(C_UDSI(c,t,0)+C_UDSI(c,t,1)+C_UDSI(c,t,2)) ;
Mtot=C_YI(c,t,0)/32.0+C_YI(c,t,1)/44.0+C_YI(c,t,2)/28.0+C_YI(c,t,3)/16.0+C_
YI(c,t,4)/18.0+C_YI(c,t,5)/2.0+C_YI(c,t,6)/28.0;
yco2= C_YI(c,t,1)/Mtot/44;

```

```

if (C_UDSI(c,t,2)>0.407*0.95 || C_UDSI(c,t,0)<0.09*0.95 || yco2<1e-3)
  k = 0.;
else
  k = 1327.0/60.0*exp(-91000/(8.3*tem));
  source=-k*(0.407*0.95-C_UDSI(c,t,2))*1200*0.044/0.012;
return source;
}

/*****
****
UDF for specifying CO production due to C-CO2 gasification
C+ CO2 ==>2CO
*****/
DEFINE_SOURCE(mass_source_co_co2gasification,c,t,dS,eqn)
{
  real source;
  real tem = C_T(c,t);
  real k, Mtot,yco2;
  real porosity;
  porosity= 0.05+0.95*(C_UDSI(c,t,0)+C_UDSI(c,t,1)+C_UDSI(c,t,2)) ;
  Mtot=C_YI(c,t,0)/32.0+C_YI(c,t,1)/44.0+C_YI(c,t,2)/28.0+C_YI(c,t,3)/16.0+C_
  YI(c,t,4)/18.0+C_YI(c,t,5)/2.0+C_YI(c,t,6)/28.0;
  yco2= C_YI(c,t,1)/Mtot/44;

  if (C_UDSI(c,t,2)>0.407*0.95 || C_UDSI(c,t,0)<0.09*0.95 || yco2<1e-3)
    k = 0.;
  else
    k = 1327.0/60.0*exp(-91000/(8.3*tem));
    source=2*k*(0.407*0.95-C_UDSI(c,t,2))*1200*0.028/0.012;
  return source;
}

/*****
****
UDF for specifying heat consumption due to C-CO2 gasification
C+ CO2 ==>2CO          dH= 172000 J/mol
*****/
DEFINE_SOURCE(heat_source_co2gasification,c,t,dS,eqn)
{
  real source;
  real tem = C_T(c,t);
  real k, Mtot,yco2;

```

```

real porosity;
porosity= 0.05+0.95*(C_UDSI(c,t,0)+C_UDSI(c,t,1)+C_UDSI(c,t,2)) ;
Mtot=C_YI(c,t,0)/32.0+C_YI(c,t,1)/44.0+C_YI(c,t,2)/28.0+C_YI(c,t,3)/16.0+C_
YI(c,t,4)/18.0+C_YI(c,t,5)/2.0+C_YI(c,t,6)/28.0;
yco2= C_YI(c,t,1)/Mtot/44;

if (C_UDSI(c,t,2)>0.407*0.95 || C_UDSI(c,t,0)<0.09*0.95 || yco2<1e-3)
  k = 0.;
else
  k = 1327.0/60.0*exp(-91000/(8.3*tem));
  source=-k*(0.407*0.95-C_UDSI(c,t,2))*1200*172000/0.012;
return source;
}

/*****
****
UDF for specifying Char consumption due to C-H2O gasification
C+ H2O ==>CO+H2
*****/
DEFINE_SOURCE(solid_FC_h2ogasificatio,c,t,dS,eqn)
{
real source;
real tem = C_T(c,t);
real k, Mtot,yh2o;
real porosity;
porosity= 0.05+0.95*(C_UDSI(c,t,0)+C_UDSI(c,t,1)+C_UDSI(c,t,2)) ;
Mtot=C_YI(c,t,0)/32.0+C_YI(c,t,1)/44.0+C_YI(c,t,2)/28.0+C_YI(c,t,3)/16.0+C_
YI(c,t,4)/18.0+C_YI(c,t,5)/2.0+C_YI(c,t,6)/28.0;
yh2o= C_YI(c,t,4)/Mtot/18;

if (C_UDSI(c,t,2)>0.407*0.95 || C_UDSI(c,t,0)<0.09*0.95 || yh2o<1e-3)
  k = 0.;
else
  k = 261276.0/60.0*exp(-131000/(8.3*tem));
  C_UDMI(c,t,4)=k*(0.407*0.95-C_UDSI(c,t,2))*C_R(c,t);
  source=k*(0.407*0.95-C_UDSI(c,t,2))*C_R(c,t);
return source;
}

/*****
****
UDF for specifying net mass production due to C-H2O gasification
C+ H2O ==>CO+H2

```

```

*****
****/
DEFINE_SOURCE(mass_source_net_h2ogasificatio,c,t,dS,eqn)
{
real source;
real tem = C_T(c,t);
real k, Mtot,yh2o;
real porosity;
porosity= 0.05+0.95*(C_UDSI(c,t,0)+C_UDSI(c,t,1)+C_UDSI(c,t,2)) ;
Mtot=C_YI(c,t,0)/32.0+C_YI(c,t,1)/44.0+C_YI(c,t,2)/28.0+C_YI(c,t,3)/16.0+C_
YI(c,t,4)/18.0+C_YI(c,t,5)/2.0+C_YI(c,t,6)/28.0;
yh2o= C_YI(c,t,4)/Mtot/18;

if (C_UDSI(c,t,2)>0.407*0.95 || C_UDSI(c,t,0)<0.09*0.95 || yh2o<1e-3)
k = 0.;
else
k = 261276.0/60.0*exp(-131000/(8.3*tem));
source=k*(0.407*0.95-C_UDSI(c,t,2))*1200*(0.002+0.028-0.018)/0.012;
return source;
}

/*****
****
UDF for specifying H2O consumption due to C-H2O gasification
C+ H2O ==>CO+H2
*****
****/
DEFINE_SOURCE(mass_source_h2o_h2ogasification,c,t,dS,eqn)
{
real source;
real tem = C_T(c,t);
real k, Mtot,yh2o;
real porosity;
porosity= 0.05+0.95*(C_UDSI(c,t,0)+C_UDSI(c,t,1)+C_UDSI(c,t,2)) ;
Mtot=C_YI(c,t,0)/32.0+C_YI(c,t,1)/44.0+C_YI(c,t,2)/28.0+C_YI(c,t,3)/16.0+C_
YI(c,t,4)/18.0+C_YI(c,t,5)/2.0+C_YI(c,t,6)/28.0;
yh2o= C_YI(c,t,4)/Mtot/18;

if (C_UDSI(c,t,2)>0.407*0.95 || C_UDSI(c,t,0)<0.09*0.95 || yh2o<1e-3)
k = 0.;
else
k = 261276.0/60.0*exp(-131000/(8.3*tem));
source=-k*(0.407*0.95-C_UDSI(c,t,2))*1200*0.018/0.012;
return source;
}

```

```

/*****
****
UDF for specifying H2 production due to C-H2O gasification
C+ H2O ==>CO+H2
****/
DEFINE_SOURCE(mass_source_h2_h2ogasification,c,t,dS,eqn)
{
real source;
real tem = C_T(c,t);
real k, Mtot,yh2o;
real porosity;
porosity= 0.05+0.95*(C_UDSI(c,t,0)+C_UDSI(c,t,1)+C_UDSI(c,t,2)) ;
Mtot=C_YI(c,t,0)/32.0+C_YI(c,t,1)/44.0+C_YI(c,t,2)/28.0+C_YI(c,t,3)/16.0+C_
YI(c,t,4)/18.0+C_YI(c,t,5)/2.0+C_YI(c,t,6)/28.0;
yh2o= C_YI(c,t,4)/Mtot/18;

if (C_UDSI(c,t,2)>0.407*0.95 || C_UDSI(c,t,0)<0.09*0.95 || yh2o<1e-3)
k = 0.;
else
k = 261276.0/60.0*exp(-131000/(8.3*tem));
source=k*(0.407*0.95-C_UDSI(c,t,2))*1200*0.002/0.012;
return source;
}

/*****
****
UDF for specifying CO production due to C-H2O gasification
C+ H2O ==>CO+H2
****/
DEFINE_SOURCE(mass_source_co_h2ogasification,c,t,dS,eqn)
{
real source;
real tem = C_T(c,t);
real k, Mtot,yh2o;
real porosity;
porosity= 0.05+0.95*(C_UDSI(c,t,0)+C_UDSI(c,t,1)+C_UDSI(c,t,2)) ;
Mtot=C_YI(c,t,0)/32.0+C_YI(c,t,1)/44.0+C_YI(c,t,2)/28.0+C_YI(c,t,3)/16.0+C_
YI(c,t,4)/18.0+C_YI(c,t,5)/2.0+C_YI(c,t,6)/28.0;
yh2o= C_YI(c,t,4)/Mtot/18;

if (C_UDSI(c,t,2)>0.407*0.95 || C_UDSI(c,t,0)<0.09*0.95 || yh2o<1e-3)
k = 0.;

```

```

else
  k = 261276.0/60.0*exp(-131000/(8.3*tem));
  source=k*(0.407*0.95-C_UDSI(c,t,2))*1200*0.028/0.012;
return source;
}

/*****
*****/
UDF for specifying heat consumption due to C-H2O gasification
C+ H2O ==>CO+H2
*****/
DEFINE_SOURCE(heat_source_h2ogasification,c,t,dS,eqn)
{
  real source;
  real tem = C_T(c,t);
  real k, Mtot,yh2o;
  real porosity;
  porosity= 0.05+0.95*(C_UDSI(c,t,0)+C_UDSI(c,t,1)+C_UDSI(c,t,2)) ;
  Mtot=C_YI(c,t,0)/32.0+C_YI(c,t,1)/44.0+C_YI(c,t,2)/28.0+C_YI(c,t,3)/16.0+C_
  YI(c,t,4)/18.0+C_YI(c,t,5)/2.0+C_YI(c,t,6)/28.0;
  yh2o= C_YI(c,t,4)/Mtot/18;

  if (C_UDSI(c,t,2)>0.407 || yh2o<1e-3)
    k = 0.;
  else
    k = 261276.0/60.0*exp(-131000/(8.3*tem));
    source=-k*(0.407*0.95-C_UDSI(c,t,2))*1200*131000/0.012;
return source;
}

```

